RADIATION INCORPORATED
SUBSIDIARY OF HARRIS-INTERTYPE CORPORATION

8105-F-1

February 29, 1972

Period:

12 January 1971 - 29 February 1972

FINAL TECHNICAL REPORT
CR-123559
OPTICAL READ/WRITE MEMORY SYSTEM COMPONENTS

NASA Contract NAS 8-26672
Request No. 1-1-40-02885
DRL No. MA-033A
DRL Line Item No. 1

Prepared For:

George C. Marshall Space Flight Center
Marshall Space Flight Center, Alabama 35812

By:

Electro-Optics Center
Radiation Incorporated
P.O. Box 1084
2320 Washtenaw Avenue
Ann Arbor, Michigan 48106

FORWARD

This report was prepared by the Electro-Optics Center of Radiation Incorporated, under Contract NAS 8-26672 with the NASA-Marshall Space Flight Center, Huntsville, Alabama. This effort is monitored by E. J. Reinbolt, Deputy Director of the Astrionics Laboratory, NASA/MSFC and G. A. Bailey who is the Contracting Officer's Representative.

The technical effort of the contract is directed by A. Kozma, General Manager and A. Vander Lugt, Director of Research. The Program Manager is D. E. Klingler. Other contributors to this report are A. A. Friesem, R. R. Basson, W. S. Colburn, G. E. Hoffmann, W-H. Lee, H. N. Roberts, F. B. Rotz, E. N. Tompkins, P. J. Peters and R. G. Zech. Section 5, concerned with storage media optimization, was written by C. M. Verber, A. H. Adelman, K. C. Brog and W. H. Jones of Battelle Columbus Laboratories.

TABLE OF CONTENTS

1
INTRODUCTION AND SUMMARY

1.1 Objectives of the Contract

The Electro-Optics Center, under Contract NAS 8-26360, has designed and fabricated the optical components of a breadboard holographic read/write memory system and has specified the parameters of the major system components: (1) a laser system, (2) an x-y beam deflector, (3) a block data composer, (4) the read/write memory material, (5) an output detector array, and (6) the electronics to drive, synchronize, and control all system components.

The objectives of the present contract (NAS 8-26672) are divided into three concurrent phases. The objective of Phase I is to supply and fabricate the major components according to the previously established specifications. The objective of Phase II is to prepare computer programs to simulate the entire holographic memory system so that a designer can balance the requirements on the various components. Included in this phase is an effort to develop a model that will describe and predict the behavior of all types of recording materials. The objective of Phase III is to conduct a development program to optimize the combined recording and reconstruction process of the high density holographic memory system.

1.2 Summary of the Work Performed During the Contract

The major effort on this contract was to fabricate the system components in such a way that their operating parameters were compatible with achieving the performance goals for the holographic memory. Included in these efforts were the design and construction of drive electronics, and the design and construction of an electronic system which controls and synchronizes the system components.

The laser system consists of two lasers, one emitting in the blue and one emitting in the red part of the visible spectrum. The longer wavelength laser is used primarily in the read/write mode of operation; both lasers are used to demonstrate the feasibility of recording more than one hologram at each storage location by using the wavelength selectivity properties of thick recording materials. The lasers supplied with the system are a Coherent Radiation Laboratories Model 52G argon laser (emitting at 488 nm) and a Coherent Radiation Laboratories Model 52G krypton laser (emitting at 647.1 nm). Both lasers operate in the TEM_{00}, single-frequency mode and both have approximately 200 mw of output power.

The x-y beam deflector is a modified Datalite Model BD-100. This device is an acousto-optic beam deflector that has a time-bandwidth product of 160 in each direction which means that it can deflect the laser beam to 80 x 80 double Rayleigh resolved hologram locations. In the present memory system, only 20 x 20 hologram locations are required in the read only mode of operation and 5 x 5 hologram locations are required in the read/write mode of operation. The present x-y beam deflector therefore is capable of working in future systems where larger hologram arrays may be used. The deflector also meets or exceeds the performance goals for efficiency, access time, stability, and optical quality. The drive electronics for the deflector are based on the use of voltage controlled oscillators which produce the incremental frequencies needed to address the hologram storage locations. This design approach offers considerable flexibility in changing the hologram format or the geometry of the system.

The read/write memory array uses photoplastic as a recording material. This device consists of a 5 x 5 array of electrically conductive pads, a thin layer of photoconductor, a thin layer of thermoplastic

and a corona discharge element. Each pad can be independently addressed for exposure, heating, reading, and erasing. The sensitivity of the material is typically 75 joules/cm^2, its resolution is greater than 1000 lines/mm, its diffraction efficiency ranges from 1 to 4% (depending on the recording parameters), and its signal-to-noise ratio is approximately 15 dB. We have made significant progress in imp7oving the operating characteristics of the photoplastic as well as in increasing the number of cycles before fatiguing. This material shows considerable promise for use in medium sized holographic memories; it is basically a thin recording material, however, so that it cannot be considered as a candidate for a mass storage system having no moving parts.

The block data composer is a matrix addressable PLZT device that converts the electrical digital signal into an optical signal that spatially modulates a laser beam. The PLZT material has the basic properties required of a block data composer (e.g., low switching voltages, high switching speeds, good contrast, good recyclability, memory, and so forth). We fabricated several preliminary devices to determine whether these known characteristics of bulk PLZT can be retained in matrix addressable devices. Although all of the characteristics were observed in sample devices, we found that it is difficult to retain all these characteristics in large matrix arrays (128 x 128 elements). The major difficulties were encountered in perfecting the fabrication process. Several bonding operations are required to fabricate the device and we found that the large diameter plates of very thin PLZT were difficult to bond without breaking. Difficulties were also encountered in uniformly polishing the thin plates; nonuniformities lead to variations in the contrast over the block data composer. Changing the applied voltage or the strain-bias tends to compensate for thickness variations, but not over the entire plate at once.

We have made significant advancements in the fabrication technology and were able to fabricate 32 x 24 element block data composers by the end of the contract. Through a refinement of these techniques and the use of different PLZT and electrode materials, it should be possible to fabricate large matrix arrays.

The photodetector array for the memory is a 32 x 24 element matrix array of phototransistors. The specifications for the two-dimensional array were based on measured performance values for a beam-lead, linear array of phototransistors. The delivered array did not, however, have either the sensitivity or the signal-to-noise ratio of the test array. As a result, several changes in the system were made during the last quarter in an effort to compensate for the reduced performance. We do not expect that photodetector performance will be a serious problem in future systems; some care is needed, however, in specifying the performance of such arrays.

Details of our work on the major system components are given in Section 4. In Section 2 we discuss some ways in which the system has been rearranged to reflect the performance characteristics of the photodetector array.

In Section 3 we report on the results of Phase II of the contract. We have written a computer program which incorporates the equations that describe the performance of each part of the holographic memory. The program is divided into four subroutines: (1) a subroutine that simulates the optical parameters so that a designer can balance the requirements on such devices as block data composer, the beam deflector, the photodetector array, and the Fourier transform lenses, (2) a subroutine that simulates the acousto-optic beam deflector to permit design tradeoffs, (3) a subroutine that calculates the laser power required in various modes of operation, and (4) a subroutine that calculates the performance of the memory for various recording materials. The fourth subroutine includes

results of our modeling of holographic recording materials. The designer generally specifies the input/output data rates, the total memory capacity, and the signal-to-noise ratio required for a given error rate. The program then simulates the entire holographic memory so that design tradeoffs can be made. The program is flexible and can be modified or updated as required.

Section 5 contains a summary of a development program, conducted by Battelle Columbus Laboratories, to optimize the combined recording and reconstruction process of a high density holographic memory system. The goal of this phase is to isolate several physical phenomona or material classes which appear to have the potential of being acceptable storage media. A set of criteria for the recording media was developed, based on the long-range goal of achieving a 10^{10} to 10^{12} bit memory having no moving parts, and used to evaluate candidate materials. The work described in Section 5 is mainly conceptual and computational; the principal conclusion is that two material classes (ferroelectric and cis-trans isomers) have the potential of satisfying many of the quantitative criteria. At present, both fail to meet the writing sensitivity criterion, but improvements in sensitivity are theoretically possible.

2

SYSTEM CONSIDERATIONS

2.1 Introduction

Under Contract NAS 8-26360, the Electro-Optics Center designed the optical portion of the feasibility test bed system and specified the operating parameters required of major system components such as the lasers, the acousto-optic beam deflectors (AOBD), the block data composer (BDC), the read/write hologram array, the photodetector array (PDA), and the control and drive electronics. The design of the optical system began by considering how the system capacity Q is related to the constructional parameters of the Fourier transform lenses and the major system components.

The objectives of this contract are to fabricate a holographic memory system in which digital data entered into a 128 x 128 element BDC can be stored in a 20 x 20 matrix array of holograms (for the read only mode of operation) or in a 5 x 5 matrix array of holograms (for the read/write/erase mode of operation). Some of the constructional parameters of the system were therefore already set before the design began. Although the design phase of the optical components was thereby partially restricted, these restrictions did not have a major impact on the final design.

It is worthwhile to summarize the findings of our study of how the capacity of the memory relates to the constructional parameters of the system. Details of the analysis can be found in Reference 1. The one-dimensional capacity Q of the system, for unity magnification, is given by

$$Q = \frac{R^2}{8\sqrt{2}\,\bar{c}c\lambda k} \quad ,$$

where R is the aperture ratio of the Fourier transform lenses, c is the spacing ratio of the bits in the BDC, $\bar{c}$ is the spacing ratio of the holograms in the hologram array, λ is the wavelength, and K is the power of

the lens. Since the system is required to operate at two wavelengths (632.8 nm and 488 nm), we carried out all the preliminary calculations for the worst case (the longer wavelength). The two-dimensional capacity of the system is given by Q^2.

Since we want to record 128 bits in 20 hologram locations, the value of Q is 2560. We used the following values for the other parameters: R = 0.5 (an f/2 lens), c = $\bar{c}$ = 1.5, and λ = 632.8 nm. The focal length of the transform lens (F = 1/K) then was calculated as being 163 mm.

The length d of each bit in the BDC is calculated from the relationship that

$$d = \frac{R}{2\sqrt{2}\, NcK} ,$$

where N = 128 is the number of elements in a row or a column of the BDC. The value of d is then 152μ. The length $\bar{d}$ of each hologram is given by

$$\bar{d} = \frac{2\lambda}{dK} ,$$

which gives $\bar{d}$ = 0.97 mm. Finally, the packing density ρ^2 will be

$$\rho^2 = \frac{N^2}{\bar{d}^2} ,$$

which is equal to $1.7(10^6)$ bits/cm^2.

The next step was to design the Fourier transform lens which has a 163 mm focal length and a 81.5 mm clear aperture. The design calculations were given in Reference 2. Two lenses for the system were fabricated by Herron Optical Company.

In parallel with this study we developed an optical layout for the overall system. The prime design consideration was that the layout provide enough flexibility so that modifications could be made in the future as new BDC's, hologram recording materials, or PDA's became available. The selected layout is shown in Figure 2.1; a complete description of this layout is given in Reference 2. The design was predicated on the use of He-Ne and Argon lasers, a 25 mm square aperture AOBD, and a BDC which diffracts light to all hologram locations. Some modifications in the major system components have required changes in this basic layout. These modifications and the attendant changes will now be considered. In each case, more detailed discussions of the performance parameters of the major components will be given later; our main interest, in this section is how these parameters affected the system layout.

2.2 Acousto-Optic Beam Deflectors

We decided, at the beginning of this contract, to fabricate an AOBD using water as the interactive medium and crystal controlled oscillators to provide the drive frequencies. Although only 20 angles are required to address the 20 holograms in a row or column, the contract requirements are to supply an 80 x 80 spot deflector that can be used in future systems. Since the hologram spacing ratio is $\bar{c} = 1.5$, the 20 spot requirement is equivalent to a 30 resolvable spot deflector requirement. We decided to fabricate the AOBD at the Electro-Optics Center for two reasons: (1) at the beginning of the program there were no AOBD's commercially available having the correct beam format and satisfying the resolution requirements, and (2) the frequency stability requirements on the drive electronics for both readin and readout were severe.

During the first two quarters of the contract we made significant progress in fabricating the water cell and its electronics. We experienced

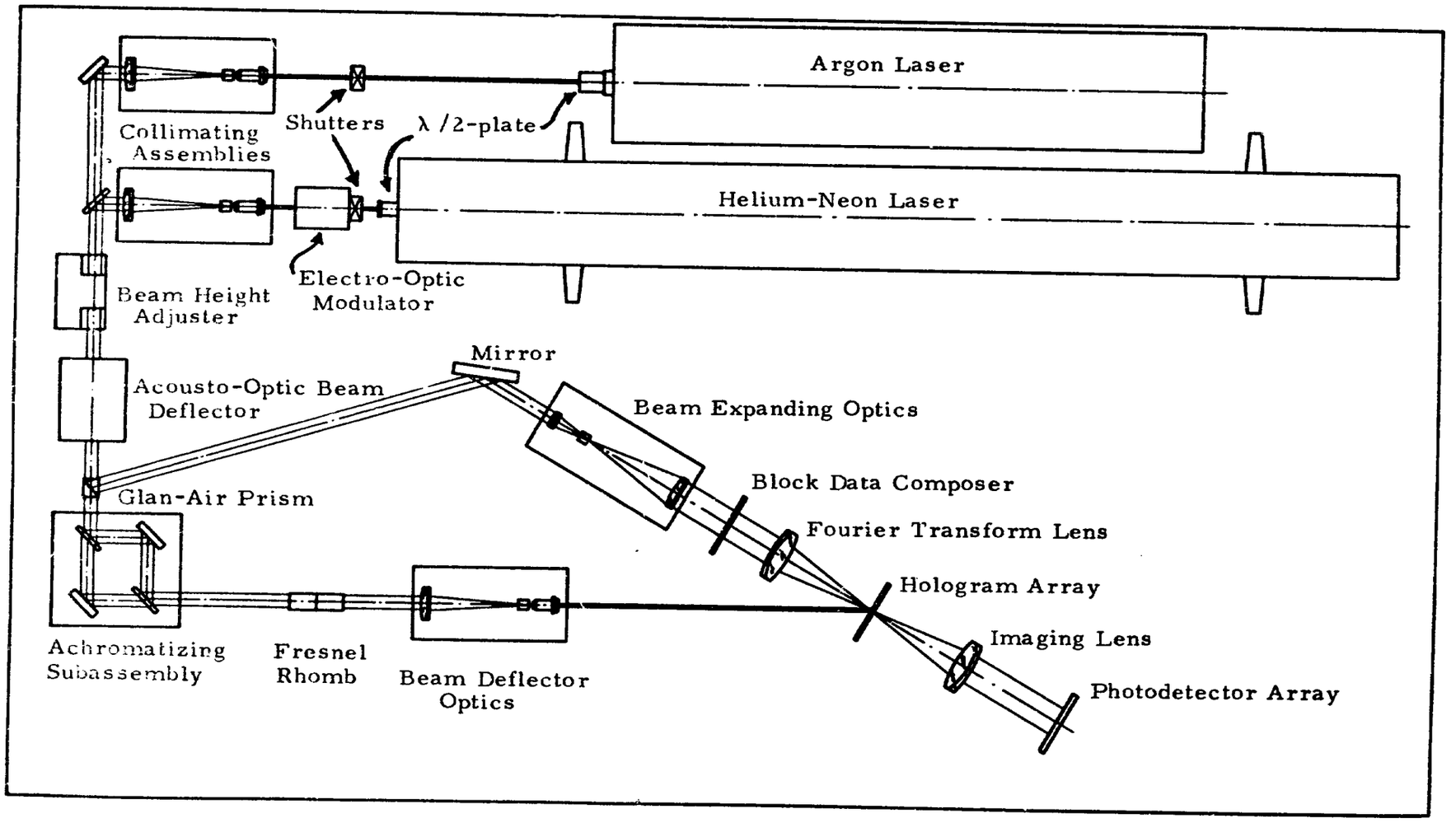

FIGURE 2.1 SYSTEM LAYOUT

some problems, however, in mounting large transducers (approximately 25 mm in diameter) and in getting good impedence matches between the transducers and the water. The latter problem caused the water temperature to rise excessively which, in turn, caused turbulence and beam instabilities. We did, nevertheless, succeed in recording holograms with the water cell by removing the effects of turbulence by circulating the water within the cell.

During the third quarter, two events occurred which led to a decision to abandon the water cell approach. First, a commercial AOBD having adequate resolution and the correct format became available. This cell is a Datalite BD-100 that is packaged into an x-y mount; a list of its specifications is given in Section 4.2. The second consideration was that we determined that the frequency stability requirements, using another design concept for the beam deflector optics, were not as severe as the requirements for the previous design concept. In the first design concept (Reference 1) the reference beams are a set of plane waves that are nearly parallel. In the second design concept (Reference 2) the reference beams have a spherical phase factor resulting from the fact that all beams originate from a given plane which is a finite distance from the hologram array.

If the reference beams were plane waves, the frequency stability would be set by the requirement that the reconstructed bit pattern does not shift when the holograms are read out. The frequency stability requirement was, therefore, $\pm(10^{-4})$. Since we are now using reference beams having spherical wavefronts, the frequency stability is only $\pm(10^{-3})$ which is set by the criterion that the readout beam is not displaced more than $\pm$10% from its position when the hologram was recorded.

The reduced frequency tolerances allowed us to design electronics based on the use of voltage controlled oscillators instead of crystal

oscillators. An additional advantage of this approach is that almost any hologram array format can be selected simply by entering a different set of voltages into the controller.

The change in AOBD's had several impacts on the layout of the system. Since the aperture of the BD-100 is 12 mm x 12 mm instead of 25 mm x 25 mm, the first change was in the focal lengths of the microscope objectives in the two collimating assemblies. These objectives have been changed to fully illuminate the aperture of the AOBD. The second impact of the change is that the incremental angle $\Delta\theta$ between resolvable spots is 0.14 milliradians instead of 0.094 milliradians. The larger value of $\Delta\theta$ meant that we had to change either the angular magnification of the beam deflector optics or the distance between the deflector optics and the hologram array. We accomplished this change by using both a different microscope objective in the deflector optics and a different distance from the deflector optics to the hologram array. We also interchanged the position of the Fresnel rhomb and the deflector optics; the rhomb is now positioned between the deflector optics and the hologram array.

The change in $\Delta\phi$ also required some changes in the signal beam optics. First, since the beam leaving the BD-100 has approximately one-half the size of the beam leaving the water cell, we had to change the optics in the beam expanding telescope slightly. The second required change was to move the beam expanding optics closer to the Glan-Air prism so that the deflected beams do not change position as a function of the AOBD address. Since the beam is expanded by a ratio of approximately 2.8 to 1, the angular magnification of the beam expanding optics is reduced by the same ratio. Thus, the angular deflection beyond the expanding optics is extremely small. The beam expanding optics are now positioned between the Glan-Air prism and the mirror.

2.3 Block Data Composer

In future systems it will be desireable to deflect the laser beam in both the reference and signal paths so that all of the available light reaches a given hologram location. In an effort to keep the system as flexible as possible and to keep it from becoming too complex, we designed the present system so that every bit in the BDC contributes light to all hologram locations in the array. There are two ways to achieve this result while maintaining good optical efficiency. The first is to use a lenslet array at the plane of the BDC and to focus the light from each element of the BDC to a point at the front focal plane of the Fourier transform lens. The light from each point focus is then collimated by the Fourier transform lens and passes through a common area that defines the boundary of the hologram array. We tested this approach using a lenslet array and found good uniformity of the light in the hologram plane. Unfortunately this lenslet array did not have a center spacing ratio that matched that of the BDC. Efforts to obtain a suitable array were unsuccessful since it would have entailed a costly development program to produce a useful array having the correct center spacing for the 128 x 128 array BDC. The costs are high primarily because the master mold is difficult to make. We believe, based on some recent experience, that it may be possible to use less expensive crossed cylindrical lenslet arrays to achieve nearly the same result as with a crossed array of spherical lenslets. We did not, however, have enough time to fully explore this approach.

The second way to cause every bit in the BDC to contribute light to every hologram location is to use a lenslet array whose geometry matches that of the hologram array. The details of this approach are given in Reference 3. The impact of this change on the system layout is that an additional lens system is needed to collimate the point focus of each lenslet element so that the plane waves pass through a common area that

defines the boundary of the BDC. Tne Fourier transform lens then accepts the light that is spatially modulated by the BDC and creates a $\bar{N} \times \bar{N}$ array of Fourier transforms located at each of the $\bar{N} \times \bar{N}$ hologram positions. Two lenslet arrays are supplied in the deliverable system; one array has a 5 x 5 matrix of lenslets for the read/write memory, the other array has a 20 x 20 matrix of lenslets for the read only memory.

One potential advantage of the lenslet array approach adopted is that a beam deflector system can be more easily incorporated into the signal beam to direct all the light to each hologram location. At least one additional mirror is required to make the signal beam deflection track the reference beam deflection.

2.4 The Photodetector Array

The photodetector array delivered by Texas Instruments has less sensitivity and a higher system noise level than we expected from the tests based on sample phototransistors. A full discussion of the characteristics of this array is given in Section 4.5. The major impact of the decrease in sensitivity and increase in noise level on the system is that the calculated laser power requirements are no longer valid. We had expected a PDA sensitivity of 20 nanowatts/bit and a signal-to-noise ratio limited primarily by dark current. The delivered array, however, requires 200 nanowatts/bit to produce an equivalent signal, and a signal-to-noise ratio limited by system noise. In order to drive the noise level down to compensate for the loss in sensitivity, we have had to replace the He-Ne laser by a krypton laser.

The krypton laser we have incorporated into the system is a CRL Model 52. The maximum power that can be delivered at 647.1 nm with an etalon (to give an adequate coherence length) is approximately 250 mw which is a factor

of 5 more power than that obtainable from the SP Model 125 He-Ne laser. This increase is not, unfortunately, enough to completely offset the reduction in the performance of the PDA and we have, therefore, attempted to minimize the loss of light in other parts of the system.

One way to reduce light losses is to reduce the beam diameter at the collimating assemblies. The result of this is that the input aperture of the AOBD is not uniformly illuminated and the spots produced by it, in conjunction with the beam deflector optics, at the hologram plane increase in size. The increased reference beam spot size is not too serious for the read/write memory because the hologram locations for the 5 x 5 photoplastic array are on 7-8 mm centers and the hologram pads are 2-3 mm wide. The problem is more serious, however, for the read only memory since it is now more difficult to produce a 1 mm diameter reference beam. Since the signal beam still causes all the information contained in the BDC to pass through a 1 mm hologram, the effect of the larger reference beam for the 20 x 20 array is to increase the possibility of cross-talk between holograms.

We have also tried to conserve light by reducing the beam diameter in the signal beam. Again, since the laser beam has a Gaussian intensity profile, the price paid for optimizing the efficiency of the system is a reduction in beam uniformity. The lack of uniformity across the lenslet array causes the intensity of the Fourier transform of the bit patterns to change at each hologram location. Since this variation in intensity can be measured, its effect can be compensated by a change in exposure at each hologram location. Obviously it would be more attractive to use a single exposure value for all hologram locations; we can, however, load a pre-determined set of exposure values in the controller so that if one exposure value is known, all others are in the proper ratio.

The revised optical layout is shown in the photograph of the completed feasibility test bed system (Figure 2.2).

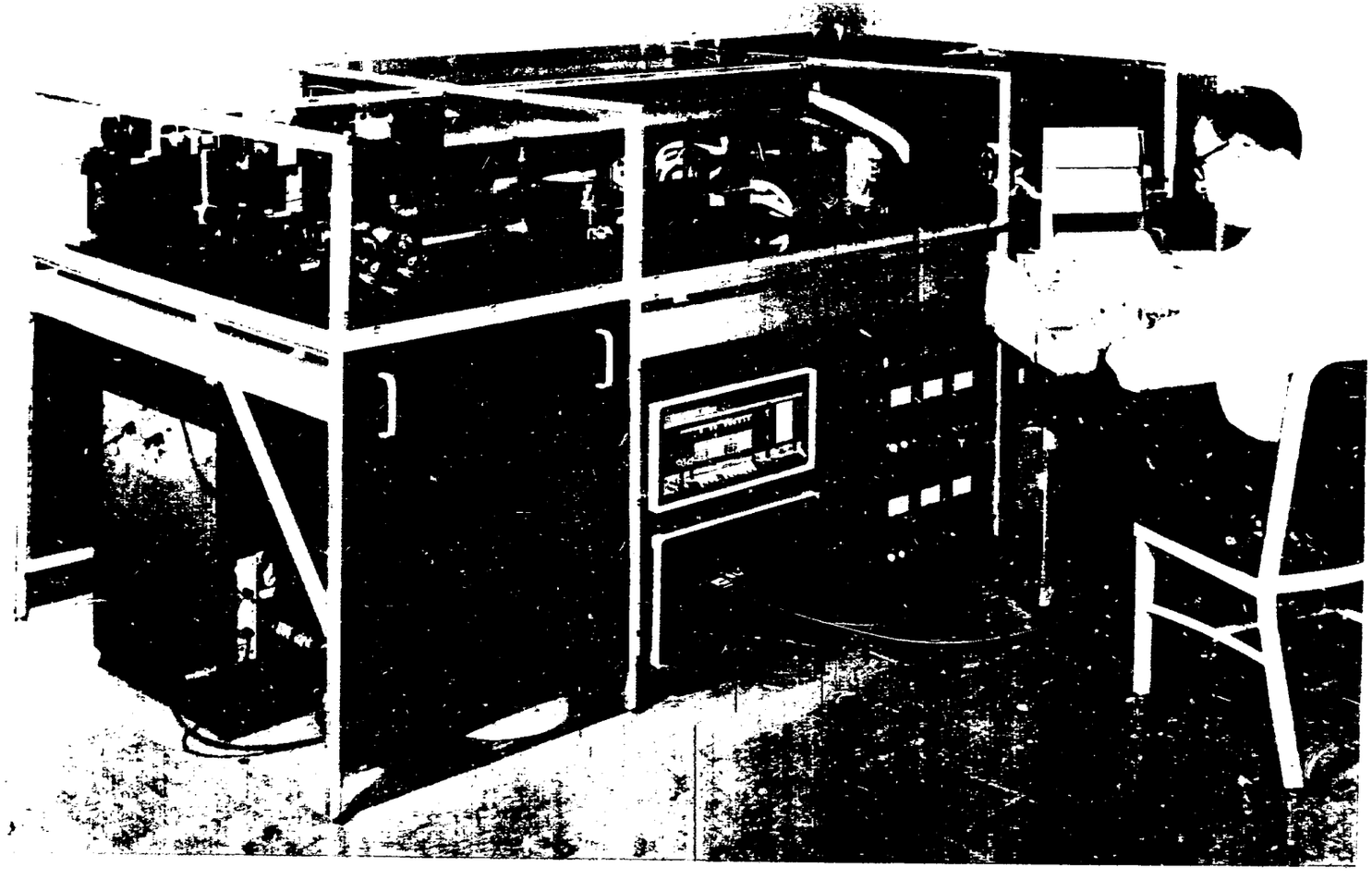

FIGURE 2.2. PHOTOGRAPH OF THE FEASIBILITY TEST BED SYSTEM

2.5 Other System Considerations

So far we have discussed how changes in the performance parameters of the major system components have significantly affected the system layout. Other changes have also affected the overall system performance to some extent. The Fourier transform lens design was based on a bit size of d = 152μ and a center spacing ratio c = 1.48. The bits should, therefore have been on 225μ center spacings and the total length of the BDC would have been 128 x 225μ = 28.8 mm. When we contacted Texas Instruments about fabricating the PDA array, they indicated that they could fabricate a 32 x 24 array on 40 mil and 50 mil centers for the 32 and 24 element directions. These spacings are equivalent to 10 mil spacings for a fully populated array and meant that the BDC center spacings would also be 10 mils (or 254μ) for unity magnification. Thus, the length of the BDC increased to 128 x 254μ = 32.5 mm which exceeds the design length by 3.7 mm or nearly 13%. The increased BDC length means that some bits are vignetted when we record in the off-axis regions of the hologram array. Furthermore, the lenslet array, in conjunction with the collimating optics, does not illuminate the BDC with a plane wave for extreme off-axis hologram positions. Thus, light from off-axis bits in the BDC do not always intercept the aperture planes of the Fourier transform lenses at equal heights. The combination of these two phenomona causes a shifting of the bit patterns at the PDA plane. The shifting is due to the increased amount of spherical aberration which had considerable impact on the fractional distortion of the bit pattern. The bits are, however, well resolved for all holograms in the array and for all positions in the BDC.

The transform lenses were designed to keep the spherical aberration small enough so that the fractional distortion is less than 0.1% over a BDC diagonal of $28.8\sqrt{2} = 40.32$ mm. The spherical aberration increases as the fourth power of the lens aperture for primary spherical aberration and as the sixth power of the aperture for secondary spherical aberration.

Thus, the secondary spherical aberration at the edge of the larger aperture will be $(1.13)^6 = 2.07$ times the original design limit. Therefore, the fractional distortion also increases for the off-axis bits and for off-axis holograms.

The fractional distortion is further increased because of the increase in the longer wavelength used (from 632.8 to 647.1 nm). Since the fractional distortion of the original design was fairly low, the total impact of all these factors is not as serious as it might have been. Nevertheless, the bit shifting for bits considerably off-axis in the BDC and for off-axis holograms is more than we would like. We have incorporated a program into the controller that causes the exerciser to disregard bits where the shift is excessive.

These considerations show that the optical design must include a knowledge of the illuminating optics as well as the exact dimensions of the BDC and the wavelength range used. The design problem does not appear to be difficult, but the changes referred to above occurred too late in the program to have the lenses redesigned and fabricated.

3

SIMULATION AND ANALYSIS PROGRAMS

There are three major tasks under the simulation and analysis program. The first task is to prepare a program in which a computer, compatible with Sigma V, is used to simulate the effects of all the operating parameters of the major components have on the performance of a holographic memory using thin recording materials. The results of this task are reported in Section 3.1.

The second task is to develop a model that will describe and predict the behavior of several types of hologram recording materials (thin and thick amplitude materials and thin phase materials). From this model we are to prepare a program in which a computer, compatible with Sigma V, will accept the measured parameters and use these data to predict the performance of the material in the memory system. The validity of the general model and its calculated performance are to be tested experimentally by measuring the diffraction efficiency, the signal-to-noise ratio, and the angular orientation and wavelength sensitivity of thick photographic films and thick dichromated gelatins. These parameters are measured as a function of exposure values and reference-to-signal beam intensity ratios. Based on the model and the experimental measurements, the performance of the recording material in the overall system will be evaluated. The results of this task are reported in Section 3.2.

The third task is to conduct a developmental program to optimize the read/write process of the high density holographic memory system. The overall goal of this task is the identification of a storage medium possessing the physical parameters to optimize the system. This program consists of the following subtasks.

(1) Conduct a survey of existing materials which show promise for use in the holographic memory.

(2) Select the most promising material and evaluate its performance in the holographic memory through experimental measurements and the use of the computer simulation program.

(3) Recommend a program to develop a suitable material possessing the physical parameters to optimize the read/write memory system.

This task was performed under a subcontract to Battelle Columbus Laboratories. The results of this task are reported separately in Section 5.

3.1 System Analysis

In References 1, 2, and 4 we gave analytical results that are useful in designing holographic memory systems. Three major analyses had been made: (1) an analysis to determine the relationships among the constructional parameters of the optical system, including the beam deflector optics, (2) an analysis of the operating parameters of the acousto-optic beam deflectors, and (3) an analysis of the laser power required for readin and readout. The computer program is written so that any or all of these three analyses can be used for system design. Later in this section we give the results of a fourth analysis in which the parameters associated with the recording material are considered. The results of this analysis are also incorporated into the system program.

In the initial stages of the design of a memory, only the optical system parameters are usually of interest. When a satisfactory system has been achieved, we consider the requirements on the acousto-optic beam deflectors, the laser source, and the recording materials. Therefore, the computer program consists of a main program and four subroutines. The main program is used to accept data and to call up the subroutines to perform the necessary computations. In the following paragraphs we

discuss the functions of the four subroutines and how they can be used in designing an optimum memory system.

3.1.1 Subroutine SYST. — The subroutine SYST is a computer program for calculating the optical system parameters. In using this program we can specify

1. Q2 - the total storage capacity of the memory, in bits;
2. NI - the number of bits in one row of the block data composer (BDC) or NH - the number of holograms in one row of the hologram array;
3. R - the aperture ratio of the lens; if not specified, R = 0.5;
4. W - the laser wavelength; if not specified, W = .0006328 mm;
5. CI - Center spacing of each bit divided by the bit diameter (related to the BDC); if not specified, CI = 1.5;
6. CH - Center spacing of each hologram divided by the hologram diameter; if not specified, CH = 1.5.

Some parameters in the list above have preassigned values so that unless the designer wants to change these values, only the values of the parameters Q2 and NI or Q2 and NH need to be supplied to the program to carry out the design calculations. After accepting the input data, the program first calculates the focal length F of the Fourier transform lenses used in the memory. The optical system is assumed to operate at unity magnification. The focal length F is given by

$$F = 16\ CI \cdot CH \cdot WM \cdot \sqrt{Q2}/R^2.$$

With F calculated, we find the diameter of the bit from

$$DI = R \cdot F/\sqrt{8}\ NI \cdot CI$$

and the diameter of the hologram from

$$DH = R \cdot F/\sqrt{8}\ NH \cdot CH$$

where $NH = \sqrt{Q2}/NI$.

This subroutine also calculates the required film packing density in bits/cm^2. The calculated value can be compared to the packing density that, for a given recording material, produces an adequate signal-to-noise ratio. Furthermore, from the fourth subroutine we can predict the resulting error rate. If the designer is forced to use a given maximum packing density (either because of recording material limitations or because a desired error rate must be achieved), he can input the film packing density. The program then automatically computes the maximum value of the aperture ratio R consistent with the value of the packing density; the aperture ratio and the wavelength are the only two constructional parameters that influence the packing density. After the main program has been called, the designer can input the values of the parameters he wants to control. We shall show, by way of an example, how each subroutine is addressed and how the output data is printed.

Suppose we want to design a 10^9 bit memory and that a 256 x 256 element block data composer is available. The following input statement is given to the computer:

```
B&INPUT Q2 = 1.E9, NI = 256, PSYST = .5.&
```

The statement, PSYST = .T., tells the main program to call the subroutine SYST, to perform the listed calculations, and to print the results. Other data supplied to the program is that the storage capacity Q2 is equal to 10^9 and the number NI of bits per dimension of the BDC is 256. The program automatically assumes that the memory is an imaging system; if NONI is typed, the calculations are based on the non-imaging set of equations.

The printout from the computer, for SYST, is organized into four sets of data. The first set includes (1) the type of system used (imaging or non-imaging), (2) the maximum wavelength, (3) the wavelength at which the calculation is to be performed, (4) the total capacity of the system, and (5) the required film packing density. This output set, for the given example, is shown below:

```
                    IMAGING SYSTEM
 DESIGN FØR MAXIMUM WAVELENGTH = 0.00063280 MM
 LASER WAVELENGTH = 0.00063280 MM
 TØTAL CAPACITY ØF THE MEMØRY SYSTEM = 0.1000E+10 BITS
 *REQUIRED FILM CAPACITY = 0.8671E+06  BITS/CM/CM
```

The next set contains lens parameters such as (1) the magnification factor (if not specified, M = -1), (2) the aperture ratio, (3) the focal length of the lens, and (4) the power of the lens. The power of the lens is included because it is needed to begin a lens design program as outlined in Reference 2. The displayed data are shown below:

```
                    LENS PARAMETERS
 *MAGNIFICATIØN FACTØR=-M/(1-M) =    1.00
  APERTURE RATIØ ØF THE LENS =    0.50
 *FØCAL LENGTH ØF THE LENS=     2881.57  MM
 *PØWER ØF THE LENS=    0.000347  1/MM
```

The next set of data contain the block data composer parameters such as (1) the number of bits per row, (2) the spacing ratio of the bits, (3) the bit diameter or length, and (4) the overall length of the BDC. The displayed data are shown below:

BDC PARAMETERS

NUMBER ØF BITS PER RØW IN BDC= 256
CENTER SPACING ØF EACH BIT/BIT DIAMETER = 1.5
BIT DIAMETER= 1.3265 MM
LENGTH ØF BDC= 509.39 MM

The fourth set of data printed out for the SYST subroutine deals with the hologram array parameters such as (1) the number of holograms per row, (2) the spacing ratio of the holograms, (3) the hologram diameter or length, and (4) the overall length of the hologram array. The displayed data is shown below:

HØLØGRAM ARRAY PARAMETERS

NUMBER ØF HØLØGRAM IN ØNE RØW ØF THE ARRAY= 124
CENTER SPACING ØF EACH HØLØGRAM/HØLØGRAM DIAMETER= 1.50
HØLØGRAM DIAMETER= 2.7492 MM
LENGTH ØF HØLØGRAM ARRAY = 511.35 MM

The symbol * shown next to some of the parameters indicates that the parameter is calculated from the parameters supplied by the designer. Because the program is based on a set of equations which maximizes the storage capacity for a given lens system, the lens focal length of 2.9 meters is the shortest that can be used to produce a storage capacity of 10^9 bits with an adequate readout SNR ratio. The design also indicates that the required storage capacity of the recording material is about 8.7×10^5 bits/cm^2. Therefore, a recording material such as Kodak 649F film can be used for such a memory.

3.1.2 Subroutine AOBD. — The function of the subroutine AOBD is to determine the requirements on the acousto-optic cell and the deflector optics. In using this program we can specify NH, CH, W, WM, and

1. MA = the angular magnification of the deflector optics, if not specified, MA = 40;
2. T = the transit time; if not specified, T = 10 microsecond; and
3. FB = the fractional bandwidth; if not specified, FB = 0.35.

If this program is called after the subroutine SYST, the program can calculate the parameters of the acousto-optic cell and the deflector optics without additional information from the designer. For example, if we have arrived at a reasonable optical design, we can turn our attention to the design of the AOBD. To do this, we want to suppress the printout of the subroutine SYST and display only the AOBD parameters. The appropriate input statement is then modified as follows:

```
B&INPUT PSYST = .F., PAØBD = .T.&
```

The first statement, PSYST = .F., will suppress the printout of the optical system parameters. The second statement, PAØBD = .T., requests the computer to printout the AOBD parameters. We obtain the following output from the computer:

```
AØBD PARAMETERS

*TIME BANDWIDTH PRØDUCT=   372
*BANDWIDTH=   37.20 MHZ
*CENTER FREQUENCY=   106.29  MHZ
TRANSIT TIME=   10.00 MICRØSECØND
FRACTIØNAL BANDWIDTH=   0.35
*FREQUENCY INCREMENT FØR   124 BEAMS=   300.00 KHZ
```

NUMBER CØDES FØR MATERIALS

1 = WATER

2 = DENSE FLINT GLASS

3 = EXTRA-DENSE FLINT GLASS

4 = FUSED QUARTZ

5 = PØLYSTYRENE

6 = KRS-5

7 = LITHIUM NIØBATE

8 = LITHIUM FLUØRIDE

9 = RUTILE

10 = SAPHIRE

MATERIAL	*BRAGG (MRADIAN)	*ANGULAR INCREMENT (MRADIAN)	*LENGTH (MM)	*PØWER (WATT)
1	21.70	0.1225	15.5	1.41
2	8.85	0.0500	38.0	14.89
3	10.85	0.0612	31.0	5.34
4	5.68	0.0318	59.7	82.26
5	13.29	0.0750	25.3	1.63
6	15.94	0.0900	21.1	0.33
7	4.54	0.0257	74.0	21.11
8	5.60	0.0316	60.0	145.56
9	3.26	0.0184	103.0	22.27
10	3.06	0.0173	110.0	451.60

PARAMETERS FØR BEAM DEFLECTØR ØPTICS

ANGULAR MAGNIFICATIØN= 40

D=DISTANCE BETWEEN EXIT PUPIL AND HØLØGRAM

MATERIAL	D(MM)
1	841.74
2	2063.62
3	1683.48
4	3242.06
5	1373.94
6	1145.85
7	4018.63
8	3258.35
9	5593.50
10	5973.64

The first set of data in the printout is the requirements on the electrical system needed to drive the acoustic cell. In our example, in order to achieve a transit time of 10 microseconds, the center frequency of the transducer must be 106 MHz and the bandwidth must be 37 MHz; the cell can then generate the 124 positions for the laser beam. The table following the data on the electrical system gives information relating to some materials that might be used in the acoustic cell. For example, if water is used, the table shows that the water cell is 15 mm long, the electrical power required to achieve 100% diffraction efficiency is 1.41 watts, and the Bragg angle of the incident beam is about 21.7 milliradians.

The distance between the exit pupil of the beam deflector optics and the hologram is given by

$$D = 0.5 \cdot L \cdot DH/(MA \cdot W)$$

where L is the length of the acoustic cell.

3.1.3 Subroutine LASER. — This program calculates the laser power needed to record the holograms and the laser power needed to retrieve the data from the memory. To use this program we can specify

1. VIN = the readin data rate; if not specified, VIN = 10^6 bits/sec
2. VOUT = the readout data rate; if not specified VOUT = 10^6 bits/sec
3. CM = the number of the channels used in readout; if not specified, CM = 1
4. UD = the detectivity of photodiodes; if not specified, UD = 10^{10}
5. SNR = the signal-to-noise ratio of the photodiodes; if not specified, SNR = 30
6. AC = the ratio of charging time to readout time, if not specified, AC = 0.5

7. EO = the exposure sensitivity of the recording material; if not specified, EO = 40.10^{-6} joules/cm^2
8. K = the reference to signal beam ratio; if not specified, K = 1
9. EFA = the efficiency of the AOBD; if not specified, EFA = 0.5
10. EFH = the efficiency of the hologram; if not specified, EFH = 0.01
11. EFDO = the efficiency of the deflector optics; if not specified, EFDO = 1
12. EFO = the efficiency of the common optics; if not specified EFO = 0.8
13. EFD = the efficiency of diffuser; if not specified, EFC = 0.028
14. EFSO = the efficiency of the signal optics; if not specified, EFSO = 1.

Because all of the parameters have a preassigned value, this program can be used following the subroutine SYST to calculate the laser power requirements. Suppose that the computer has just finished printing out the AOBD parameters in the previous example and that we have achieved a satisfactory design. We can now examine the laser power requirement by typing in

```
B&INPUT PAØBD = .F., PLASER = .T., VIN = 1.E8, VØUT = 1.E8&
```

The statement, PAØBD = .F., will suppress the printout of the AOBD parameters. In using this program we want to find the requirements on the laser when we write data on the hologram and when we read out data from the hologram at a rate, say, of 10^8 bits/second. The following printout provides us the laser power requirements and all the values of the parameters used in the calculations.

LASER POWER REQUIREMENTS

*AVERAGE READIN PØWER= 0.27E+01 WATTS
*PEAK READØUT PØWER (CHARGE STØRAGE)= 0.36E-01 WATTS
*AVERAGE READØUT PØWER (CHARGE STØRAGE)= 0.18E-01 WATTS
*PEAK READØUT PØWER (CW)= 0.92E+01 WATTS
*AVERAGE READØUT PØWER (CW)= 0.46E+01 WATTS
READIN DATA RATE= 0.10E+09 BITS/SECØND
READØUT DATA RATE= 0.10E+07 BITS/SECØND
DETECTIVITY ØF PHØTØDIØDE = 0.10E+11
EXPØSURE SENSITY ØF RECØRDING MATERIAL= 0.40E-40 JØULES/CM**2
REFERENCE TØ SIGNAL BEAM RATIØ= 1
*GLAN-AIR PRISM SPLITTING RATIØ= 0.0021
EFFICIENCY ØF AØBD= 0.5000
EFFICIENCY ØF HØLØGRAM= 0.0100
EFFICIENCY ØF DEFLECTØR ØPTICS= 1.0000
EFFICIENCY ØF ØTHER ØPTICS= 0.8000
EFFICIENCY ØF BDC= 0.0800
EFFICIENCY ØF DIFFUSER= 0.0280
EFFICIENCY ØF SIGNAL ØPTICS= 0.9500
SIGNAL TØ NØISE RATIØ ØF PHØTØDIØDE= 30.0000
RATIØ ØF CHARGING TIME TØ TØTAL READØUT TIME= 0.5000
NUMBER ØF CHANNELS IN READØUT= 1.
*TØTAL READØUT TIME PER HØLØGRAM= 0.6554E-01 SECØNDS
*DISCHARGE TIME= 0.50E-06 SECØNDS

For the set of parameters given, it requires 2.7 watts of laser power to record the hologram and 360 milliwatts of laser power to retrieve the data from the hologram at a data rate of 10^8 bits/second. The details as to the relationship of the laser power to the various parameters have been discussed in Reference 4.

3.1.4 Subroutine XFILM. — Since the analysis of how the film recording parameters influence the system performance was completed during the fourth quarter, we begin our description of Subroutine XFILM with a discussion of some of the fundamental concepts relating to film modeling. The modeling of a recording material can be approached in two ways. In principle the best, but yet most difficult, approach is to start with the basic structure of the recording material and build up a model to explain the different observable parameters of the recording material. This approach was used as early as 1922[5] to study the response of the photographic emulsion. Since then many different models have been proposed for photographic emulsions.[6] These models are adequate to explain the general behavior of the photographic emulsion but yet fail to characterize the precise characteristics of any real photographic emulsion. This implies that the number of parameters used in these models is not large enough to represent all real emulsions. During the second quarter we selected a modified checker board model to derive the relationships among parameters such as the exposure, transmissivity, modulation transfer function, and noise spectrum of the emulsion. In Figure 3.1 we show the T_a vs E curve based on the model and an experimentally derived curve for Kodak 649F. As can be seen, it is not possible to select the values of the parameters of the model to fit the real emulsion over a significant exposure range. It is even more difficult to set up models for phase recording material because little is known about the microscopic structure of the clusters of phase centers that constitute the hologram.

A second approach to this problem is to first measure the observable parameters of the recording material. Then we represent the dependence of these observables on the exposure by functions having a finite number of parameters. From this functional dependence we derive the performance of the recording material. Observable parameters for a recording material are, for example, the diffraction efficiency, the modulation transfer function,

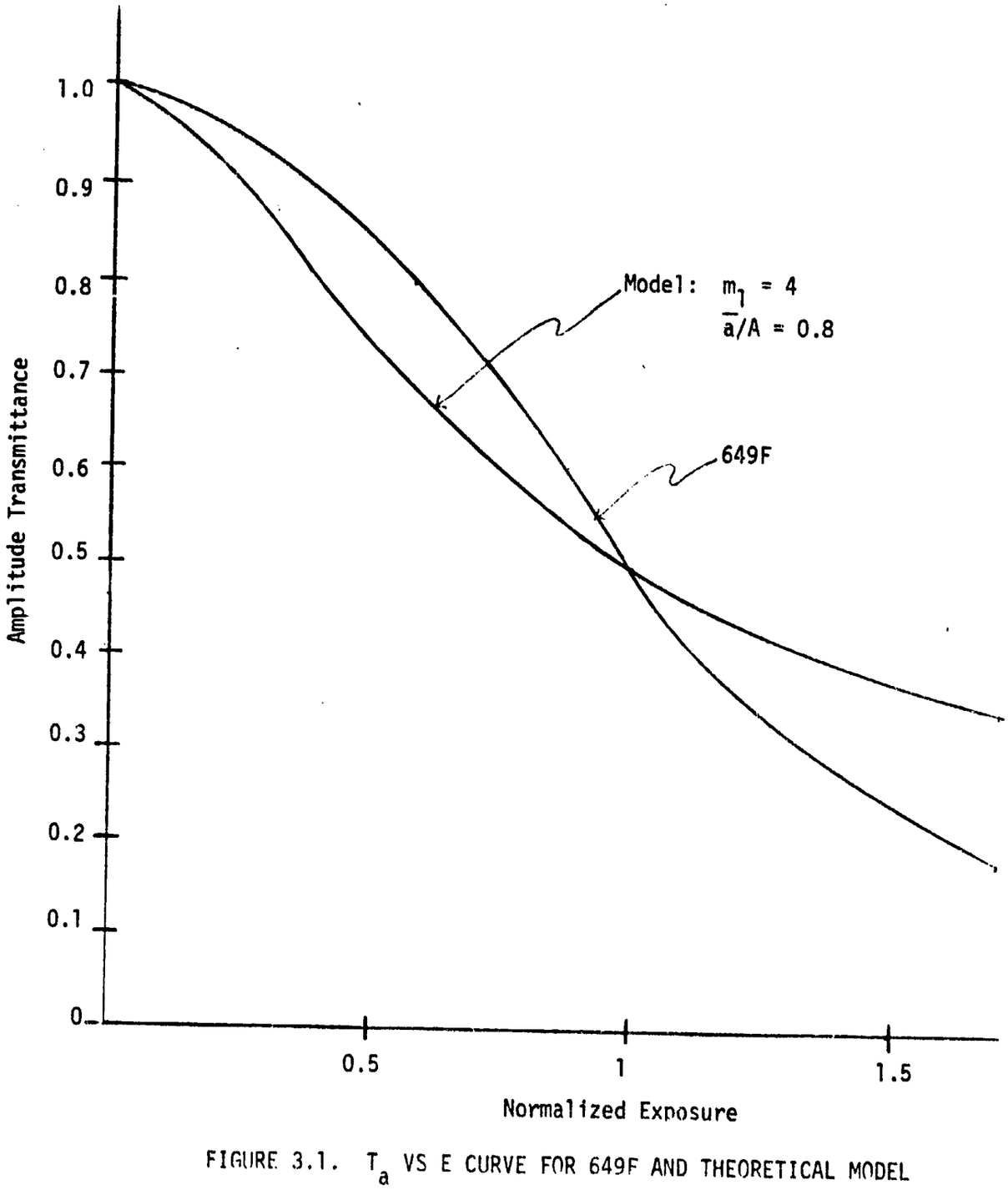

FIGURE 3.1. T_a VS E CURVE FOR 649F AND THEORETICAL MODEL

the transmissivity, and the Wiener spectrum of the scattering of the recording elements. Based on these observable parameters, for example, we found functional relationships that adequately represent the transmittance versus exposure curve for Kodak 649F. The dependence of the transmittance on the exposure is approximated by $1/(1 + (E/E_0)^2)$, where $E_0 \approx 40$ μjoules/cm^2. The Wiener spectrum of the film grain noise is derived from a checkerboard model. Using these formula we can actually determine the performance of the film. We then measured a number of films to study whether they can also be represented by the same model by changing some of the parameters in the model. Figure 3.2 shows the T_a-E curves for some representative emulsions and a curve based on the model. There are enough variations to believe that this model is not sufficiently general.

The approach that we used is, in a way, circuitous because the observables that we measure for the recording material are essentially the performance parameters that we hope to predict for the material. Therefore, we believe that the best method for evaluating the performance of a recording material is to measure the observable parameters and use these observables directly in the system program to predict the performance of the memory. Details of the experimental procedures and techniques can be found in Reference 7. In the following paragraphs we discuss how the observable parameters (discrete data points) can be represented as continuous functions of the independent variable so that the computer program can more efficiently calculate the performance of the memory for all values of the independent variable within a given range.

In holographic applications the recording material can be classified as a thin material or a thick material. This classification is not based only on the physical thickness of the material, since the same material can be regarded as thick or thin depending on how it is used. The criterion for determining the thickness of the recording material is given by a parameter Q defined by Kogelnik[8] as

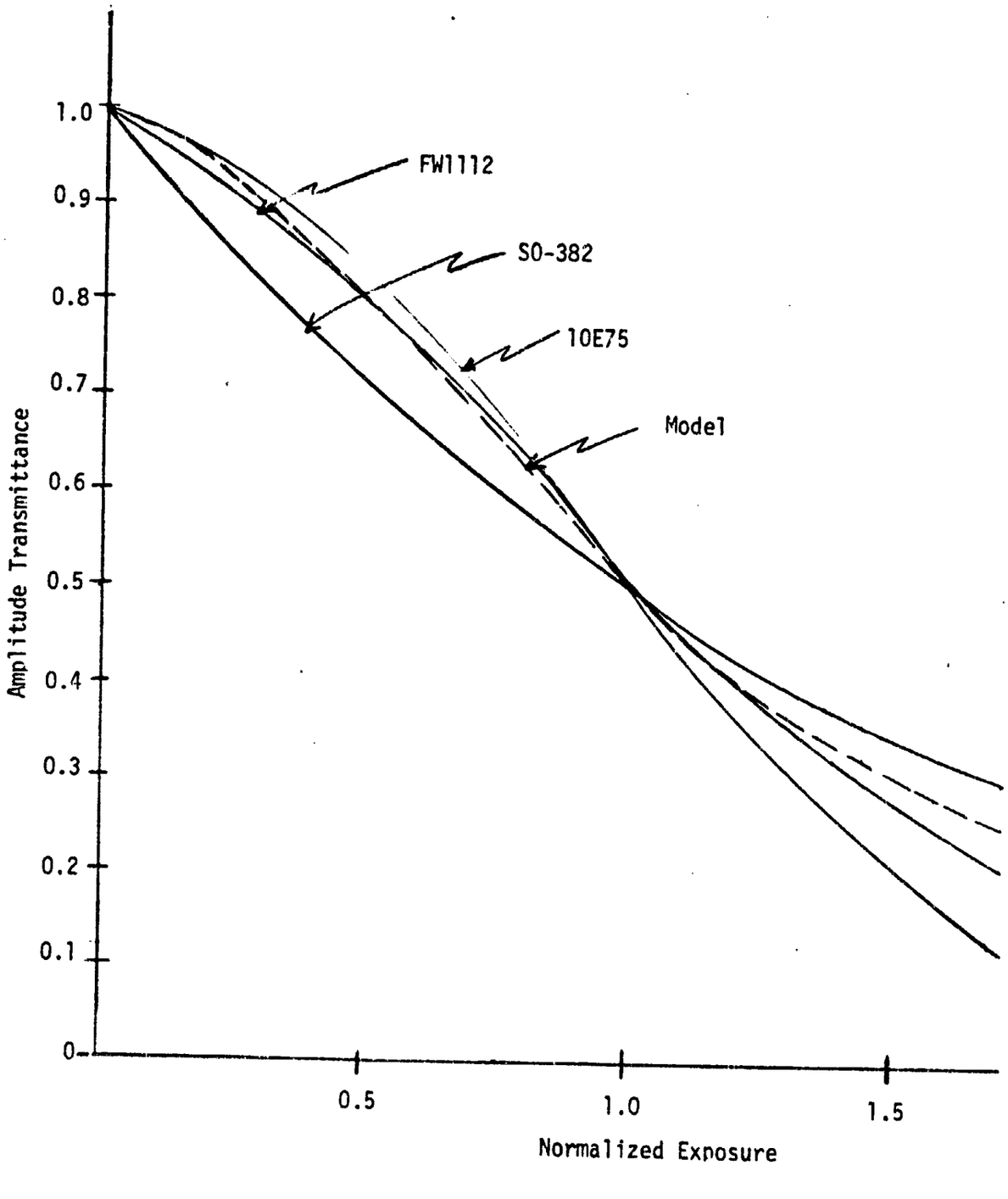

FIGURE 3.2.1 T_a VS E CURVE FOR THEORETICAL MODEL AND FINE-GRAINED FILMS

$$Q = 2\pi\lambda d/n_o\Lambda^2$$

where λ is the wavelength of the laser beam, d is the physical thickness of the material, n_o is the refractive index of the material, and Λ is the spacing between the fringes recorded on the hologram. According to Kogelnik a hologram recorded on a recording material is a thick hologram only when Q is larger than 10. For example, the physical thickness of Kodak 649F emulsion is 16μm. If a hologram is recorded with a 1μm fringe spacing using an He-Ne laser, the parameter Q is approximately 40. Therefore, the hologram recorded on a 16μm emulsion under these conditions is actually a thick hologram. On the other hand, if the fringe spacing Λ is 2.5μm, the hologram will be a thin one. This indicates that we can carry out the experimental study of thin and thick holograms using the same type of recording material as long as we choose the fringe spacing Λ properly.

We performed a series of experiments on the Kodak 649F emulsion, using it both as an absorptive and as a phase recording material. When it is used as phase material we remove the silver in the emulsion and sensitize the relatin with amonium dichromate according to a technique described by Chang[9]. After exposure and development, the resulting hologram has very little absorption; the information is carried as variations in the optical path length in the emulsion. The experimental results are then approximated by equations that form the basis for our film model. The film model is then put in a subroutine program called XFILM.

Before we proceed to explain how the program can be used to investigate the performance of two types of recording material, we shall briefly describe the film model. In studying the characteristics of the Kodak 649F emulsion we found that the performance of any emulsion can be characterized by its T_a-E (the amplitude transmittance versus exposure) curve and the

Wiener spectrum of its grain noise.[10] For the 649F emulsion, the T_a-E curve can be approximated by the function

$$T_a = \frac{1}{1 + (\frac{E}{E_o})^2} ,$$

where E is the exposure and E_o is equal to 40μjoules/cm^2. The Wiener spectrum was measured by Burkhardt[11] and can be approximated by[7]

$$\Phi(f) = 1 - T_a)T_a \exp(-.00248f)10^{-8},$$

where f is the spatial carrier frequency. Based on these two equations we derived the diffraction efficiency and the SNR of the hologram recorded on the emulsion.[10] The diffraction efficiency (in percent) of the hologram is given by

$$DIF = 400\ K\ T_a^2(1 - T_a)^2/(1 + K)^2 ,$$

where K is the reference beam to signal beam ratio. The diffraction efficiency DIF is usually derived for grating holograms. For holograms of more complex objects, the efficiency is slightly lower due to the fluctuation on the modulation and the transmittance of the hologram. The reduction in diffraction efficiency is generally of the order of 60% for highly structured objects. We also showed in Reference 10 that the signal-to-noise ratio SNR is equal to

$$SNR = DIF/\Phi(f)P,$$

where P is the packing density of the hologram in bits per square centimeter.

The relationship given above for diffraction efficiency is valid only for thin holograms ($Q < 10$). For $Q > 10$, the theory of thick holograms shows that the diffraction efficiency is given by

$$DIF = 100\ T_a^2 \sinh^2 [.5\alpha\sqrt{K}/(K+1)]$$

where $\alpha = -2 \cos \theta_B \log_e(T_a)$ and θ_B is the Bragg angle of the recording. Therefore, this relationship will be used to calculate the diffraction efficiency whenever Λ is less than 2.5μm (for any 16μm thick emulsion). In other words, if the carrier frequency of the hologram causes Q to be more than 10, the thick hologram formation will be used to calculate the diffraction efficiency. This set of equations then forms the basis for our film model. This model was found to be adequate for films belonging to the class of higher resolution emulsions. For example, films such as FW1112 also manufactured by Kodak fit our model quite well. But we also found films that cannot be adequately described by the model during our investigation. This procedure shows, nevertheless, the steps that must be taken to measure the observable parameters so that functional relationships can be provided to the subroutine.

The model for the phase material is based on our experimental results for dichromated gelatin emulsions prepared using Chang's technique. We found that over a wide region of exposure the incremental change in the refractive index of the sensitized gelatin is linearly proportional to the exposure. However, if a certain exposure is exceeded, some phenomena within the gelatin makes the performance of the material highly unpredictable. Within the predictable range of exposure, the diffraction efficiency was found to be

$$DIF = 100 \sin^2(Es/\sqrt{K} \cos \theta_B)$$

where E is the exposure in units of microjoules/cm^2 and s is the sensitivity coefficient. This relationship is valid for thick materials ($Q > 10$). However for thin materials ($Q < 10$) the diffraction efficiency is given by

$$DIF = 100\ J_1^2\ (Es/\sqrt{K}),$$

where $J_1(x)$ is the Bessel function of the first kind of order one. In the computer program that calculates the performance of the recording material, the Bessel function is approximated by a polynomial. Therefore, the value of $J_1(x)$ is only accurate for $|x| < 3$. In the program an error message will be printed out whenever $Es/\sqrt{K}$ exceeds 3. For reasonable exposure the values of $Es/\sqrt{K}$ should always be less than 3 and our approximation for $J_1(x)$ is adequate.

The noise mechanism inside that phase material is more complicated than for absorptive materials because the material itself does not contain a significant number of scattering centers. Hence, the degradation in the signal reconstructed from the hologram is primarily caused by the nonlinear characteristics of the material. We measured the signal-to-noise ratio (SNR) of the material using techniques described in Ref. (10) and we found that the signal-to-noise ratio can be approximated by

$$SNR = 3.5\ DIF\ EXP\ (.00248) \times 10^8/P[.5(E/E_o\sqrt{K})^2 + 1]^{1.5}$$

for the particular material cited above. This approximation is based on the general behavior of the SNR and its value relative to Kodak 649F emulsion.

These two film models can be interrogated through the subroutine program XFILM which will be described below.

Subroutine XFILM

The subroutine XFILM is a program for calculating the general characteristics of absorptive and phase material. In using this program we must specify

1. ITYPE - The type of material to be investigated.
   ITYPE = 'PHSE' for phase material and
   ITYPE = 'ABSUR' for absorptive material
2. EX = Exposure in units of microjoules/cm^2. Ex is the exposure due to the reference beam for phase material and EX is the total exposure for absorptive material.
3. REF = Angle in degree subtended by the reference beam and the normal of the hologram.
4. W = Laser wavelength in millimeters.
5. FILM = Packing density of the hologram for the purpose of calculating SNR in bits/cm^2
6. K = reference beam to signal beam ratio.

The following examples will illustrate how the program can be used. The following statement is given to the computer.

```
& INPUT W = .0005, FILM = 1.E6, K = 10
EX = 400, REF = 30, PFILM = .T.&
```

The statement PFILM = .T. tells the main program to call the subroutine XFILM. For input data given above, the printout from the computer is

```
FILM TYPE=ABSØR
DIFFRACTIØN EFFICIENCY=  0.94 percent
SIGNAL TØ NØISE RATIØ=115.93
EXPØSURE =      400.00 MICRØJØULES/CM*CM
REFERENCE TØ SIGNAL BEAM RATIØ= 10.00
PACKING DENSITY=  0.10E+07 BITS/CM*CM
WAVELENGTH=     0.000500 MM
CARRIER FREQUENCY=   1000.0000 LINES/MM
```

If we want to study the phase material, we then type in

```
& INPUT, ITYPE = 'PHASE', EX = 4000 &
```

The following is the printout from the computer.

```
FILM TYPE=PHASE
DIFFRACTIØN EFFICIENCY=  1.55 PERCENT
SIGNAL TØ NØISE RATIØ=442.17
EXPØSURE =      4000.00 MICRØJØULES/CM*CM
REFERENCE TØ SIGNAL BEAM RATIØ= 10.00
PACKING DENSITY=  0.10E+07 BITS/CM*CM
WAVELENGTH=     0.000500 MM
CARRIER FREQUENCY=    1000.0000 LINES/MM
```

Suppose now we want to change the K-ratio to 1. We type in

```
& INPUT K = 1 &.
```

The computer printout is

```
FILM TYPE=PHASE
DIFFRACTIØN EFFICIENCY= 14.83 PERCENT
SIGNAL TØ NØISE RATIØ=170.21
EXPØSURE =    4000.00 MICRØJØULES/CM*CM
REFERENCE TØ SIGNAL BEAM RATIØ=  1.00
PACKING DENSITY= 0.10E+07 BITS/CM*CM
WAVELENGTH=     0.000500 MM
CARRIER FREQUENCY=  1000.0000 LINES/MM
```

As can be seen, by increasing the K-ratio we increase the effect of the intermodulation noise. As a result the signal-to-noise ratio is lower than before.

3.1.5 Conclusions. — It should be noted that the film modeling as used here applies to two particular kinds of phase materials and is based on external measurable parameters. In this sense the modeling and the resulting system equations are consistent with the procedures used in the other three subroutines. For example, in the first subroutine we calculate the focal length of the Fourier transform lens. A lens having the required focal length can be fabricated using various glass types, curvatures, thicknesses, and spacings. These parameters are internal parameters which determine the external parameter of interest (the focal length). In the same sense, a film having a required signal-to-noise ratio can be fabricated by using different grain sizes, quantium efficiencies, and quantum thresholds. These internal parameters affect the external parameters, but in a way that is much less well understood (relative to, say, a lens design), as we noted earlier. In the next section we report on our efforts to characterize the external parameters of the film using the known internal parameters and show why this kind of modeling is inadequate.

A listing of the complete computer program for the system analysis is given on the following pages.

```
00100C  IN USING THE PRØGRAM FØR THE FIRST TIME, YØU MUST SPECIFY
00110C
00120C  (1) THE TØTAL STØRAGE CAPACITY ØF THE SYSTEM -Q2-
00130C
00140C  (2) EITHER
00150C       THE NUMBER ØF BITS PER RØW ØF THE BDC -NI-
00160C      ØR
00170C       THE NUMBER ØF HØLØGRAMS PER RØW ØF THE HØLØGRAM ARRAY -NH-
00180C
00190C  (3) EITHER
 0200C            THE APERTURE RATIØ ØF THE LENS -R-
00210C      ØR
00220C            THE FILM RECØRDING CAPACITY(BITS/CM**2) -FILM-
00230C
00240C  (4) THE APERTURE RATIØ ØF THE HØLØGRAM -S-
00250C      ***ØTHERWISE S=0.5 ***
00260C
00270C  (5) THE TYPES ØF RECØRDING SYSTEM
00280C        FØR NØNIMAGING SYSTEM, SET NØNI=1
00290C        FØR IMAGING SYSTEM,    SET NØNI=0
00300C
00310C  (6) THE MAXIMUM WAVELENGTH USED IN THE SYSTEM (MM) -WM-
00320C      THE ØPERATING WAVELENGTH (MM) -W-
00330C      ***SET W=0, IF YØU WANT W=WM ***
00340C
00350C  (7) THE TRANSIT TIME (MICRØSECØNDS) -T- AND THE FRACTIØNAL
00360C      BANDWIDTH -FB- ØF THE AØBD
00370C      ***ØTHERWISE T=10,  FB=0.35  ***
00380C
00390C  (8) ANGULAR MAGNIFICATIØN ØF THE DEFLECTØR ØPTICS -MA-
00400C      ***ØTHERWISE MA=40  ***
00410C
00420C  (9) THE ENERGY REQUIRED BY EACH ELEMENT ØF THE PDA(JØULES) -UD-
00430C      ***ØTHERWISE UD=3.E-12  ***
00440C
00450C  (10) EXPØSURE SENSITIVITY ØF RECØRDING MATERIAL(JØULES/CM**2)
00460C       -E0-      ;***ØTHERWISE E0=40.E-6  ***
00470C
00480C  (11) REFERENCE-TØ-SIGNAL BEAM RATIØ -K-
00490C       ***ØTHERWISE K=1  ***
00500C
00510C  (12) THE INPUT DATA RATE(BITS/SECØNDS) -VIN-
00520C       THE ØUTPUT DATA RATE(BITS/SECØNDS) -VØUT-
00530C       *** ØTHERWISE VØUT=VIN=1.E6  ***
00540C
00550C  (13) THE EFFICIENCY ØF THE HØLØGRAM -EFH-
00560C       THE EFFICIENCY ØF THE AØBD -EFA-
00570C       THE EFFICIENCY ØF THE DEFLECTØR ØPTICS -EFD0-
00580C       THE EFFICIENCY ØF THE REST ØF THE ØPTICS -EFØ-
00590C       THE EFFICIENCY ØF THE BDC -EFB-
```

```
00600C        THE EFFICIENCY ØF THE DIFFUSER -EFD-
00610C        THE EFFICIENCY ØF THE SIGNAL ØPTICS -EFSØ-
00620C        ***ØTHERWISE
00630C                        EFH=.01
00640C                        EFA=.5
00650C                        EFDØ=.95
00660C                        EFØ=.8
00670C                        EFB=.08
00680C                        EFD=.028
00690C                        EFSØ=.95      *****
00700C
00710C  (14) TYPE ØF RECØRDING MATERIAL-ITYPE-
00720C       ITYPE='PHASE'  ØR ITYPE='ABSØR'
00730C
00740C  (15) EXPØSURE-EX-
00750C
00760C  (16) ANGLE BETWEEN THE REFERENCE BEAM AND THE NØRMAL
00770C       ØF THE HØLØGRAM-REF-
00780C
00790C  (17) PSYST=.TRUE.  ,IF YØU WANT TØ PRINT ØUT THE RESULTS ØF
00800C       THE SYSTEM DESIGN
00810C       ***ØTHERWISE SET PSYST=.FALSE. ***
00820C
00830C  (18) PAØBD=.TRUE.  ,IF YØU WANT TØ PRINT ØUT THE AØBD DATA
00840C       ***ØTHERWISE SET PAØBD=.FALSE.  ***
00850C
00860C  (19) PLASER=.TRUE.  ,IF YØU WANT TØ PRINT ØUT THE LASER PØWERS
00870C       ***ØTHERWISE SET PLASER=.FALSE.  ***
00880C
00890C  (20) PFILM=.TRUE>  ,IF YØU WANT TØ PRINT ØUT FILM DATA
00900C      ***ØTHERWISE SET PFILM=.FALSE.  ***
00910C
00920C       ********************************************************
00930C
00940C       AFTER THE FIRST ITERATIØN, PUT IN ØNLY THØSE PARAMETERS
00950C       THAT YØU WANT TØ CHANGE
00960C
00970C       ********************************************************
00980C
00990C       USE THE FØLLØWING FØRMAT FØR SUPPLYING THE DATA TØ
01000C       THE PRØGRAM
01010C
01020C       &INPUT R=.5,S=.25,W=.000488,Q2=1.E10&
01030C
01040C       ********************************************************
01050C
01060C       TERMINATE THE PRØGRAM AT THE END ØF AN ITERATIØN BY TYPING
01070C
01080C       &INPUT ØUT=.TRUE.&
01090C
```

```
01100C        ********************************************************
01110C
01120C
01130C
01140 REAL M
01150 LØGICAL PFILM,ØUT,PSYST,PLASER,PAØBD
01160 CØMMØN /ØPT/ R,S,Q2,M,NØNI//K,DI,NI,NH,CI,CH,W,WM,FILM,DH
01170&/LAS/PULSE,CM,SNR,AC,UD,EØ,EFA,EFH,EFDØ,EFØ,EFB,EFD,EFSØ,VIN,VØUT
01180 CØMMØN/AØ/T,FB,MA
01190 CØMMØN/FMØD/EX,REF,DIF,ITYPE
01200 NAMELIST /INPUT/R,S,NI,NH,Q2,M,NØNI,W,WM,FILM,T,FB,MA,UD,EØ,
01210&K,EFH,EFA,EFDØ,EFØ,EFB,EFD,EFSØ,VIN,VØUT,PAØBD,PSYST,PLASER,ØUT
01220&,CH,CI, PULSE,CM,SNR,AC,EX,REF,ITYPE,PFILM
01230 TYPE3
01240 3 FØRMAT(' EXECUTIØN',/,/,/)
01250 1 ACCEPT INPUT
01260 IF(ØUT) GØ TØ 2
01270 IF(PSYST) CALL SYST
01280 IF(PAØBD) CALL AØBD
01290 IF(PLASER) CALL LASER
01300 IF(PFILM) CALL XFILM
01310 GØ TØ 1
01320 2 STØP
01330 END
01340C
01350C
01360C
01370C
01380 SUBRØUTINE SYST
01390 REAL M,M1
01400 CØMMØN /ØPT/ R,S,Q2,M,NØNI//K,DI,NI,NH,CI,CH,W,WM,FILM,DH
01410 R2=SQRT(2.)
01420 IF(TFILM.EQ.FILM) FILM=0.
01430 IF(MH.NE.NH) NI=0
01440 IF(MH.EQ.NH) NH=0
01450C
01460C  INITIALIZE THE UNSPECIFIED PARAMETERS
01470C
01480C
01490C  NUMBER ØF HØLØGRAMS PER RØW=NH
01500 IF(NH.EQ.0) NH=1*(SQRT(Q2)/NI+.5)
01510 MH=NH
01520C
01530C  NUMBER ØF BITS PER RØW=NI
01540 IF(NI.EQ.0) NI=1*(SQRT(Q2)/NH+.5)
01550C
01560C  APERTURE RATIØ ØF HØLØGRAM=S
01570 IF(S.E).0) S=.5
01580C
01590C  APERTURE RATIØ ØF LENS=R
```

```
01600 IF(R.EQ.0) R=.5
01610C
01620C  CENTER SPACING/BIT DIAMETER RATI0=CI
01630 IF(CI.EQ.0) CI=1.5
01640C
01650C  CENTER SPACING/H0L0GRAM DIAMETER=CH
01660 IF(CH.EQ.0.) CH=1.5
01670C
01680C  MAXIMUM WAVELENGTH=WM ; 0PERATING WAVELENGTH=W
01690 IF(WM.EQ.0) WM=.0006328
01700 IF(W.EQ.0) W=WM
01710C
01720C  MAGNIFICATI0N=M ;  MAGNIFICATI0N FACT0R=M1
01730 IF(M.EQ.0) M1=1
01740 IF(M.NE.0) M1=M*1./(1.+M)
01750C
01760C  FILM CAPACITY(BITS/CM*CM)=FILM
01770 IF(FILM.NE.0) R=.40*CI*W*SQRT(FILM)/(N0NI+1)
01780C
01790C  N0RMALIZE CH F0R TW0 WAVELENGTH 0PERATI0NS
01800C
01810 CH=CH*WM/W
01820C
01830C  T0TAL ST0RAGE CAPACITY=Q2 ;  Q1=SQRT(2*Q2)
01840C
01850 Q1=SQRT(Q2)*2
01860C
01870C  P0WER 0F THE LENS=XK
01880 XK=R**2*M1/(8.*CI*CH*W*Q1)
01890 IF(N0NI.EQ.1) XK=S*R*.5/(CI*CH*W*Q1)
01900C
01910C  DIAMETER 0F A BIT IN BDC=DI
01920 DI=R/(2*R2*XK*CI*NI)
01930 IF(N0NI.EQ.1) DI=R/(CI*NI*XK*R2)
01940C
01950C  DIAMETER 0F H0L0GRAM
01960 DH=2*W/(DI*XK)
01970C
01980C  IF FILM IS N0T SPECIFIED, CALCULATE FILM
01990C
02000 TFILM=100.*(NI/DH)**2
02010 IF(FILM.EQ.0) FILM=TFILM
02020C
02030C  F0CAL LENGTH 0F LENS=YK=1/XK
02040C
02050 YK=1./XK
02060C
02070C  LENGTH 0F BDC
02080 AI=DI*CI*NI
02090C
```

```
02100C  LENGTH ØF HØLØGRAM ARRAY
02110 AH=DH*CH*NH
02120C
02130C  PRINT ØUT SYSTEM PARAMETERS
02140 IF(NØNI.EQ.0) TYPE10
02150 IF(NØNI.EQ.1) TYPE11
02160 TYPE1,WM,W,Q2,FILM
02170 IF(NØNI.EQ.1) TYPE12,YK
02180 1 FØRMAT(' DESIGN FØR MAXIMUM WAVELENGTH=',F12.8,4H  MM,/,/,
02190&1X,'LASER WAVELENGTH=',F12.8,'  MM',/,/,
02200&' TØTAL CAPACITY ØF THE MEMØRY SYSTEM=',E12.4,' BITS',/,/,
02210&1X,'REQUIRED FILM CAPACITY=',E12.4,'  BITS/CM/CM',/)
02220 IF(NØNI.EQ.0) TYPE3
02230 IF(NØNI.EQ.0) TYPE2,M1,R,YK,XK
02240 2 FØRMAT(1X,'MAGNIFICATIØN FACTØR=-M/(1-M)=',F12.2,/,
02250&1X,'APERTURE RATIØ ØF THE LENS=',F12.2,/,
02260&1X,'FØCAL LENGTH ØF THE LENS=',F12.2,'   MM',/,
02270&1X,'PØWER ØF THE LENS=',F12.6,'  1/MM')
02280 3 FØRMAT(/,/,/,1X,'LENS PARAMETERS',/,/,/)
02290 TYPE4
02300 4 FØRMAT(/,/,/,1X,'BDC PARAMETERS',/,/,/)
02310 IF(NØNI.EQ.1) TYPE5,R
02320 5 FØRMAT(1X,'APERTURE RATIØ ØF BDC=',F12.2)
02330 TYPE6,NI,CI,DI,AI
02340 6 FØRMAT(1X,'NUMBER ØF BITS PER RØW IN BDC=',I6,/,
02350&1X,'CENTER SPACING ØF EACH BIT/BIT DIAMETER=',F12.2,/,
02360&1X,'BIT DIAMETER=',F12.4,'  MM',/,
02370&1X,'LENGTH ØF BDC=',F12.2,'  MM')
02380 TYPE7
02390 7 FØRMAT(/,/,/,1X,'HØLØGRAM ARRAY PARAMETERS',/,/,/)
02400 IF(NØNI.EQ.1) TYPE8,S
02410 8 FØRMAT(1X,'HØLØGRAM LENGTH TØ FØCAL LENGTH RATIØ=',F12.2)
02420 TYPE9,NH,CH,DH,AH
02430 9 FØRMAT(1X,'NUMBER ØF HØLØGRAM IN ØNE RØW ØF THE ARRAY=',I6,/,
02440&1X,'CENTER SPACING ØF EACH HØLØGRAM/HØLØGRAM DIAMETER=',F12.2,/,
02450&1X,'HØLØGRAM DIAMETER=',F12.4,'  MM',/,
02460&1X,'LENGTH ØF HØLØGRAM ARRAY=',F12.2,'  MM',/,/,/)
02470 10 FØRMAT(/,/,10X,'IMAGING SYSTEM',/,/)
02480 11 FØRMAT(/,/,10X,'NØNIMAGING SYSTEM',/,/)
02490 12 FØRMAT(1X,'FØCAL LENGTH ØF THE LENS=',
02500&F12.2,'   MM')
02510 RETURN
02520 END
02530C
02540C
02550C
02560C
02570 SUBRØUTINE AØBD
02580 CØMMØN /AØ/ F,FB,MA//K,DI,NI,NH,CI,CH,W,WM,FILM,DH
02590 DIMENSIØN BA(10),RN(10),RHØ(10),BA(10),DB(10)
```

```
02600 DATA BV/1.55,3.8,3.1,5.97,2.53,2.1 ,7.4,6.,10.3,11./
02610 DATA RN/1.33,1.72,1.92,1.46,1.59,2.6,2.25,1.39,2.6,1.76/
02620 DATA RH0/1.,4.8,6.3,2.2,1.06,7.4,4.7,2.6,4.26,6.95/
02630 BA(1)=.695E-4
02640C
02650C INITIALIZE UNSPECIFIED PARAMETERS
02660C
02670C  FRACTIONAL BANDWIDTH=FB
02680 IF(FB.EQ.0) FB=.35
02690C
02700C  TRANSIT TIME= T (MICROSECONDS)
02710C
02720 IF(T.EQ.0) T=10.
02730C
02740C ANGULAR MAGNIFICATION OF DEFLECTOR OPTICS=MA
02750C
02760 IF(MA.EQ.0) MA=40
02770 IF(FB.EQ.0) FB=.35
02780C BANDWIDTH(MHZ)=2*NUMBER OF HOLOGRAM/TRANSIT TIME(MICROSECOND)
02790C
02800 F1=2*NH*CH/T
02810C
02820C   TIME BANDWIDTH PRODUCT=TRANSIT TIME X BANDSIDTH
02830C
02840 ITBP=2*NH*CH
02850C
02860C  NORMALIZED FRACTIONAL BANDWIDTH
02870C
02880 FB=WM*FB/W
02890C
02900C CENTER FREQUENCY=BANDWIDTH/FRACTIONAL BANDWIDTH
02910C
02920 FC=F1/FB
02930C
02940C FREQUENCY INCREMENT=BANDWIDTH/NUMBER OF HOLOGRAM (KHZ)
02950C
02960 F2=F1/NH*1000.
02970C
02980C PRINT GENERAL INFORMATION ON AOBD
02990C
03000 TYPE1,ITBP,F1,FC,T,FB,NH,F2
03010 1 FORMAT(/,/,/,/,1X,'AOBD PARAMETERS',/,/,/,
03020&' TIME BANDWIDTH PRODUCT=',I10,/,
03030&' BANDWIDTH=',F12.2,'  MHZ',/,
03040&' CENTER FREQUENCY=',F12.2,'  MHZ',/,
03050&' TRANSIT TIME=',F12.2,'  MICROSECOND',/,
03060&' FRACTIONAL BANDWIDTH=',F12.2,/,
03070&' FREQUENCY INCREMENT FOR ',I4,'  BEAMS=',F12.2,'  KHZ',/,/,/)
03080C
03090C COMPUTE AOBD PARAMETERS FOR 10 DIFFERENT MATERIALS
```

```
03100C
03110 TYPE2
03120 2FØRMAT('     NUMBER CØDES FØR MATERIALS',/,/,
03130&'  1= WATER',/,
03140&'  2= DENSE FLINT GLASS',/,
03150&'  3= EXTRA-DENSE FLINT GLASS',/,
03160&'  4= FUSED QUARTZ',/,
03170&'  5= PØLYSTYRENE',/,
03180&'  6= KRS-5',/,
03190&'  7= LITHIUM NIØBATE',/,
03200&'  8= LITHIUM FLUØRIDE',/,
03210&'  9= RUTILE',/,
03220&' 10= SAPHIRE',/,/,/,/,/)
03230C
03240C
03250 TYPE3
03260 3 FØRMAT(' MATERIAL',3X,'BRAGG',4X,'ANGULAR INCREMENT',3X,
03270&'LENGTH',3X,'PØWER',/,
03280&10X,'(MRADIAN)',6X,'MRADIAN)',8X,'(MM)',4X,'(WATT)',/)
03290 DØ 4 I=1,10
03300 XRN=(RN(I)**3+RN(I)-2./RN(I))**2
03310C
03320C PØWER REQUIRED TØ PRØDUCE 100% DIFFRACTIØN EFFICIENCY
03330C
03340 PT=4.5*10.**12*RHØ(I)*(.001*W)**2*BV(I)**3/XRN
03350C
03360C CELL LENGTH
03370C
03380 D=BV(I)*T
03390C
03400C DISTANCE BETWEEN EXIT PUPIL AND HØLØGRAM
03410C
03420 DB(I)=.5*D*DH/W/MA
03430C
03440C BRAGG ANGLE=WAVELENGTH*CENTER FREQUENCY/VELØCITY
03450C
03460 BRAGG=500.*W*FC/BV(I)
03470C
03480C ANGULAR INCREMENT BETWEEN SPØT
03490C
03500 DBRAG=2*FB*BRAGG/NH
03510C
03520C
03530C
03540 TYPE5,I,BRAGG,DBRAG,D,PT
03550 4 CØNTINUE
03560 5 FØRMAT(4X,I2,6X,F5.2,9X,F6.4,9X,F6.1,2X,F6.2)
03570 TYPE6,MA
03580 6 FØRMAT(/,/,/,' PARAMETERS FØR BEAM DEFLECTØR ØPTICS',/,/,
03590&' ANGULAR MAGNIFICATIØN=',I10,/,/,/,
```

```
03600&' D=DISTANCE BETWEEN EXIT PUPIL AND HØLØGRAM',//,/,
03610&' MATERIAL',21X,'D (MM)')
03620 DØ 7 I=1,10
03630 7 TYPE8,I,DB(I)
03640 8 FØRMAT(4X,I2,15X,F12.2)
03650 TYPE9
03660 9 FØRMAT(/,/,/)
03670 RETURN
03680 END
03690C
03700C
03710C
03720C
03730 SUBRØUTINE LASER
03740 CØMMØN /LAS/PULSE,CM,SNR,AC,UD,EØ,EFA,EFH,EFDØ,EFØ,EFB,EFD,EFSØ,
03750&VIN,VØUT//K,DI,NI,NH,CI,CH,W,WM,FILM,DH
03760C
03770C  INITIALIZE UNSPECIFIED PARAMETERS
03780C
03790C   DETECTIVITY ØF EACH PHØTØDIØDES=UD
03800 IF(UD.EQ.0) UD=1.E10
03810C
03820C  NUMBER ØF CHANNELS USED IN READØUT=CM
03830 IF(CM.EQ.0) CM=1.
03840C
03850C  RATIØ ØF CHARGING TIME FØR THE DETECTØR TØ READØUT IIME=AC
03860 IF(AC.EQ.0) AC=.5
03870C
03880C   SIGNAL TØ NØISE RATIØ FØR THE DETECTØR=SNR
03890 IF(SNR.EQ.0) SNR=30.
03900C
03910C  EFFICIENCY ØF AØBD=EFA
03920 IF(EFA.EQ.0) EFA=.5
03930C
03940C  EFFICIENCY ØF HØLØGRAM=EFH
03950 IF(EFH.EQ.0) EFH=.01
03960C
03970C  EFFICIENCY ØF BEAM DEFLECTØR ØPTICS=EFDØ
03980 IF(EFDØ.EQ.0) EFDØ=1.
03990C
04000C  EFFICIENCY ØF THE REST ØF THE ØPTICS=EFØ
04010  IF(EFØ.EQ.0) EFØ=.8
04020C
04030C  EFFICIENCY ØF BDC=EFB
04040 IF(EFB.EQ.0) EFB=.08
04050C
04060C  EFFICIENCY ØF DIFFUSER=EFD
04070 IF(EFD.EQ.0) EFD=.028
04080C
04090C  EFFICIENCY ØF SIGNAL ØPTICS=EFSØ
```

```
04100 IF(EFS0.EQ.0) EFS0=.95
04110C
04120C  REFERENCE BEAM T0 SIGNAL BEAM RATI0=K
04130 IF(K.EQ.0) K=1
04140C
04150C  EXP0SURE REQUIRED F0R THE REC0RDING MATERIAL=E0 (J0ULES/CM**2)
04160 IF(E0.EQ.0) E0=40.E-6
04170C
04180C  INPUT DATA RATE=VIN (BITS/SEC0ND)
04190 IF(VIN.EQ.0) VIN=1.E6
04200C
04210C  0UTPUT DATA RATE=V0UT (BITS/SEC0ND)
04220 IF(V0UT.EQ.0) V0UT=1.E6
04230C
04240C  CALCULATE READIN LASER P0WER
04250C
04260C  GLAN-AIR PRISM SPLITTING RATI0=XM
04270 XM=K*EFB*EFD*EFS0/(EFD0+K*EFB*EFD*EFS0)
04280C
04290C  READIN AVERAGE P0WER
04300 PIN=K*E0*VIN/(K+1.)/(FILM*XM*EFA*EF0*EFD0)
04310C
04320C  CALCULATE READ0UT LASER P0WER
04330C   PULSE WIDTH 0F PULSE LASER=PULSE
04340 IF(PULSE.NE.0) AC=PULSE/(NI*NI)*V0UT
04350C
04360C  T0TAL READ0UT TIME PER H0L0GRAM=TT
04370 TT=NI*NI/V0UT
04380 TCD=CM*(1.-AC)/V0UT
04390C
04400 P01=SQRT(V0UT/AC)*SNR*0.1*DI*NI/(UD*EFH*EFA*EFD0*EF0)
04410 P03=NI*P01/SQRT(CM)
04420 P02=P01*AC
04430 P04=P03*AC
04440C
04450C  PRINT 0UT DATA
04460C
04470 TYPE1,PIN,P01,P02,P03,P04,VIN,J0UT
04480 TYPE2,UD,E0,K,XM,EFA,EFH,EFD0,EF0,EFB
04490&,EFD,EFS0,SNR,AC,CM,TT
04500C
04510 1 F0RMAT(/,',/,/,/,1X,'       LASER P0WER REQUIREMENTS',/,/,/,/,
04520&' AVERAGE READIN P0WER=',E12.2,'  WATTS',/,
04530&' PEAK READ0UT P0WER(CHARGE STORAGE)=',E12.2,' WATTS',/,
04540&' AVERAGE READ 0UT P0WER(CHARGE ST0RAGE)=',E12.2,' WATTS',/,
04550&' PEAK READ0UT P0WER(CW)=',E12.2,' WATTS',/,
04560&' AVERAGE READ0UT P0WER(CW)=',E12.2,' WATTS',/,
04570&'  INPUT DATA RATE=',E12.2,'  BITS/SECOND',/,
04580&' 0UTPUT DATA RATE=',E12.2,'  BITS/SECOND')
04590 2 F0RMAT(' DETECTIVITY 0F PHT0DI0DE=',E12.2,/,
```

```
04600&' EXPØSURE SENSITY ØF RECØRDING MATERIAL=',E12.2,'  JØULES/CM**2'
04610&,/,' REFERENCE TØ SIGNAL BEAM RATIØ=',I10,/,
04620&' GLAN-AIR PRISM SPLITTING RATIØ=',F12.4,/,
04630&' EFFICIENCY ØF AØBD=',F12.4,/,
04640&' EFFICIENCY ØF HØLØGRAM=',F12.4,/,
04650&' EFFICIENCY ØF DEFLECTØR ØPTICS=',F12.4,/,
04660&' EFFICIENCY ØF ØTHER ØPTICS=',F12.4,/,
04670&' EFFICIENCY ØF BDC=',F12.4,/,
04680&' EFFICIENCY ØF DIFFUSER=',F12.4,/,
04690&' EFFICIENCY ØF SIGNAL ØPTICS=',F12.4,/,
04700&' SIGNAL TØ NØISE RATIØ ØF PHØTØDIØDE=',F12.4,/,
04710&' RATIØ ØF CHARGING TIME TØ TØTAL READØUT TIME=',F12.4,/,
04720&' NUMBER ØF CHANNELS IN READØUT=',F12.0,/,
04730&' TØTAL READØUT TIME PER HØLØGRAM=',E12.4,' SECØNDS')
04740 TYPE3,TCD
04750 3 FØRMAT(' DISCHARGE TIME=',E12.2,' SECØNDS',/,/,/)
04760 RETURN
04770 END
04780 SUBRØUTINE XFILM
04790 REAL NØISE
04800 CØMMØN /FMØD/EX,REF,DIF,ITYPE
04810&//K,DI,NI,NH,CI,CH,W,WM,FILM,DH
04820 IR='PHASE'
04830 FR=SIN(REF/180*3.1415927)/W
04840 TYPE8
04850 8 FØRMAT(/,/,/,/,'       FILM MØDEL',/,/,/)
04860 IF(ITYPE.EQ.IR) GØ TØ 4
04870C
04880C
04890C  ABSØRPTIVE MATERIAL
04900C
04910C
04920 TA=1./(1.+(EX/400.)**2)
04930 NØISE=TA*(1-TA)*EXP(-.00248*FR)*1.E-8/0.529/(1-0.529)
04940 IF(FR.LT.500.) GØ TØ 1
04950 UT=-2*CØS(REF/360.*3.1415927)*ALØG(TA)
04960 DIF=100*(TA*SINH(.5*UT/(K+1)*SQRT(K*1.)))**2
04970 GØ TØ 2
04980 1 DIF=400*K*TA**2*(1-TA)**2/(1+K)**2
04990 2 SNR=DIF/(NØISE*FILM)
05000 TYPE3,ITYPE,DIF,SNR,EX,K,FILM,W,FR
05010 3 FØRMAT(1X,'FILM TYPE=',A5,
05020&/,' DIFFRACTIØN EFFICIENCY=',F6.2,' PERCENT',/,
05030&' SIGNAL TØ NØISE RATIO=',F6.2,/,
05040&' EXPØSURE =',F12.2,' MICRØJØULES/CM*CM',/,
05050&' REFERENCE TØ SIGNAL BEAM RATIØ=',F6.2,/,
05060&' PACKING DENSITY=',E10.2,' BITS/CM*CM',/,
05070&' WAVELENGTH=',F12.6,' MM',/,
05080&' CARRIER FREQUENCY=',F12.4,' LINES/MM',/)
05090 GØ TØ 6
```

```
05100C
05110C
05120C  PHASE MATERIAL
05130C
05140C
05150 4 S=.9546984E-4
05160 NØISE=EXP(-.00248*FR)*1.E-8
05170 IF(FR.GT.500)
05180& DIF=100*(SIN(EX*S/SQRT(K*1.)/CØS(REF/360.*3.1415927)))**2
05190 IF(FR.LE.500) DIF=100*(BESJ(S*EX/SQRT(1.*K)))**2
05200 ER=S*EX/SQRT(K*1.)
05210 IF((FR.LE.500).AND.(ER.GT.3)) TYPE7
05220 7 FØRMAT(' PRØGRAM ERRØR,PLEASE CØNSULT MANUAL')
05230 E0=400
05240 IF(FR.LE.500) E0=2000.
05250 SNR=3.5*DIF/NØISE/FILM/(.5*(EX/SQRT(1.*K)/E0)**2+1)**1.5
05260 TYPE3,ITYPE,DIF,SNR,EX,K,FILM,W,FR
05270 6 RETURN
05280 END
05290 FUNCTIØN BESJ(X)
05300 DIMENSIØN C(6)
05310 DØUBLE PRECISIØN  Y,Y1,BESJ
05320 DATA C/-.56249985,.21093573,-.03954289,.00443319,
05330&-.00031761,.00001109/
05340 Y=(X/3.)**2
05350 Y1=1.
05360 BESJ=.5
05370 DØ 1 I=1,6
05380 Y1=Y*Y1
05390 BESJ=BESJ+C(I)*Y1
05400 1 CØNTINUE
05410 BESJ=X*BESJ
05420 RETURN
05430 END
```

3.2 Model for Thin Recording Materials

We developed a model for photographic film which is the most commonly used thin absorptive recording material. This model can be used to account for the characteristics of photographic films used in holographic applications. The model is based on the following four assumptions and with reference to Figure 3.3:

(1) The photosensitive grains in the film emulsion are circular,

(2) An unsensitized grain can be found in each cell with probability p,

(3) The probability that a grain has an area between a_0 and $a_0 + \Delta a$ is $p_a(a_0)\Delta a$,

(4) When the grains are exposed to light for a total exposure E, the probability that a grain with area a_0 is sensitized and becomes opaque after chemical development is $P(0|a_0, E)$.

The photosensitive grains in a real emulsion generally have many different shapes. However, because the grains also have random orientations, the shape of the grain averaged over an ensemble of films will appear to be circular; this observation suggests the first assumption. In the second assumption the probability p determines the population density of the unsensitized grains can be shown to be equal to p/A where A is the area of the cell shown in Figure 3.3. The third assumption allows the film grains to have a distribution of sizes. Later on when we use these assumptions to derive the characteristics of the film we assume that the probability of having overlapping grains is zero or extremely small. The probability $P(0|a_0,E)$, in the last assumption, is used to control the sensitivity of each grain during exposure.

In the following sections we shall use these assumptions to derive the amplitude transmittance versus exposure (T_a-E) curve, the diffraction efficiency (DE), the Wiener spectrum $\Phi(u,v)$ of the film grain noise, and the modulation transfer function (MTF) of the photographic film M(u,v).

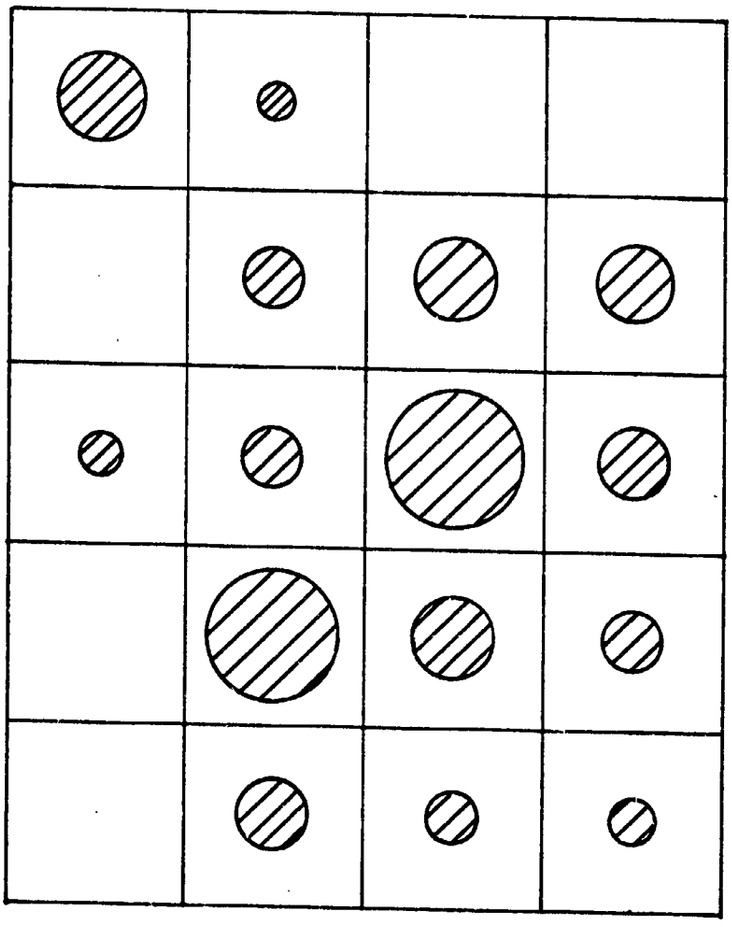

FIGURE 3.3. Film Model

3.2.1 Amplitude Transmittance Versus Exposure Curve. — From the sketch shown in Figure 3.3, we can represent the amplitude transmittance of a film sample which has been exposed and developed by

$$t(x,y) = 1 - \sum_{n=1}^{N} \sum_{m=1}^{N} \xi(a_{nm})\, w(x-nd,\, y-md;\, a_{nm}),$$

where $\xi(a)$ is a random variable which has values 1 or 0 with probabilities $q = pP(0|a,E)\, p_a(a)\Delta a$ and $1-q$. The probability q is equal to the probability that a cell contains an opaque grain with area a. The function $w(x,y;\, a)$ which represents the circular grains is given by

$$w(x,y;\, a) = \begin{cases} 1 & \text{for } \pi(x^2 + y^2) \leq a; \\ 0 & \text{otherwise .} \end{cases}$$

The constant d is the center spacing between cells. The average spatial transmittance of the film sample is equal to

$$t = \frac{1}{N^2 A} \iint t(x,y)\, dxdy \qquad (3\text{-}3)$$

$$= 1 - \frac{1}{N^2 A} \sum_{n=1}^{N} \sum_{m=1}^{N} \xi(a_{nm})\; a_{nm} \;,$$

where $A = d^2$. Because $t(x,y)$ is binary, the average transmittance t is both the amplitude transmittance and the intensity transmittance. The transmittance t can be measured experimentally. Now we shall average t over an ensemble of film samples. The ensemble average of t is given by

$$\langle t \rangle = 1 - \frac{1}{N^2 A} \sum_{n=1}^{N} \sum_{m=1}^{N} \int_0^\infty a_{nm} pP(0|a_{nm},E) \; p_a(a_{nm}) \, da_{nm}. \qquad (3\text{-}4)$$

Since $\{a_{nm}\}$ have the same statistical properties, we can write t as

$$\langle t \rangle = 1 - \frac{p}{A} \int_0^\infty a \, p(0|a,E) \, p_a(a) \, da \; . \qquad (3\text{-}5)$$

Suppose that $p_a(a) = \delta(a-A)$ and $P(0|a,E) = 1$. We find that $\langle t \rangle = 1 - p$ which is the same as the result obtained by O'Neil[12] using the checkerboard model. Because the intensity transmittance is the same as the amplitude transmittance for a binary film model, the density of the exposed film is equal to

$$D = -\log \langle t \rangle \qquad (3\text{-}6)$$

In holography the film amplitude transmittance function is used instead of the film density because the systems are linear in light amplitudes. However, for phase type material the phase retardation of the light wave will be proportional to a function similar to D in Eq. (3-6).

The exposure E influences the average amplitude transmittance $\langle t \rangle$ through $P(0|a,E)$. An analytical expression of the probability $P(0|a,E)$ as a function of the exposure E and grain size a has been developed by Silberstein in 1922[5]. Since his theory is pertinent to our film modeling,

we shall briefly discuss his derivation of $P(0|a,E)$. According to Silberstein's theory, if a grain is to be developed, it must absorb a certain minimum number of photons which will depend on the wavelength of the exposure and may also change from grain to grain. In any case it is necessary to describe the sensitivity of the grain by two numbers; (1) the probability ε that a photon incident on a grain is absorbed by that grain, and (2) the minimum number, m, of absorbed photons required to make a grain developable. The numbers ε and m are often referred to as the quantum efficiency and the quantum threshold respectively. With the usual assumption of Poisson distributed photon arrivals, the probability that a grain with known sensitivity parameters (ε,m) becomes opaque during development is given by

$$P(0|a,E) = \sum_{k=m}^{\infty} \frac{1}{k!} (\varepsilon E a \lambda/hc)^k \exp[-\varepsilon E a \lambda/hc]$$

$$= 1 - \sum_{k=0}^{m-1} \frac{1}{k!} (\varepsilon E a \lambda/hc)^k \exp[-\varepsilon E a \lambda/hc] \qquad (3\text{-}7)$$

where h is the Plank's constant, λ is the wavelength of the exposure radiation, and c is the speed of light.

In order to further develop an analytical expression for <t>, we need to know the probability density function $p_a(a)$. It was found that the distribution of the grain size can be approximated by a log-normal distribution[13]. However, for our model we assume that $p_a(a)$ has the form

$$p_a(a) = \frac{1}{\bar{a}} \exp(-\frac{a}{\bar{a}}) \qquad (3\text{-}8)$$

where $\bar{a}$ is the average grain size. For a > 0 the exponential distribution can also be a good approximation for the grain size distribution. By substituting Eqs. (3-7) and (3-8) into Eq. (3-5) and integrating, we get

$$\langle t \rangle = 1 - \frac{\bar{pa}}{A} + \sum_{k=0}^{m-1} \frac{\bar{a}p(k+1)}{A} \frac{E^k}{\left(\frac{\varepsilon\lambda}{hc}\right)^2 \left(\bar{a}E + \frac{hc}{\varepsilon\lambda}\right)^{k+2}} \quad . \tag{3-9}$$

We can find the average transmittance for two limiting cases. For E = 0, we can show that $\langle t \rangle = 1$ and for $E = \infty$, the average transmittance $\langle t \rangle$ approaches $1 - \frac{Pa}{A}$. If all the cells inside the emulsion contain a grain before exposure (i.e., p = 1) and $\bar{a} = A$, the average transmittance for extremely long exposure will be 0. Therefore, the amplitude transmittance versus exposure characteristics of the film can be completely specified by (1) the population density p, (2) the average area of the grains $\bar{a}$, (3) the quantum efficiency ε, and (4) the quantum threshold m.

3.2.2 Diffraction Efficiency. — Another parameter of interest in holography is the diffraction efficiency of the recording material. The diffraction efficiency of a hologram is proportional to the square of the normalized slope of the T_a-E curve. The normalized slope η of the T_a-E curve is defined as $E\frac{d\langle t \rangle}{dE}$. Using our previous results the normalized slope of the T_a-E curve is equal to

$$\eta = \sum_{k=1}^{m-1} \frac{\bar{a}p(k+1)}{A} \frac{E^k \left(\frac{khc}{\lambda\varepsilon} - 2\bar{a}E\right)}{\left(\frac{\lambda\varepsilon}{hc}\right)^2 \left(aE + \frac{hc}{\lambda\varepsilon}\right)^{k+3}} - \frac{2\bar{ap}}{A} \frac{E}{\left(aE + \frac{hc}{\lambda\varepsilon}\right)^3} \tag{3-10}$$

and the diffraction efficiency is proportional to

$$DE = \eta^2 \tag{3-11}$$

29

3.2.3 Wiener Spectrum of Film Grain Noise. — The random distribution of the film grain inside the emulsion causes the transmitted light to scatter. The measure of the scattering caused by the film grain is provided by the Wiener spectrum defined as

$$\Phi(u,v) = \left\langle \left| \iint \left[t(x,y) - \langle t(x,y) \rangle \right] e^{-j2(ux+uy)} \, dxdy \right|^2 \right\rangle, \qquad (3\text{-}12)$$

where $\langle\ \rangle$ indicates an ensemble average over the random variable a and $\langle t(x,y) \rangle$ is the average transmittance function. For a given film sample, $\langle t(x,y) \rangle$ is the average transmittance of the film sample at (x,y). The film grain noise is a fluctuation of the amplitude transmittance about its average transmittance. The Wiener spectrum $\Phi(u,v)$ can be written as

$$\Phi(u,v) = \frac{1}{N^2 A} \left\langle \left| \sum_{n=1}^{N} \sum_{m=1}^{N} \left[\langle \xi(a_{nm}) \rangle - \xi(a_{nm}) \right] \right.\right.$$

$$\left.\left. \iint w(x-nd;\ y-md;\ a_{nm}) e^{-j2\pi(ux+uy)} \, dxdy \right|^2 \right\rangle$$

$$= \frac{1}{N^2 A} \left\langle \left| \sum_{n=1}^{N} \sum_{m=1}^{N} a_{nm} \left[\langle \xi(a_{nm}) \rangle - \xi(a_{nm}) \right] \right.\right.$$

$$\left.\left. \frac{J_1(2\sqrt{\pi a_{nm}}\,\omega)}{\omega\sqrt{\pi a_{nm}}} \, e^{-j2\pi(mdu+ndv)} \right|^2 \right\rangle, \qquad (3\text{-}13)$$

where $\omega = \sqrt{u^2 + v^2}$ and $J_1(x)$ is the Bessel function of the first kind, of order one. Now we shall carry out the ensemble average over the variable ξ.

Because the grains in each cell are statistically independent and have the same probability density, the cross terms in the summations vanishes and we obtain

$$\Phi(\omega) = \frac{1}{\pi A_\omega^2} \langle a[\xi(a) - \langle \xi(a) \rangle]^2 \; J_1^2 (2\sqrt{\pi a}\omega) \rangle \qquad 3\text{-}14)$$

When we carry out the ensemble average over the random variable a, the Wiener spectrum $\Phi(u,v)$ becomes

$$\Phi(\omega) = \frac{p}{\pi A_\omega^2} \int_0^\infty a J_1^2 (2\sqrt{\pi a}\omega) \quad P(0|a,E) \; [1-pP(0|a,E)] \; p_a(a) \; da \qquad (3\text{-}15)$$

We shall not attempt to substitute $P(0|a,E)$ and $p_a(a)$ into Eq. (3-12) to find an expression in closed form for $\Phi(\omega)$. When we test this film model, we should compute $\Phi(\omega)$ numerically using a digital computer. In order to check the accuracy of the expression for $\Phi(\omega)$ we assume again that $p_a(a) = \delta(a-A)$ and $P(0|a,E) = 1$. With such assumption the Wiener spectrum is

$$\Phi(\omega) = Ap(1-p) \frac{J_1^2 (2\sqrt{\pi A}\omega)}{\pi \omega^2 A} \qquad (3\text{-}16)$$

This result is the same as that predicted by the checkerboard model with circular grains.

3.2.4 Modulation Transfer Function (MTF). — Using this film model we can also derive the dependence of modulation transfer function of the film on the different film parameters. Suppose that we expose the film using a light beam which app7oximates a two-dimensional Dirac delta function. The impulse response of the film according to the film model will take the form

$$m(x,y) = \xi(a) * w(x,y;\, a) \quad .$$

The modulation transfer function M(u,v) is the modulus of the Fourier transform of m(x,y). Therefore, M(u,v) is equal to

$$M(u,v) = \xi(a) \left| \iint w(x,y;\, a)\, e^{-j2(ux+uy)}\, dxdy \right| \qquad (3\text{-}17)$$

$$= a\xi(a) \left| J_1(2\sqrt{\pi a}\omega)/\omega\sqrt{\pi a} \right| \quad ,$$

where $\omega^2 = u^2 + v^2$.

The ensemble average of M(u,v) is

$$\langle M(u,v)\rangle = p \int_0^\infty aP(0|a,E)\, p_a(a) \left| \frac{J_1(2\sqrt{\pi a}\omega)}{\sqrt{\pi a}\omega} \right| da \cdot \qquad (3\text{-}18)$$

Another transfer function of interest is the intensity transfer function which is equal to $M^2(u,v)$. The ensemble average of $M^2(u,v)$ can be shown to be equal to

$$\langle M^2(u,v)\rangle = p \int_0^\infty a^2 P(0|a,E)\; p_a(a)\, \frac{J_1^{\,2}\,(2\sqrt{\pi a}\omega)}{\omega^2 \pi a}\; da \,. \qquad (3\text{-}19)$$

3.1.5 Conclusion. — This simple model is useful in helping us to partially understand the dependence of the observable parameters of the film on its microscopic structures. For example, in Eq. (3-7) we observe that the exposure sensitivity of the film is dependent upon the grain size, the quantum efficiency of the grain, and the quantum threshold required

for development. We can make a film more sensitive to exposure by using larger grains. However, from Eq. (3-19) we find that the larger grains produce poorer resolving power for the film. This type of trade off for the different properties of photographs is common in a real emulsion. For instance, Kodak 649F has a fine grain but a low exposure sensitivity; a film such as Tri-X has high exposure sensitivity but lower resolving power.

As noted in Section 3.2, this kind of model is not adequate for our purposes because it is not general enough to take into account the variations of the quantum efficiency and quantum threshold from grain to grain. Moreover in a real emulsion the silver halide grains are distributed in the volume of the emulsion instead of the surface as in the model. The best method for evaluating the performance of a recording material is still to measure the observable parameters directly and to use these in the system program.

4
MAJOR COMPONENTS

The major components supplied on this contract are (1) two lasers, one emitting light in the blue or green and the other emitting light in the red, (2) an x-y orthogonal acousto-optic beam deflector (AOBD), (3) a block data composer (BDC), (4) a read/write hologram array and a read-only array, (5) a photodetector array (PDA), and (6) a controller and the required drive and synchronizing electronics. In the following sections we report on the results obtained during the contract period in each area.

4.1 Lasers

Based on expected photodetector array sensitivities of 20 nw/bit or less and the expected optical and hologram efficiencies, we calculated that we would need approximately 60-70 mw of output power from the longer wavelength laser and 250-280 mw of output power from the shorter wavelength laser. Also, in order to adequately demonstrate multiple hologram storage at each location, we want to maximize the difference in wavelength between the two lasers. We decided therefore to select a He-Ne laser (632.8 nm) and an argon laser (488 or 514.5 nm) for use in the memory system.

The Spectra-Physics Model 125 He-Ne laser has set a standard for high power output at 6328Å; it also is highly reliable and has good amplitude stability. We specified that the delivered laser shall produce at least 75 mw of power (which is often achieved) and, at our special request, an output beam that is linearly polarized to one part in ten thousand. The high degree of polarization is desirable to maximize the performance

of the polarizing beamsplitter used to adjust the reference-to-signal beam intensity ratio. The delivered laser met all the specifications and was incorporated into the memory system in the second quarter.

We purchased a Coherent Radiation Laboratories Model 52G to complete the laser specification and procurement requirements; this argon laser is rated at two watts multimode, multiline. In single frequency TEM_{00} operation, it is expected that at least 280 mw of power will be available at 488 nm. Wavelength selection is by means of a thermally compensated prism-reflector mechanism. Single mode (longitudinal) operation will be obtained using a Cervit^{R} spaced etalon. Our experience indicates that this type of etalon eliminates mode hopping and, to a large extent, amplitude fluctuations. Insertion loss of the etalon is about 6 dB. The Model 52G will operate with plasma tube currents less than 25 amperes. This, together with a graphite bore structure, should yield an extended period of uninterrupted operation.

We received the Coherent Radiation Model 52G argon laser in the second quarter. We detected an incorrect tube pressure on the laser pressure meter when the unit was first operated. During shipment the glass near the tube seal developed a crack allowing the tube to reach atmospheric pressure. Coherent Radiation promptly replaced the tube. The laser then operated with a multimode, multiline power output well over the two watts

specification. After we installed the Cervit etalon and the Brewster prism wavelength selector, we measured the single wavelength, single longitudinal mode power available at the major spectral lines operating at plasma tube currents of 20, 25, and 30 amperes.

	20a	25a	30a
514.5 nm	272 mw	480 mw	670 mw
496.5 nm	58 mw	102 mw	158 mw
488.0 nm	224 mw	390 mw	565 mw
476.5 nm	78 mw	140 mw	202 mw
457.9 nm	18 mw	34 mw	49 mw

Operation with the plasma current below the maximum rating will extend the operating life of the tube. Operation at 488 nm with 25 ampere plasma current provides 390 mw of power which should be adequate for the system.

As pointed out in Section 2, the delivered photodetector array has significantly less sensitivity than we expected, based on our initial tests; this problem is discussed in detail in Section 4.5. The reduced sensitivity (approximately a factor of 10) meant that our laser power requirements increased by a factor of 10. During the fourth quarter we therefore replaced the SP-125 He-Ne laser with a CRL Model 52 krypton laser.

The CRL Model 52 krypton laser is characterized by its high output power in the red part of the visible spectrum, especially at 647.1 nm. At this wavelength, using a standard flat rear reflector with a boradband dielectric coating, about 250 mw of TEM_{00}, multimode power is emitted. We have replaced the infinite radius rear reflector with a 3 meter radius mirror which is dielectric coated for maximum power at 647.1 nm. With this modification more than 400 mw of TEM_{00} multimode power can be obtained.

To insure the recording of high quality holograms, the laser must not only oscillate in the fundamental spatial mode (TEM_{00}) but also in a single temporal mode, i.e., in a single frequency. Single frequency operation of the laser is obtained by means of an uncoated glass etalon. Because the transmission properties of the etalon depend both on its position relative to the plasma tube axis and its temperature, we added a temperature-controlled oven to increase single frequency stability. The oven maintains the etalon at about 40°C to within ±.01°C. Mode-hopping is eliminated and, in addition, amplitude stability is greatly enhanced. Typically, about 40 percent of multimode power is converted into single frequency power. As the plasma tube ages, this percentage will generally decrease.

Periodic maintainance is required for optimum performance from a krypton laser. The gain of the 647.1 nm line, for example, is not high even though high power is obtained once oscillation is initiated. A closed laser, operated in a reasonably clean, environmentally controlled area, should not require maintainance more often than once every two weeks. Under less favorable environmental conditions, maintanance may be required weekly or more often.

Laser maintainance primarily involves cleaning the optical surfaces. The main cause of power loss and erratic laser operation is dirty Brewster windows. The Brewster windows should be cleaned with reagent grade methyl alcohol and a soft lens tissue. Laser mirrors and the internal wavelength selecting prism are the next most common cause of power loss. They should be cleaned in a similar manner to the Brewster windows. Also, it should be noted that krypton laser mirrors are soft dielectric coated. They are easily damaged by rough handling or cleaning, high relative humidity, and extended exposure to ultraviolet radiation. Damage to the mirrors is detected not only by a decline in power but also by difficulty in obtaining oscillation at certain wavelengths, especially, 647.1 nm.

4.2 Acousto-Optic Beam Deflector

The reference and readout beam addresses in the holographic memory are controlled by a two-dimensional acousto-optic beam deflector (AOBD). The AOBD operates as a Bragg-mode deflector and produces x and y angular variations of an incident laser beam by the application of different frequencies to each of two independent transducers. The AOBD output beams are angularly magnified by the beam deflector optics and projected onto the hologram plane as 1 mm diameter beams.

In Reference 2 we analyzed the angular stability and repeatability requirements for the AOBD given the geometry of the test bed system. The angular stability during the recording operation is found by determining the maximum allowable angular change that will cause the carrier frequency fringe pattern to shift by 1/10 of a fringe spacing. The result of this analysis showed that an angular stability, at the hologram plane, of ±0.144 milliradians is required. Since the beam deflector optics have an angular magnification of approximately 16, this requirement means that the AOBD must be stable (over the exposure time) to ±0.09 milliradian.

A second stability requirement arises from the need to keep the reconstructed bit pattern fixed on the photodetector array. In Reference 1 we analyzed one beam deflector optics approach in which the reference and readout beams were collimated and nearly parallel. Based on this system, we found that the AOBD must be stable to ±0.057 milliradian. Later, in Reference 2, we proposed an alternative beam deflector concept in which the reference and readout beams are not collimated, but originate from a source plane that is a finite distance from the hologram plane. The reference and readout beams therefore have a spherical instead of a plane wavefront. Angular stability is, therefore, no longer based on keeping

tne bit pattern fixed on the photodetector array, but on the requirement that the readout beam is not displaced more than ±10% of the hologram size. Since we use a three Rayleigh resolution criterion between adjacent holograms (for the 20 x 20 array) and since the deflection angle between holograms with the preset cell is 0.14 milliradians, this requirement means that the AOBD stability must be at least ±0.144/(10)(1.5) = 0.096 milliradians.

Both requirements on the angular stability are about equal; yet the requirement is easily met using modest drive electronics. If we convert the angular stability requirement to a fractional frequency tolerance, we find that the drive electronics must be stable to ±0.1%.

We began fabrication of an AOBD using water as the interactive medium. We selected the water cell approach because there were, at that time, no commercially available cells that met all our requirements. Our efforts to fabricate the water cell are documented in References 1, 3 and 14. Although we were successful in meeting most of the design goals, we were not completely successful in perfecting our mounting techniques and we still experienced problems with thermal heating of the water. Nevertheless, we did record and reconstruct holograms using a water cell. In the third quarter an AOBD became available that met all the design goals; we therefore purchased a Datalite AOBD for use in the system. In the remainder of this section we discuss the operating parameters of this cell and its associated drive electronics.

The primary requirements on the AOBD deflection system are:

(1) to deflect the laser beam over arrays of 5 x 5 and 20 x 20 hologram positions, offset at 30° to the normal; each beam diameter to be 1 mm,

(2) to operate over a wavelength range from 488 to 647.1 nm, and

(3) to operate with an overall frequency stability of ±0.1%.

Other design goals are that the diffraction efficiency should be 50% for the x-y combination (70% per cell) at the center frequency and a time-bandwidth product of 160 per cell.

The Datalite deflector and associated drive electronics used in the system were built to meet the specifications. The nominal access time of the cell is 4 μsec and the nominal frequency bandwidth is 40 MHz which meets the requirement of a time-bandwidth product of 160. For the smaller 20 x 20 and 5 x 5 arrays it is not necessary to use the full time-bandwidth product of the cell. We chose, therefore, to use a bandwidth at 488 nm which ensures that we have no more than 1.5 dB loss at the edge hologram position (3 dB) at the corners and which gives an average of three Rayleigh resolution performance between positions in the 20 x 20 array and an average of 12 Rayleigh resolution performance for the 5 x 5 array.

4.2.1 Fundamental Relationships. — Table 4.1 shows the incremental angles between adjacent spots and the incremental frequencies needed to generate them. The relationships between these values is a function of the AOBD, as expressed by the Bragg equation, and the geometry of the optics. The relevant expressions used to generate the values listed in the table are as follows:

(a) $\Delta\theta = \frac{\Delta f \lambda}{V}$,

where $\Delta\theta$ is the incremental angle at the exit pupil of the AOBD, Δf is the incremental frequency, λ is the wavelength of the laser beam, and V is the acoustic velocity in the medium;

(b) $\Delta\theta_{488} = \Delta\theta_{647.1}$,
that is, identical spacings for both wavelengths;

TABLE 4.1. AOBD DEFLECTION PARAMETERS

	X DEFLECTION			Y DEFLECTION		
	Incremental Deflection Angle in 'x' ($\Delta\theta_x \pm .01$)MR	* ($\Delta F_x \pm 0.7$)MHz	Rayleigh Resolution R	Incremental Deflection Angle in 'y' ($\Delta\theta_y \pm .01$)MR	* ($\Delta f_y \pm 0.7$)MHz	Rayleigh Resolution R
20 x 20 Array 4880A°	0.12	0.866	3.3	0.14	1.000	3.8
20 x 20 Array 6471A°	0.12	0.654	2.5	0.14	0.755	2.9
5 x 5 Array 4880A°	0.48	3.464	13.2	0.56	4.000	15.2
5 x 5 Array 6471A°	0.48	2.616	10	0.56	3.020	11.6

*All tolerances on incremental deflection angle and incremental frequency are a function primarily of the stability of the frequency of the drive electronics which is specified as better than 0.1% over 10°C temperature range.

(c) $R = \frac{\Delta f}{40\ MHz}$,

where R is the number of Rayleigh resolutions between spots;

(d) $\Delta\theta_x = \Delta\theta_y \cos\theta$,

where θ is the offset angle (30°), $\Delta\theta_x$ is the incremental angle in the x-direction and $\Delta\theta_y$ is the incremental angle in the y-direction; and

(e) $\Delta\theta_{5 \times 5} = 4\Delta\theta_{20 \times 20}$,

where $\Delta\theta_{5 \times 5}$ is the incremental angle for the 5 x 5 array and $\Delta\theta_{20 \times 20}$ is the incremental angle for the 20 x 20 array.

4.2.2 Optical Efficiency. — The overall optical efficiency η_o of the AOBD may be defined as the percentage of incident light that is diffracted into the required order, i.e., the first order X and first order Y. It may be further broken down into the following product:

$$\eta_o = \eta_{oc} \cdot \eta_{1x} \cdot \eta_{1y}$$

where η_{oc} is the efficiency of the optics within the cell and is the percentage of light transmitted with no R.F. applied.

η_{1x} is the first order diffraction efficiency in X

η_{1y} is the first order diffraction efficiency in Y.

Both η_{1x} and η_{1y} are functions of Bragg angle and R-F drive power. Bragg angle adjustments on the AOBD are provided which should not be wavelength dependent, but are. They may be set to optimize either wavelength c.

somewhere in between to give good Bragg diffraction at both wavelengths. R-F power is controllable from the front panel of the AOBD electronics and again is a compromize for the two wavelengths. One watt of R-F power is optimum for 647.1 nm whereas 0.5 watts is all that is needed for 488.0 nm. With both Bragg and R-F power level controls at optimum setting for 647.1 nm, the following efficiencies were recorded at center frequency:

at 6471 $\eta_{oc} = 70\%$, $\eta_{1x} = 70\%$, $\eta_{1y} = 70\%$

$$\eta_o = (70\%)^3 = 35\%$$

at 4880 $\eta_{oc} = 50\%$, $\eta_{1x} = 70\%$, $\eta_{1y} = 70\%$

giving $\eta_o = 50/100 \times 70/100 \times 70/100 = 25\%$.

4.2.3 Bragg Angle Adjustments. — As already described, a Bragg-angle adjustment exists on each cell but there are also fine adjustments. To operate at all, the beam entering the AOBD should be nearly axial, in which case the beam should also leave the AOBD axially. Thus, provided the AOBD is horizontal, a horizontal incident beam will be diffracted. This setup procedure results in a close to optimum efficiency, but to maximize the efficiency it has been found necessary to move the beam off-axis slightly. To facilitate this the AOBD is mounted on an adjustable stand which can be oriented finely in three dimensions to maximize the Bragg angle. Only then should the fine adjustments on the cell body be adjusted. The orientation controls on the stand and the fine Bragg controls are essentially independent.

If the Bragg angle is optimized as described above in one wavelength, it should be nearly optimum at the other wavelength. To maximize efficiency at the second wavelength, independent fine adjustments must

made to the incoming beam so that none of the previous adjustments for the first wavelength are disturbed.

4.2.4 AOBD Electronics. — The flexibility of the electronics has enabled effectively continuous frequency control over the entire operating frequency range of the AOBD (50 - 90 MHz). It is therefore possible to completely program the different frequency increments listed in Table 4.1. It is also possible to change those values at some future time if operation at different optical wavelengths is required, or if the size or scale of the hologram array is altered.

Frequency control is obtained by controlling a voltage to a voltage controlled oscillator (VCO) which is heavily temperature compensated (Fig. 4.1). Temperature compensation is accomplished by means of a compensation current which is detected by a thermister bridge in the VCO package. The amount of compensation required to stabilize the VCO output frequency is linear to a first order approximation. Forced cooling of the electronics further helps reduce temperature effects.

Figure 4.2 is a calibration of the VCO. It will be seen that the characteristic is not linear so that equal frequency increments are generated by unequal voltage increments. This necessitates a look-up table in the computer to store a set of calibration numbers for the particular array of frequencies to be generated.

The R-F power is controlled by the D.C. voltage fed to the power amplifiers. Control is achieved by varying the gain of the transistors in the amplifiers. This method of control is particularly useful here since there is no interaction between frequency and voltage.

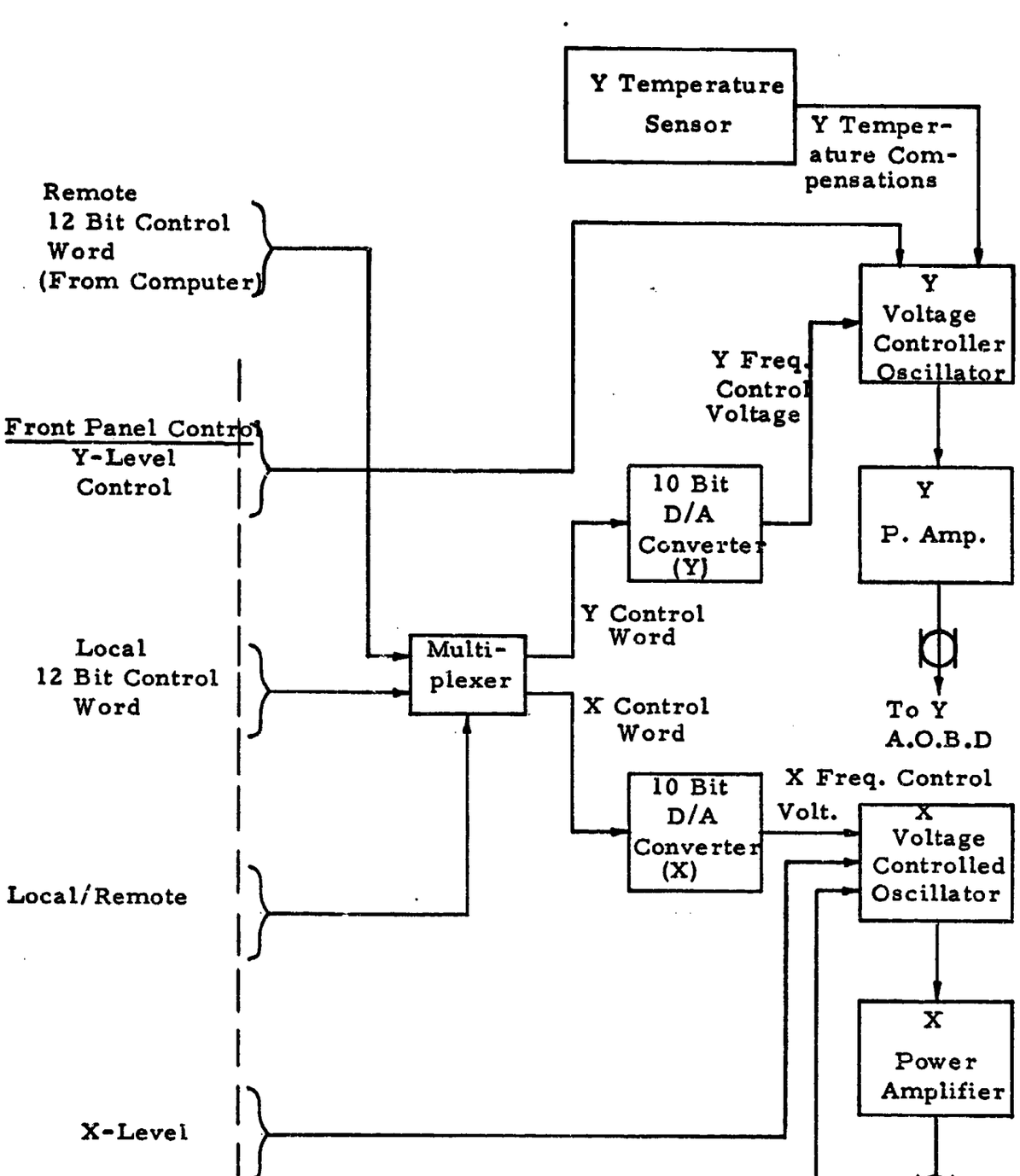

FIGURE 4.1 ELECTRONIC DRIVE CIRCUITRY

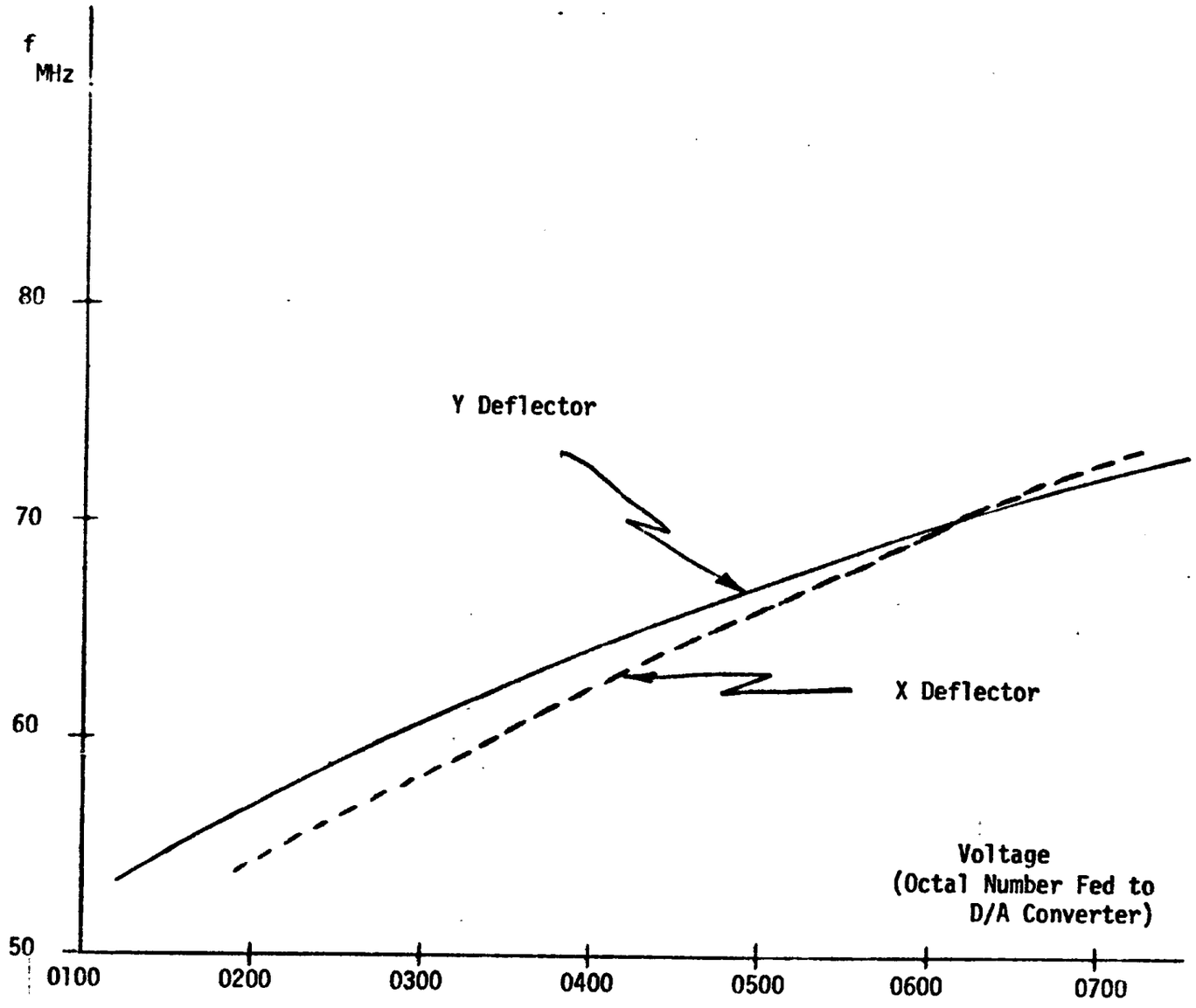

FIGURE 4.2. FREQUENCY/VOLTAGE CALIBRATION FOR VCO'S

Any future attempt to linearize the voltage-frequency characteristic and increase the stability of the oscillator would involve a complete phase-locked loop with an elaborate count-down chain if any degree of flexibility is to be maintained. A worthwhile excercise would be to close-loop the VCO with a photo-diode array placed at the hologram array. The photo-diode array could sense the exact position of the reference beam and feed back any connecting voltages required to correct beam position errors. Such a system would have to be time shared such that the AOBD electronics were only phase-locked while a hologram was not being usefully addressed. The advantages of such a system would be that all beam variations due to the lasers and mirrors as well as the AOBD could be eliminated together.

4.2.5 Time-Bandwidth Product. — In Reference 1 we derived expressions for the time-bandwidth product of an AOBD. The basic relationships are that the total included deflection angle θ is given by

$$\theta = \frac{\lambda f}{V} \quad ,$$

where λ is the wavelength, f is the total electrical bandwidth, and V is the velocity of the acoustic wave in the medium. The minimum resolvable angle, for Rayleigh resolution, is

$$\theta_{min} = \lambda/D \quad ,$$

where D is the length of the cell normal to the optical axis. The number of resolvable elements is then

$$n = \frac{\theta}{\theta_{min}} = \frac{D}{V} f ,$$

Since D/V is equal to the transit time τ of the acoustic wave, we can say that $n = f\tau$ which is equal to the time-bandwidth product of the cell.

For the spots to be well resolved, we require that each spot be double Rayleigh resolved so that $\bar{N} = n/2$. One of the requirements on the AOBD is that it produce $\bar{N} = 80$ addressable positions so that the time-bandwidth product must be equal to 160. The Datalite cell has a manufacturers quoted transit time of 4 μsec and a bandwidth of 40 MHz (50-90 MHz) so that the advertized time-bandwidth product is 160 as desired.

This analysis is incomplete, however, because it does not fully account for the performance of the cell in terms of the diffraction efficiency as a function of spot position. We discussed this question in Reference 1 with respect to the parameters associated with the water cell. Unfortunately, the theory that relates the diffraction efficiency to the spot position is not fully developed and rests, to a large extent, on empirically derived formulae.

The diffraction efficiency of the AOBD is determined not only by the fractional bandwidth of the drive electronics, but is also a function of several parameters of the interactive medium. The medium for the Datalite cell is glass, but the exact values of its parameters such as refractive index, velocity of propagation, specific density, modulus of elasticity, and so forth are not known. It is impossible, therefore, to theoretically compute the performance of the cell with respect to its diffraction efficiency at all spot positions.

We have measured the performance of the cell when operated in the 80 x 80 spot position mode and have found that the diffdaction efficiency at the corner spot position is an average of 6 dB down from the central position at 488 nm and an average of 8 dB down at 647.1 nm. There is some lack of symmetry in the response which is due to some residual impedence mismatch in the transducers and, perhaps, to a slight mismatch in Bragg angle. Figure 4.3 demonstrates that the cell is capable of producing 80 x 80 double Rayleigh resolved spots. Four spots are shown in the outer corner of the array along with a central group of nine spots. The variation in the intensity of the central nine spots is due to variations in exposure times; our shutter mechanism is not consistent in the 1-3 millisecond range. Since the outer four spots are weaker than the central spots, different exposures were used at the corners than in the center so that the relative intensity differences are not evident in the photograph.

4.2.6 Conclusions. — The performance of the Datalite cell meets all of our design goals except, perhaps, for overall efficiency. Some improvement might be expected by using better coatings on the glass surfaces within the cell (several lenses in addition to the glass interactive medium) to minimize reflection losses. The coatings in the present cell are broadband coatings needed to operate the cell over a range of wavelengths; for any one wavelength significant improvements could be made. It is also likely that the cylindrical optics within the cell contribute to the light losses. A summary of the AOBD operating parameters is given in Table 4.2.

FIGURE 4.3. 80 X 80 ARRAY FORMAT (DOUBLE RAYLEIGH RESOLUTION)

TABLE 4.2. SPECIFICATION AOBD

1.	The diffracted beams emerge from each cell as a plane wave to within $\lambda/8$ at 5500A°, for all positions of the diffracted beam.		
2.	The temperature coefficient of the diffraction angle is less than 2×10^{-5} per °C.		
3.	The input impedance is 50Ω.		
4.	Diffraction efficiency is > 50% per cell.		
5.	The frequency increment between adjacent beams (at exit pupil of AOBD with 3 Rayleigh criteria)	λ = 488 nm 1 MHz	λ = 6471 755 KHz
6.	The angular increment between adjacent beams (at exit pupil of AOBD with 3 Rayleigh criteria)	0.14 MR.	0.14 MR.
7.	Bandwidth (for 20 angular positions)	20 MHz	15.1 MHz
8.	Deflection Resolution 100 positions (Rayleigh criteria)		
9.	Aperture	1.2 cm x 1.2 cm	
10.	Laser Wavelength	4300Å to 7000Å (System optimized for the wavelength range of 4880A° to 5145A°)	
11.	Deflection Angular Range	16 minutes at 5145°	
12.	Optical Transmission	50% nominal	
13.	Optical Noise	All spurious components within any single resolution element are 20 dB down	
14.	Output Beam Characteristic	1.2 x 1.2 cm diffraction limited beam	
15.	Random Access Time	4 microseconds maximum	

It will be noticed that only a (4μs x 20 MHz), 80 time bandwidth product is used (in the 20 x 20 array) out of the total capability of 160 time bandwidth product.

4.3 Block Data Composer

The digital data is entered into the holographic memory system by a block data composer (BDC). The BDC provides a two-dimensional spatial array of successive blocks of data extracted from the input data stream. Each array of data spatially modulates a laser beam which is directed to a storage location where it interferes with the reference beam to form a hologram.

In this section, the BDC goals are reviewed and related to results achieved during the contract. The PLZT material characteristics[15-20] are summarized and tabulated, and various BDC configurations are discussed. Experimental data obtained during the program is presented and related to BDC performance. A description of the solution to the half-select disturbance problem is presented and techniques for strain-biasing PLZT are reviewed. Transparent electrode material tradeoffs for the BDC and PLZT polishing and contrast uniformity are considered. Other fabrication details, including photoresist-etching techniques, are discussed and the BDC electronics are described. The more significant problem areas are reviewed and conclusions and recommendations are given. In Appendix A the details of electro-optic light modulation with PLZT are presented; experimental data is included to relate the polarization hysteresis and strain-bias properties to switchable birefringence and light intensity modulation.

4.3.1 Review of Goals for BDC Performance. — Constraints imposed by the overall holographic memory system and by the various devices within the system affect the BDC configuration and the BDC performance requirements[2,21,22]. For example, the center spacings between BDC elements and the element dimensions are related to the size of optical components, to lens focal lengths, and to the size of each hologram in the memory. Also, the BDC must register with the PDA during readout. The contrast of the BDC affects the signal-to-noise ratio of the output data which is, in turn, related to bit error rates. The optical efficiency of the BDC affects the laser output power requirements. The switching speed of the light modulating elements in the BDC affects the input data rates at which the system can function. Switching voltage requirements impact the drive circuitry and power supply designs. These and other considerations strongly affected the particular configuration and performance goals established for the BDC at the inception of this program. The goals are summarized below:

(1) Number of light modulating elements: 128 x 128 = 16,384.
(2) Center spacing between elements: 0.15 to 0.25 mm.
(3) Overall dimensions: 20 x 20 mm to 40 x 40 mm.
(4) Input bit rate: 10^6 bits/sec.
(5) Contrast: 100/1.
(6) Optical efficiency: 30 percent.
(7) Peak switching voltage: $\leq$300 volts.
(8) Effects of wavelength changes: Maximum change in efficiency and contrast of 30 percent between 488.0 nm and 632.8 nm.

In addition to numerous smaller devices, two full 32 x 24 element BDC's with 10 x 1.25 mm center spacings and a total size of 30 x 32 mm were fabricated and tested. With the special drive electronics assembled

for the 32 x 24 element BDC's, rows of 32 elements were composed at the rate of one row every 120 μsec for an effective input data rate of $(32/20) \times 10^6 = 0.27 \times 10^6$ bits/sec. Each row of the 128 x 128 BDC is switchable at the same rate; the effective data rate achievable is therefore $(128/120) \times 10^6 = 1.07 \times 10^6$ bits/sec. Higher rates are achievable with increased switching voltages (higher than the 75 and 150 volt levels used for the above tests).

Local contrasts of 50/1 have been measured in the 32 x 24 element BDC's after optimizing the strain-bias level for the region of the array under investigation. Thickness variations in the PLZT plate cause the optimum strain-bias levels to vary over the full BDC aperture. The contrast can be uniformly optimized over regions in which thickness variations are less than about ±2 microns. Typical profiles of polished PLZT plates indicate thickness variations in excess of ±10 microns over the full aperture. The problem of polishing PLZT plates to achieve more uniform thickness has been considered in detail on this program. Improvements have been made but more effort is required to completely solve the uniform thickness problem.

The optical efficiency of modulating elements in the Plexiglas-PLZT structure with chromium-gold (Cr-Au) transparent electrodes (80 to 100Å of gold) is typically 10 to 15 percent (excluding the absorption losses in the polarization analyzer). Tests with small 5 x 5 element BDC's with sputtered indium oxide electrodes indicate that optical efficiencies in excess of 40 percent can be achieved.

Switching voltages for the 32 x 24 element BDC's are typically 75 to 150 volts. The drive circuitry design permits levels up to 150 and 300 volts. For a particular PLZT plate thickness b and level of strain-bias S_x, the switching voltages may vary by ±7 percent without significantly altering contrast or optical efficiency.

One of the 32 x 24 element BDC's has been operated at both 514.5 nm and 632.8 nm. Scattering in the PLZT is stronger at the shorter wavelength; both contrast and optical efficiency are reduced by less than 30 percent. The optimum strain-bias level changes with wavelength but optimum conditions can be achieved (over local regions of a full array) for both wavelengths.

An important feature not noted in the performance goals is the need for the BDC to be immune from half-select disturbance effects as data is switched into successive rows during block composition. Early in the program these effects were considered to be a problem, but the switching procedure was modified and this problem was solved. Half-select disturbances do not degrade contrast and are therefore no longer a problem.

In summary, the bit rate, switching voltage, and wavelength range goals have been met or exceeded. Contrasts of 50/1 have been achieved over subregions of the full 32 x 24 element BDC aperture; non-uniformity of contrast resulting from PLZT thickness variations is a problem which requires further investigation. Optical efficiencies (excluding analyzer losses) of 10 to 15 percent are typical with Cr-Au electrodes and can be increased to 40 percent with indium oxide electrodes. Half-select disturbance effects are not a problem.

4.3.2 Characteristics of Strain-Biased PLZT. — The control media for the BDC is PLZT. In this section we describe this material and review the parameters of PLZT that are important for BDC applications. In Table 4.3 we summarize these parameters.

TABLE 4.3

SELECTED PHYSICAL, ELECTRICAL, AND OPTICAL PROPERTIES OF PLZT-7/65/35

Bulk density:	ρ_b = 7.85 g/cc (99.9% of theoretical)
Curie temperature:	$T_c \approx 150°C$
Relative dielectric constant:	$\varepsilon_r \approx 1600$
Coercive electric field:	$E_c \approx 8.0$ KV/cm
Maximum remanent polarization (saturated; electric field OFF):	$P_R \approx 35$ μcoul/cm^2
Optical transmission range:	0.4 to 6 microns
Index of refraction:	n_o = 2.5 at 0.633 microns
Net birefringence at P_R (unstrained):	$\overline{n_R} \approx 0.011$
Practical optical Transmissivity (with In_2O_3 electrodes):	T > 0.4
Absorption and scattering losses in polished plates about 0.1 mm thick:	A + S < 0.1
Contrast ratios	
Maximum achieved (Sandia):	R_{cm} = 4000
Practical range (32 x 24 BDC):	$10 \leq R_{cB} \leq 50$
Lifetime (with In_2O_3 electrodes):	$N_L > 10^9$ cycles
Half-wave voltage and rise-time in linear EO mode (driving from P_R; with strain; no memory):	$V_{\lambda/2}$ < 350 volts; τ_r < 0.1 μsec
Typical half-wave ON voltage range and switching time with long-term memory:	35 Volts ≤ + V_1 ≤ 100 Volts; τ_s < 100 μsec
Typical half-wave OFF voltage range and switching time with long-term memory:	70 Volts ≤ -V_2 ≤ 200 Volts; τ_s < 100 μsec
Typical thickness range for half-wave memory switching with strain-bias and transparent electrodes:	0.075 mm ≤ b ≤ 0.150 mm
Typical linear strain required to cause fracture:	$S_x \geq 4 \times 10^{-3}$ mm/mm (tension)

PLZT is an acronym which refers to a new class of electro-optic materials.[15-20] These electro-optic materials are transparent ferroelectric ceramics formed by hot-pressing mixtures of lead zirconate ($PbZrO_3$), lead titanate ($PbTiO_3$), and lanthanum oxide (La_2O_3). The designation PLZT-x/y/z is used, where x denotes the atomic percent of La present and y/z is the $PbZrO_3/PbTiO_3$ ratio obtained after hot-pressing. The most promising compositions for BDC applications are those with x in the 6 to 8 percent range and y/z in the 62/38 to 66/34 range.[15,16] In this range of compositions, PLZT has both memory and high optical efficiency. Of these, the particular composition PLZT-7/65/35 has been extensively tested during this program. All experimental data presented in this report were obtained with PLZT-7/65/35. Hereafter we will use the acronym PLZT to refer only to PLZT-7/65/35, unless otherwise specified.

This class of polycrystalline materials is the first known to have strong electro-optic effects along with excellent optical transmissivity in the visible and near infrared (0.4 to 6 microns). Absorption and scattering losses are under 10 percent with plate glass quality surface finishes in plates as thick as 0.25 mm.[15] Uncoated polished plates have transmissivities in the 55 to 65 percent range. Reflection losses are in excess of 30 percent because of the high index of refraction ($n_o \simeq 2.5$). The same plates exhibit increased transmissivities when tin doped indium oxide (In_2O_3:SnO_2) transparent electrodes of the proper thickness ($\simeq$0.3 microns) are applied. The In_2O_3:SnO_2 also acts as an antireflection coating (an index matching medium).

The electro-optic effects are related to the electrical polarizability of the ferroelectric ceramics. Changes in electrical polarization fields are accompanied by changes in birefringence.[15,16] In the mode of operation of particular interest, the PLZT is strain-biased and can be electrically

switched within a range of birefringence states by voltage pulses of controlled amplitude and duration. The voltage is applied between transpartent electrodes on opposite faces of the PLZT to produce an electric field parallel to the light propagation direction. Any state change induced in this manner can persist indefinitely with zero applied voltage and zero power dissipation; this long-term memory property is extremely important for achieving memory in the BDC. Subsequent voltage pulses of equal or lower amplitude and the same polarity will not disturb ON and OFF states. A detailed discussion of techniques for exploiting this inherent memory property for display applications is presented in Appendix A.

Procedures for more uniformly hot-pressing PLZT and for reducing scattering levels by oxygenation have been developed during the past year. The material which is now obtained from Honeywell has notably lower scattering levels than earlier batches. Further improvements are anticipated in PLZT properties.

An interesting development has recently been reported.[27] PLZT can be hot-pressed such that domain (or crystallite) sizes are in the 4 to 8 micron range as opposed to the materials we presently use which have 1 to 3 micron domain sizes. The material with larger domains can be switched with longitudinal electric fields (no strain-bias required) between low and high scattering level states. Contrasts of 1000/1 have been observed and no polarizers are required. Memory still exists and switching fields are similar to those for the smaller domain materials. Optimum thicknesses are around b = 250 microns, which is much easier to achieve with uniformity than b = 100 microns. Element center spacings of 250 microns may be difficult to achieve, but 500 microns appears reasonable. This modulating concept will be carefully investigated in subsequent phases of the BDC development program.

4.3.3 BDC Configurations. — The BDC's to be tested in the holographic memory system consist of a polished PLZT plate, transparent and opaque Cr-Au electrodes, and a Plexiglas substrate. The polished PLZT plates are 50 to 56 mm in diameter and have a nominal thickness of $b = 0.11$ mm. The modulating elements are defined by the intersections of transparent Cr-Au electrode strips which are deposited on the two PLZT faces. Thicker opaque Cr-Au electrodes are deposited on the PLZT at the ends of each transparent electrode to mate with Cr-Au electrodes on the Plexiglas.

Photographs of one of the 32 x 24 element BDC's are shown in Figure 4.4. The upper photograph is a close-up of the PLZT-Plexiglas structure with all electrodes evident. The PLZT plate is 50 mm in diameter. The "Radiation" symbol is a letterhead on the white paper under the device. Small circular tabs of thick Cr-Au can be seen at the ends of the transparent electrode strips on the upper PLZT face. Similar tabs are on the lower face; they are mated to the thick Cr-Au electrodes on the Plexiglas which extend under the PLZT. The tabs on the upper face are connected to the thick Cr-Au strips by 5 mil gold wires. Indium solder is most often used, but thermocompression and ultrasonic bonding techniques can also be used to bond to the tabs on the PLZT. The first, third, fifth, etc., rows are accessed from one end and the second, fourth, sixth, etc., rows from the other. A similar division is made for the columns. The lower photograph shows the same BDC after all leads have been attached and after it has been placed in the strain-biasing jig.

For the 32 x 24 element BDC's, the elements are on 1.0 mm and 1.25 mm centers and lie within a 32 x 30 mm rectangle. The transparent electrode widths are half the center spacings. This configuration precisely matches the 32 x 24 element PDA.

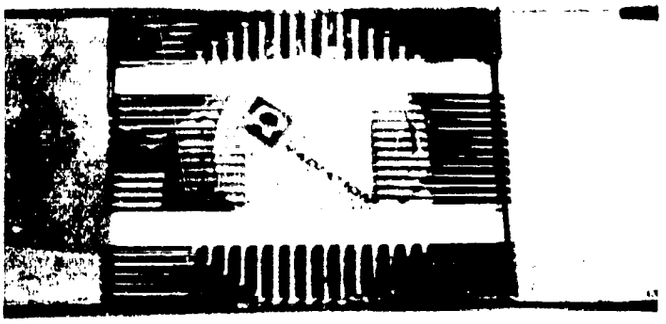

(a) BDC with "Radiation" Letterhead on Paper Under PLZT

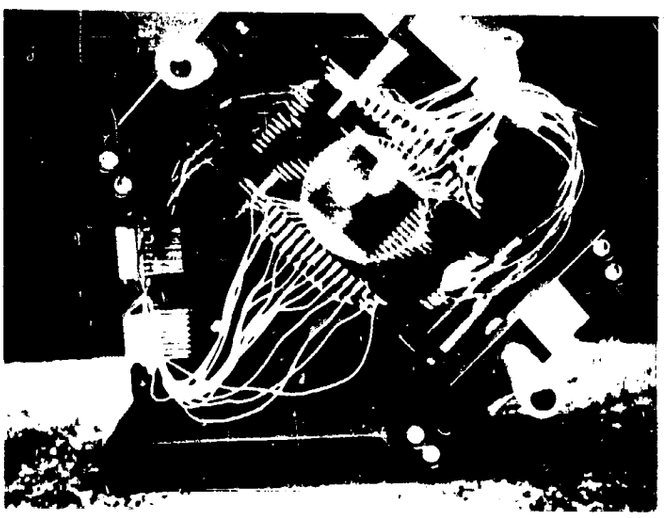

(b) BDC in Strain-Bias Jig

FIGURE 4-4. A 32 x 24 ELEMENT BDC

The 128 x 128 element BDC's appear quite similar to the 32 x 24 element BDC's (see Figure 4.4). The transparent electrode strips are 0.15 mm wide and are on 0.25 mm centers in both directions. All 16,384 elements lie within a 32 x 32 mm square. Alternate transparent electrodes are accessed from opposite edges of the square on both the upper and lower PLZT faces. As in the case for the 32 x 24 element BDC's, contact to the lower electrodes is achieved by pressure contact with thick Cr-Au electrodes on the Plexiglas which mate with extended tabs on the PLZT from the ends of the transparent electrodes. The upper tabs are connected to the corresponding thick electrode strips on the Plexiglas with 2 to 5 mil gold wire.

The patterns for the 32 x 24 element BDC's are formed by vacuum depositing through thin (2 mil) beryllium-copper masks. The masks are made from photographic transparencies by photoresist-etching techniques. The patterns for the 128 x 128 element BDC's are too fine for metal masking procedures. Photoresist-etching techniques are used directly on the PLZT plates to form these patterns (see Section 4.3.9).

These configurations represent what we consider to be reasonable design approaches. More investigation is required to refine these configurations and overcome some problems which have been encountered as noted in Section 4.3.9.

In Section 4.3.6 we describe a BDC configuration in which PLZT is bonded to precompressed fused quartz or glass. This configuration has considerable appeal for those situations in which the strain-bias level can be essentially fixed. The compactness, flatness, and ruggedness of this configuration are important considerations.

The most effective configuration for the BDC is expected to evolve as fabrication procedures are developed and refined.

4.3.4 Experimental Data. — In this section we present the more important experimental data accumulated on the BDC phase of the program. The emphasis in these experiments is on determining those factors which significantly affect the BDC performance characteristics. Several experiments have been carried out to determine the effects of PLZT thickness nonuniformities on contrast and optimum strain-bias levels. From these efforts we have concluded that these thickness nonuniformities represent the most significant fabrication problem. We have determined what degree of thickness uniformity is required (see Section 4.3.8). The PLZT polishing procedures have been improved, and we are closer to the required uniformities. Other BDC performance characteristics considered in the following paragraphs include switching speed and optical efficiency.

Four rows in a 5 x 5 element BDC were selected for row-switching tests with memory; the fifth row had cracks which formed during fabrication. The thickness of the 19 mm diameter PLZT disc, measured at several positions near the outer edge, varies from 95 to 100 microns; larger variations occur toward the center of the plate. The array elements are 2.0 mm square with 1.0 mm guard bands between adjacent elements on all sides. The transparent electrodes are Cr-Au electrodes. Except as noted, all data were taken with a tensile strain-bias level of $S_x = 2.3 \times 10^{-3}$ mm/mm. The PLZT is bonded with DER 332 epoxy to a 3.2 mm thick Plexiglas plate. Strain is applied to bending the 100 x 50 mm Plexilas plate in a double fulcrum bending jig.

In Figures 4.5a through 4.5d the strain-axis is vertical and the light is polarized at 45 degrees to the vertical. The polarization analyzer is adjusted to pass the component perpendicular to the polarization direction of the incident beam. The 4 x 5 element BDC is illuminated by the central portion of a 75 mm diameter collimated beam at 632.8 nm; a phase

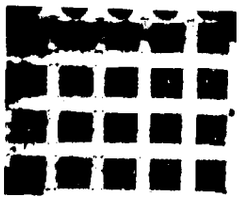

(a) ALL ROWS OFF

(b) ROWS 2 AND 4 SWITCHED ON

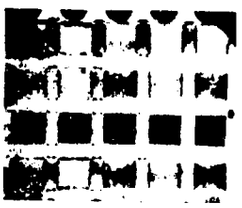

(c) ROWS 1,2, AND 4 SWITCHED ON

(d) ALL ROWS SWITCHED ON

(e) SAME AS (a) EXCEPT STRAIN-BIAS REDUCED TO ZERO

86022-1

FIGURE 4.5. ROW-SWITCHING OF A 4 X 5 ELEMENT ARRAY

compensator is not used. The BDC was imaged through a Glan-laser polarizer (the analyzer) onto a plane containing Polaroid film to obtain the data shown in Figure 4.5.

The five columns are electrically connected together, but each of the four rows can be independently excited. In Figure 4.5a all four rows have been placed in the OFF state by applying $2V_1$ = +160 volts to each row electrode; all column electrodes are held at V = 0 for all of these data. In Figure 4.5b rows two and four have been switched to the ON state by applying $-V_1$ = -80 volts to the second and fourth row electrodes; the first and third row electrodes were floating during the switching of rows two and four. In Figure 4.5c row one has also been switched to the ON state by $-V_1$ = -80 volts while all other row electrodes floated. In Figure 4.5d row three has also been switched to the ON state so that the full 4 x 5 array is ON. The ratio of ON and OFF intensities in this device ranges from about 4/1 to 20/1.

In Figure 4.5e the effect of strain on the polarization state of light transmitted by the PLZT is demonstrated. The full array was placed in the OFF state, identical to the state shown in Figure 4.5a, and then the strain was reduced to zero. The photograph in Figure 4.5e was taken after the strain was removed.

A 32 x 24 element BDC has been tested in a mode similar to that described above for the 4 x 5 device. Since the 32 x 24 device has been extensively tested before the photographs in Figures 4.6, 4.7, and 4.8 were obtained, electrical access to several rows had been lost. The light intensity changes to be noted in Figures 4.7 and 4.8 occur along rows 5, 7, 9, 11, and 13 (counting downward from the top row). Polarized light, incident on a diffuser, is used to illuminate the device; the depolarizing effects of the diffuser tend to degrade the contrast slightly.

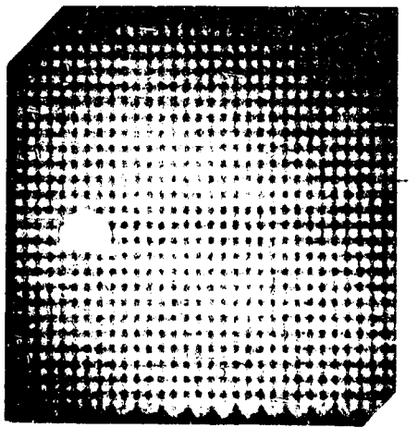

FIGURE 4-6. IMAGE OF 32 x 24 ELEMENT BDC WITH THE ANALYZER REMOVED

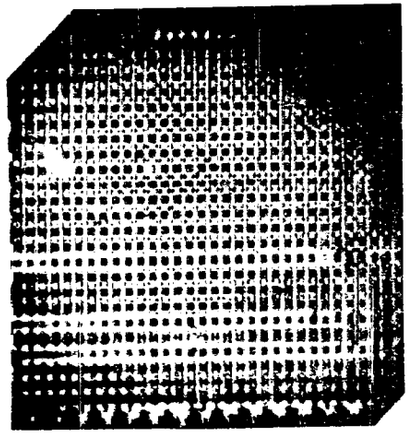

(a) State After -150 Volt Pulse Then a +75 Volt Pulse (Switchable Elements Are OFF)

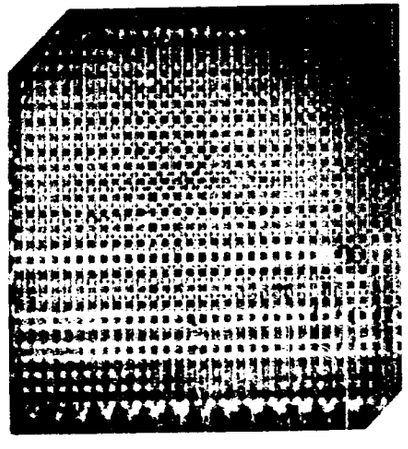

(b) State After a +150 Volt Pulse (Switchable Elements Are ON)

FIGURE 4-7. SWITCHING OF A 32 x 24 ELEMENT BDC WITH $S_x = 1.65 \times 10^{-3}$ mm/mm.

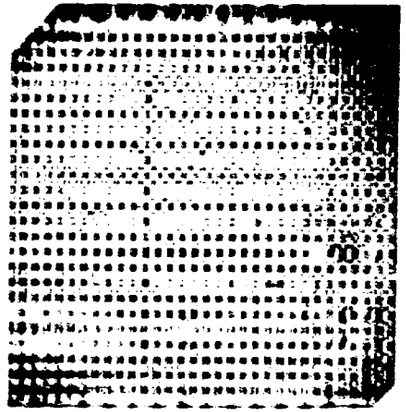

(a) State After -150 Volt Pulse Then a +75 Volt Pulse (Switchable Elements Are ON).

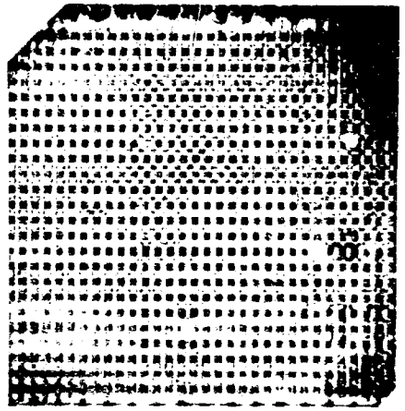

(b) State After a +150 Volt Pulse (Switchable Elements Are OFF).

FIGURE 4-8. SWITCHING OF A 32 x 24 ELEMENT BDC WITH $S_x = 2.1 \times 10^{-3}$ mm/mm

The PLZT in the 32 x 24 device was polished by Honeywell. The 50 mm diameter plate has a nominal thickness of b = 112 microns with thickness variations of $\delta b = \pm 10$ microns over the region occupied by the 32 x 24 array. The elements are 0.5 x 0.625 mm and are on 1.0 x 1.25 mm centers. The transparent electrodes are Cr-Au with sheet resistances of about 30 ohms per square. Optical efficiency per element is about 11 percent with most of the loss in the Cr-Au electrodes. The PLZT is bonded with DER 332 epoxy to a 3.2 mm thick Plexiglas substrate. The 32 x 24 element BDC in the strain-bias jig is shown in Figure 4.4.

In Figures 4.7 and 4.8 the strain axis is horizontal; otherwise, the relative orientation of the polarization axes is the same as for the 4 x 5 device. A phase compensator is not used. A Polaroid sheet polarizer is used for the analyzer.

A photograph of the 32 x 24 array with the analyzer removed is shown in Figure 4.6. All electrically accessible columns are connected together. In Figures 4.7 and 4.8 attention should be concentrated on the fifth through thirteenth rows from the top.

In Figure 4.7 the strain-bias level is $S_x = 1.65 \times 10^{-3}$ mm/mm. The switchable elements are placed in an OFF state by the application of a -150 volt pulse followed by a +75 volt signal (see Figure 4.7a). The ON state is reached by applying a +150 volt pulse to elements in an OFF state (see Figure 4.7b).

In Figure 4.8 the strain-bias level is $S_x = 2.1 \times 10^{-3}$ mm/mm. The switchable elements are placed in an ON state by the application of a -150 volt pulse followed by a +75 volt pulse (see Figure 4.8a). The OFF state is reached by applying a +150 volt pulse to elements in an ON state (see Figure 4.8b). Contrasts were measured for 20 elements (the seventh through the twenty-seventh) in row eleven after optimizing the strain-bias level

for maximum contrast at the center of the row. The contrast varied from 8/1 to 35/1 for these 20 elements; in other regions of this plate, contrasts of 50/1 were achieved. The elements nearest the array edges are in a steep thickness roll-off region of the PLZT. The contrast variations are related to thickness variations; this relationshp is considered in detail in Section 4.3.8.

It is signficiant to note that the relationship between OFF and ON states and the drive voltage sequence is inverted for the two levels of strain-bias discussed above. Contrasts are improved for the higher strain-bias level by about a factor of two. Nevertheless, the capability of inverting the digital logic states by changing only the strain-bias level is demonstrated. Furthermore, it is clear that more than one level of strain-bias can be examined to optimize contrast.

Switching speeds for the 32 x 24 element BDC's operated in the mode which provides immunity to half-select disturbances are essentially the same as for the previously considered mode. The important results are summarized here. The PLZT thickness (nominal) is b = 112 microns. For pulse widths τ_m down to 100 μsec, the two voltage levels required for switching are V_1 = 75 volts and $2V_1$ = 150 volts. For τ_m = 25 μsec, the voltages V_1 = 100 volts and $2V_1$ = 200 volts provide switching, but with some sacrifice in contrast (less than a factor of two). An important observation is the insensitivity of contrast to switching voltage amplitude variations. For $\tau_m \geq 100$ μsec, the two voltages can be varied over the ranges $70 \leq V_1 \leq 80$ volts and $140 \leq 2V_1 \leq 160$ volts with contrast changes staying within the range of experimental measurement accuracy. This property relaxes the design constraints on the drive circuitry.

Measurements of thickness variations in polished PLZT plates have been made interferometrically and by comparing relative phase retardations along a diamter of the BDC. We analyzed and tested techniques for monitoring PLZT thickness profiles during and after polishing. Several

interferometric approaches can be used. A particularly simple one is to illuminate a PLZT plate with collimated laser light and to image the interfering reflections from the front and back surface onto a viewing plane. A more flexible means for determining thickness profiles is to use a Mach-Zehnder interferometer. An example of Mach-Zehnder interferometer data with three 19 mm diameter polished PLZT plates is shown in Figure 4.9. The PLZT plates, each having a nominal thickness of 100 microns, were held between clean glass slides and placed in one leg of the interferometer. An image of each sample is shown in Figure 4.9. The interferometer was adjusted in each case to display any circular or elliptical patterns present in the PLZT; interference patterns caused by the glass supports do not significantly affect our interpretation of the fringes due to the PLZT plate. The straight line background pattern in the field surrounding the circular plates provides a measurement of the amount and direction of wedge in each plate. Similarly, the near elliptical patterns are measures of curvature superimposed on the wedge. As an example, the total thickness variation measured from Figure 4.9c is about 32 microns with a curved surface modulated on a wedge. The wedge is believed to result mainly from improper adjustment of polishing motion and from misalignment of the polishing apparatus. The curvature is believed to result mainly from a nonuniform wax thickness during final polishing. Optical monitoring techniques are being used during polishing to correct for such errors.

Samples of polished PLZT plates have been received from Bell Telephone Laboratories for test and evaluation in our facilities. We placed one of these plates in the Mach-Zehnder interferometer and obtained the pattern shown in Figure 4.10. This BTL plate is 21.5 mm in diameter and has a nominal thickness of 100 microns. The magnification of this pattern is

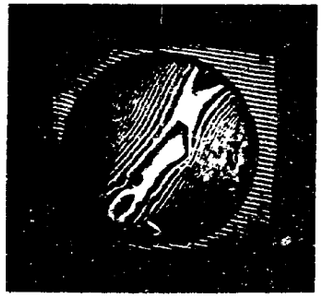

(a)

(b)

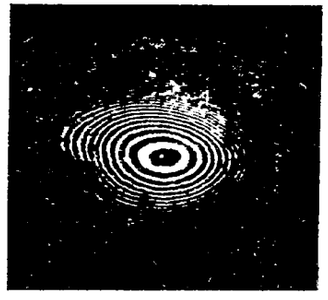

(c)

FIGURE 4.9. POLISHED PLZT THICKNESS PROFILE DATA FROM A MACH-ZEHNDER INTERFEROMETER

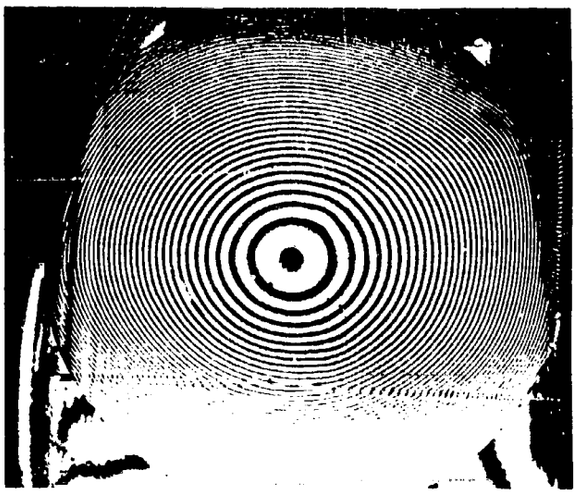

FIGURE 4-10. THICKNESS PROFILE DATA FOR A POLISHED PLZT PLATE FROM BELL TELEPHONE LABORATORIES

approximately twice that of these in Figure 4.9. There is negligible wedge in the BTL plates, but the curved surfaces which cause the circular interference patterns show that the thickness varies by about 20 microns from center to edge of the particular plate shown in Figure 4.10. The other three BTL samples had more severe thickness errors. BTL personnel indicated that these are not typical "good" results and are sending better samples for our evaluation.

Another valid measurement of thickness variations can be obtained from nonmemory mode switching characteristics using a Babinet-Soliel phase comp4ensator with the BDC and the polarization analyzer. A preliminary partial 32 x 32 element BDC was tested in this way. The strain-bias level was fixed at $S_x = 1.85 \times 10^{-3}$ mm/mm for these tests. One row along a diameter was tested. Figure 4.11 shows the nonmemory electro-optic switching characteristics for four elements along a common row of the 32 x 32 device. The clean trace in each case is the 255 volt pulse applied to the element under test. Note that the voltage risetime is nearly 6 μsec and the fall time is nearly 11 μsec; these limitations are imposed by the drive circuitry. The noisier trace is the light received through the element under test at a photomultiplier tube. Zero light and zero voltage levels are both along the bottom of the graticule. The Babinet-Soliel compensator in the optical arrangement was adjusted to obtain a minimum light transmission state at the sixth element with zero volts applied. The important feature to note in each case is the variation in the light level at the beginning of each trace (before the voltage starts). It is clear that the light level with zero volts applied for the second and twentieth elements is not at zero; as the voltage begins to rise for these elements, the light intensity first dips toward zero then begins to rise. By readjusting the Babinet-Soliel compensator for the second and twentieth elements, we obtained conditions essentially identical to those observed at the fifth and sixth elements. The amount of optical path length

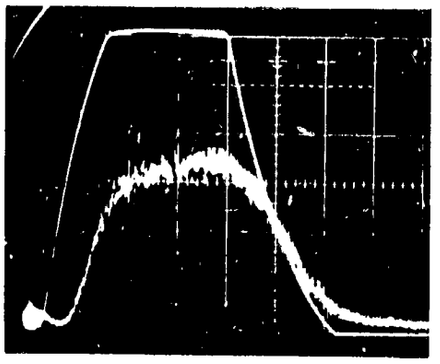

(a) Element #2

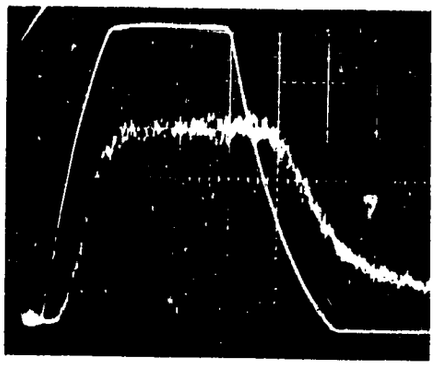

(b) Element #5

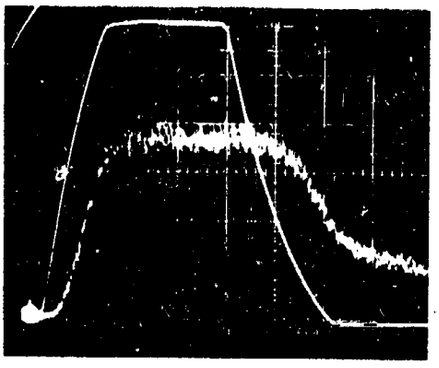

(c) Element #6

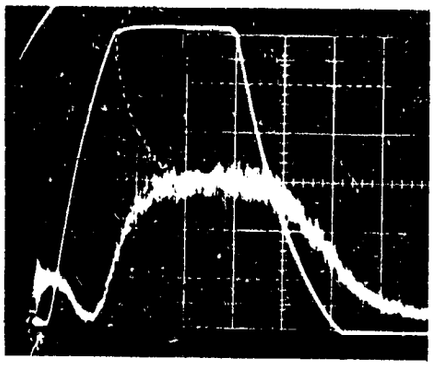

(d) Element #20

Clean Traces: Drive Voltage - 43 Volts/Division
Noisy Traces: Relative Light Intensity Transmitted
Sweep Speed: 5 μsec/Division

FIGURE 4.11. NONMEMORY ELECTRO-OPTIC SWITCHING WITH DEVICE OF FIGURE 4.8 (a) AT VARIOUS POSITIONS ALONG A COMMON ROW; STRAIN BIASED TO 1.85 X 10^{-3} mm/mm.

difference read from the compensator relative to the sixth element was 0.065λ for the second element and 0.141λ for the twentieth element. These readings correspond to PLZT plate thickness variations in the 14 to 30 micron range.

Nonmemory mode switching speed tests have also been carried out. Several 0.5 x 0.625 mm elements driven one at a time by a transistor circuit have been switched from OFF to ON to OFF in less than 0.5 μsec. The 0.2 μsec rise and fall times were limited by the drive circuitry. The peak voltage was 255 volts. The 2.2 RC risetime limit of each element is near 0.1 μsec and will be even lower for smaller elements. Typical voltage and corresponding light intensity traces are shown in Figure 4.12a. A 4 x 5 element BDC operated in the nonmemory mode is shown in Figure 4.12b; one row is switched ON with 160 volts applied to it while the photograph was taken. The contrast ratio is greater than 40/1.

The changes in the dielectric constant ε_r of PLZT-7/65/35 with strain-bias level S_x and voltage were measured. For a fixed voltage, ε_r increases with S_x. At $S_x = 3 \times 10^{-3}$mm/mm, ε_r is about 1.7 times larger than at $S_x = 2 \times 10^{-3}$mm; ε_r is about 1.9 times smaller at 200 volts than at zero volts. The changes in ε_r with S_x and voltage are monotonic.

Memory mode lifetime tests were performed on several test devices. In the longest continuous test, a 60 Hz voltage signal reaching ±190 volts (peak) was applied to a 5 x 5 element BDC which had Cr-Au electrodes. Over 2×10^6 cycles were accumulated before the test had to be discontinued (due to equipment requirements). No changes were detected in the performance characteristics of the test device. In a nonmemory mode lifetime test with +100 volt pulses applied at 50 kHz, over 10^9 cycles were accumulated with no change in device performance; Cr-Au electrodes were also used on this device.

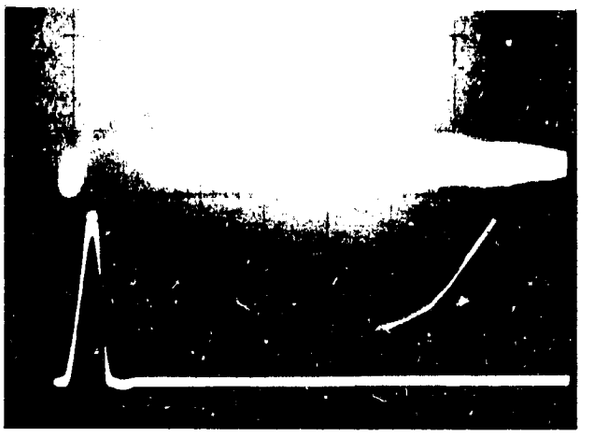

(a) Top: Photomultiplier Tube Output
(Relative Light Intensity)
Bottom: PLZT Drive Voltage
(255 Volt Peak)
Horizontal (Both): 0.5 Microseconds/Division

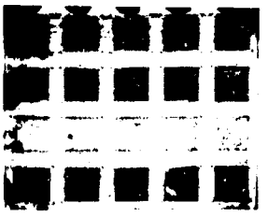

(b) No Voltage on Rows 1, 2, and 4
Voltage on Row 3 is +160 Volts

FIGURE 4-12. RISE TIME AND I-V SIGNAL DATA WITH STRAIN-BIASED PLZT IN A NONMEMORY MODE.

Electrical polarization versus drive voltage hysteresis data were obtained and related to the birefringence characteristics of the PLZT. These data are presented and discussed in Appendix A. Data relating switchable birefringence $\overline{\Delta n}$ to strain-bias level S_x are also presented and discussed in Appendix A.

4.3.5 Half-Select Disturbance Compensation. — A technique for fully compensating the half-select disturbance effects has been conceived [18,26] and implemented in the drive electronics design. Tests with switching pulse widths down to 100 μsec have confirmed total compensation. For pulse widths of 25 μsec, compensation is adequate but about 30 percent higher drive voltages are required.

The data in Appendix A in Figure A-4 clearly indicate that optical transmission states in PLZT are a function of the history of electrical control signals in a nonlinear manner. The specific sequence of electrical control signals which is used to matrix address a two-dimensional array of display elements is not explicitly shown in these data. We shall describe this sequence in some detail in the next paragraphs.

PLZT exhibits a voltage-controlled mode of operation[18] in addition to the hysteresis characteristics demonstrated in Figure A-4. A strained plate which has been electrically poled by the application of a large voltage (V_0 +250 volts for b = 0.1 mm) operates in this mode without half-select disturbances as follows.

The application of sequential voltage pulses of amplitude $-2V_1$ followed by $+V_1$ produces a birefringence state which will not change for any subsequent voltage pulses in the $0 < V < +V_1$ range; the birefringence state is "controlled" by the $+V_1$ voltage level. However, any single pulse with $V > V_1$ will produce a new birefringence state different from that

following the $+V_1$ pulse (or pulses). In particular, a pulse with $V = +2V_1$ will produce a significantly different birefringence state. With proper design, the state following $+V_1$ will correspond to a light transmission minimum (OFF) and the state following $+2V_1$ will correspond to a light transmission minimum (OFF) and the state following $+2V_1$ will correspond to a maximum (ON), or vice versa. An element in either of these states will not change during the application of a large number of subsequent $+V_1$ pulses. The voltage V_1 will fall in the 35 to 100 volt range (strain, speed, and thickness dependent). The element can be reset and prepared to receive new data by applying a $+2V_1$ pulse followed by a $-2V_1$ pulse.

The switching characteristics for a single element described in the preceding paragraph can be expolited for matrix addressing a two-dimensional array of elements. Figure 4.13 shows that disturbance signals generated during row-at-a-time writing do not exceed $+V_1$. All of the possible disturbance combinations for any NxN array are illustrated in this example. The column electrodes are activated in parallel during each row writing sequence. All columns receiving ON signals are pulsed with $+2V_1$ and all others are held at $+V_1$. The row receiving data is grounded and all others are held at $+V_1$. A fully composed BDC is erased by first applying $+2V_1$ to all columns and grounding all rows and then reversing this voltage. At this point $+V_1$ could be applied to all columns with all rows grounded, but this step is not required.

The effective data rate is N/τ_m where N is the number of bits per row and τ_m is the interval between the times when row composing commands are given.

4.3.6 Strain-Bias Techniques for PLZT. — Several techniques can be used to produce a linear strain in PLZT. The procedure most often used for test devices[17,19] is illustrated in Figure 4.14. The PLZT is bonded

(a) Block to be composed:

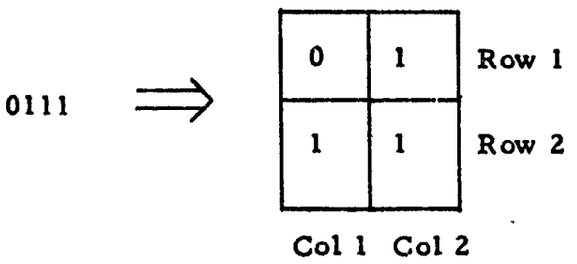

(b) Voltage pattern for writing onto Row 1 (with potential differences across BDC elements shown at electrode interssections):

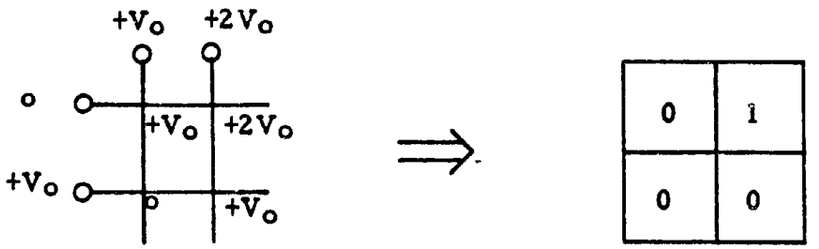

(c) Voltage pattern for writing onto Row 2:

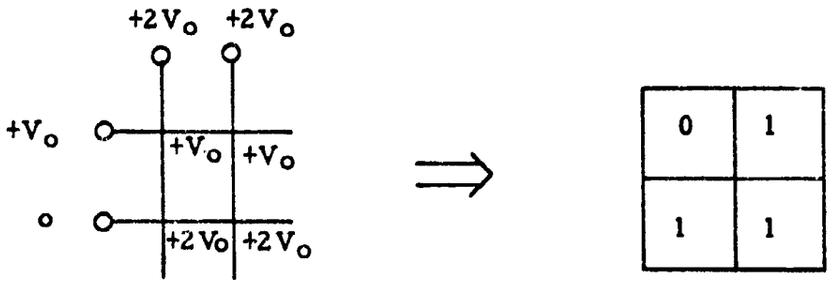

FIGURE 4-13

Voltage Drive Sequence for Composing with Compensated Half-Select Distrubance Technique.

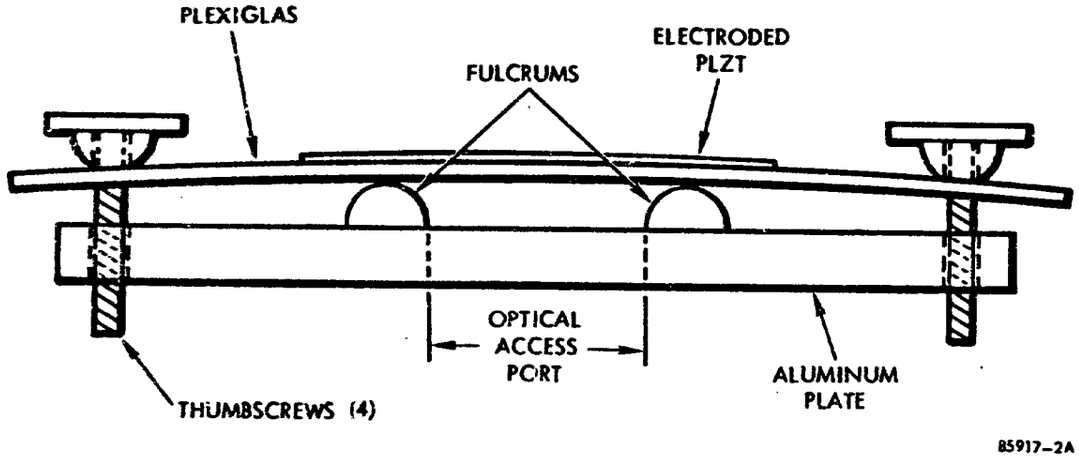

FIGURE 4-14. STRAIN-BIASING PLZT BY BENDING PLEXIGLAS IN A SPECIAL JIG.

with a transparent epoxy to a Plexiglas plate. The device is placed in a jig which forms the Plexiglas into a large radius of curvature bend. The convex surface acquires a linear tensile strain and the concave surface acquires a linear compressive strain. Tensile strain is preferred because it produces stronger electro-optic effects.[19] A tensile strain-bias is imparted to the PLZT in the situation depicted in Figure 4.14. With this bent Plexiglas approach, the strain-bias level can be varied easily. This feature is desirable for test devices but is not needed when the optimum strain-bias level is known and can be set by other means.

Other techniques for producing a linear strain-bias have been developed. In Figure 4.15 a particularly appealing procedure is indicated for producing a strain-bias without curved surfaces. The ability to vary the strain-bias level easily is lost, but the compactness, flatness, and ruggedness of the structure may offset this disadvantage. The technique depicted in Figure 4.15 takes advantage of the fact that glass and fused quartz can tolerate high levels of compressive strain (higher than steel) without cracking. A glass or fused quartz block is placed in a special jack and compressed until the compressive strain (relative dimension change) is equal to the tensile strain required in the PLZT plate. A PLZT plate is then bonded to one of the strained faces. After the epoxy sets, the compressive force on the quartz block is released; a linear tensile strain is thereby developed in the PLZT. The resulting structure is compact and flat.

The optical quality of quartz blocks can be extremely high at modest cost, since the state-of-the-art in glass and fused quartz preparation and polishing is highly developed and geared to high volumes. The blocks can be trimmed with a diamond saw so that the PLZT plate completely covers one face of the block. This feature is important because it permits a large BDC to be assembled from small modular BDC's while maintaining regular element center spacings, even across module intersections. With this

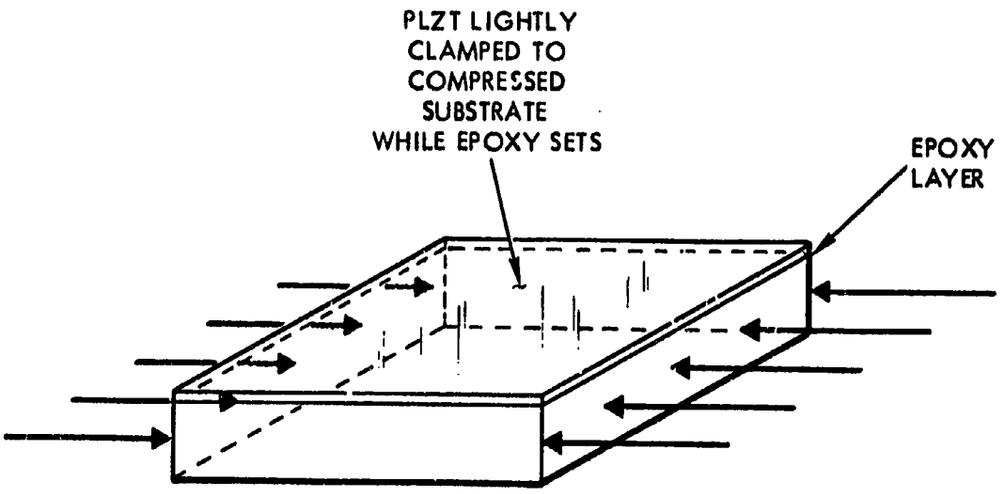

STEP 1: LIGHTLY CLAMP A PLZT PLATE TO A PRE-COMPRESSED TRANSPARENT SUBSTRATE (SUCH AS GLASS) WHILE THE EPOXY CURES AND SETS.

$$S_p \approx 0$$
$$S_g < 0$$

STEP 2: AFTER THE EPOXY HAS FULLY CURED, RELEASE THE COMPRESSION IN THE SUBSTRATE AND TRANSFER A TENSILE STRAIN TO THE PLZT.

$$S_p > 0$$
$$S_g \approx 0$$

86270-4

FIGURE 4-15. STRAIN-BIASING PLZT BY PRE-COMPRESSING A GLASS OR FUSED QUARTZ SUBSTRATE.

technique, access to the transparent electrode strips on the top and bottom faces of the PLZT can be provided in several ways. One approach is to extend the electrodes around to the four edges of each block so that electrical interconnections with adjacent modules can be made by fitting them together, with slight pressure. The drivers connected to the electrodes on modules around the BDC periphery are thereby connected to full rows and columns.

The precompressed glass or fused quartz approach for strain biasing the PLZT is a potentially important procedure for developing design criteria for larger BDC's in subsequent phases of the program.

Photographs of test devices fabricated in our facilities are presented in Figures 4.4 and 4.16. The bent Plexiglas technique is illustrated in Figure 4.4. The device shown in Figure 4.16 is on fused quartz which was compressed while the epoxy bond cured and set. Preliminary tests have been made with the fused quartz devices but more extensive testing remains to be done.

The various strain-bias jigs fabricated for test devices were analyzed prior to construction and tested with resistance-wire strain gages after completion. The actual strain-bias levels versus deflection of the ends of the plates were within 10 percent of the predicted values in all cases. Uniformity of strain-bias along a diagonal in the region occupied by a 32 x 24 and a 128 x 128 element BDC was measured. The rate of change of strain-bias with deflection of the Plexiglas plate ends was uniform to better than 10 percent along this diagonal. Uncertainties in the zero relative strain-bias level and in strain gage properties exist and can account for much of this variation.

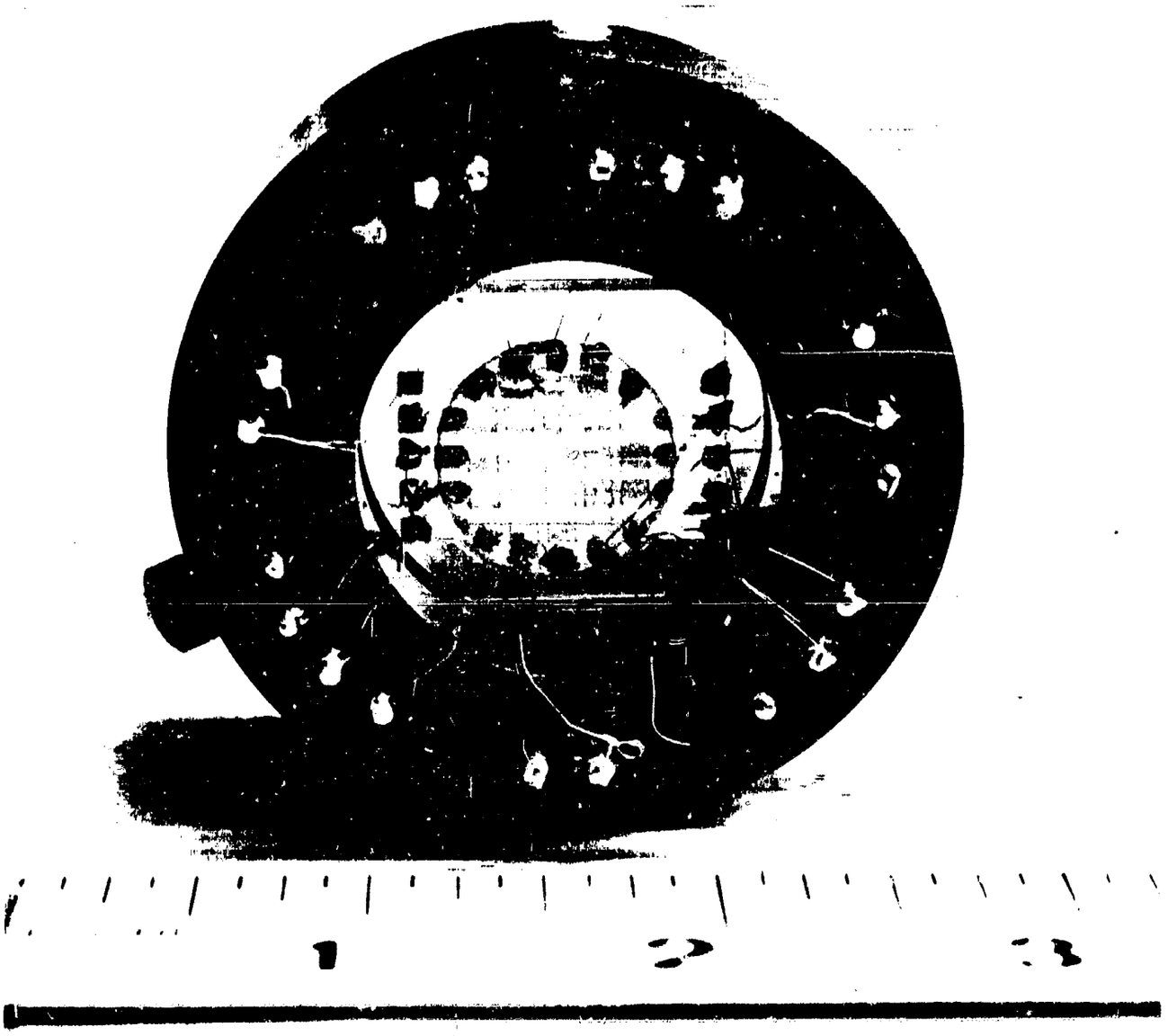

FIGURE 4-16. A 5 x 5 ELEMENT BDC TEST DEVICE OF STRAIN-BIASED PLZT ON PRE-COMPRESSED FUSED QUARTZ.

4.3.7 Transparent Electrode Material. — Throughout the program the transparent electrode materials have been thin chromium-gold (Cr-Au) films in all but two test devices. All Cr-Au films were vacuum deposited onto the PLZT plates and substrates in our facilities. A sequence of tests were performed to characterize the Cr-Au films. Transparent films of various thicknesses were deposited and data on film thickness t_{cg}, optical transmissivity T_{cg}, and resistivity R_{cg} were compiled. The transparent Cr-Au films, used on over 80 percent of the test devices, were characterized by t_{cg} = 8.0 nm, T_{cg} = 0.8, and R_{cg} = 30 ohms per square. For two such films on opposite PLZT faces, T_{cg}^2 = 0.64.

The Cr was evaporated from a tungsten rod coated with Cr. The amount of Cr deposited was controlled by controlling the length of time Cr was received at the PLZT plate with a clock and a shutter. Typically, a film of less than 0.5 nm of Cr is used to improve the adherence of the Au layer which follows.

The Au was evaporated from a boat. Measured lengths of 5 mil gold wire were placed in the boat and totally evaporated to produce the desired film thickness. Calibration data relating the film thickness to the mass of Au used and to the separation of the PLZT from the boat were generated early in the program.

Several 19 mm diameter polished PLZT plates received sputter deposited transparent electrodes of tin doped indium oxide (In_2O_3:SnO_2). Two test devices were fabricated with these; one was tested extensively. The performance of this device was very similar to those fabricated with Cr-Au films; the optical efficiency was much improved, however. With Cr-Au films, BDC optical efficiencies of 10 to 15 percent were noted. With the In_2O_3:SnO_2 films, optical efficiencies in excess of 40 percent were obtained. The

adherence of the In_2O_3:SnO_2 films was excellent; attempts to scratch the film off failed until enough pressure was applied with a steel stylus to gouge the PLZT. The Cr-Au films were much easier to remove, although they usually passed the Scotch tape test.

The improvement in optical efficiency of the In_2O_3:SnO_2 films is attributable to two effects: reduced absorption losses and antireflection (AR) coating effects. To optimize the AR coating effects, the thickness of the film must be properly controlled. In the test device, the 40 percent and larger optical efficiencies were noted in regions where the film had the correct thickness to AR coat for the 632.8 nm wavelength normally used.

In general, the In_2O_3:SnO_2 films are preferred because of the higher optical efficiencies, better adherence, and the potential for longer device lifetimes.[17] However, the Cr-Au films are adequate for many device tests and applications.

4.3.8 PLZT Polishing and Contrast Considerations. — Improvements in the surface finish and thickness uniformity of polished PLZT plates have been made during this program. Further improvements in thickness uniformity are required to improve the uniformity of contrast over the full BDC area.

The best polishing results with 50 mm diameter PLZT plates have been obtained in our facilities and by the material supplier (Honeywell). Nominal thicknesses in the 100 to 120 micron range have been achieved with thickness variations down to ±10 microns over the central 75 percent of 50 mm diameter polished plates. Before we describe the special polishing procedures that have been tested and discuss our interpretation of the cause of the thickness variations, we analyze the effect of these variations on contrast. The analysis is related to experimental data on a 32 x 24 device.

Contrast is defined here as the ratio of the light intensity transmitted by an element in the ON state to that transmitted by that element in the OFF state. Strain-bias variations and temperature variations will also degrade contrast. Temperature changes with ±10°C of room temperature do not significantly affect the contrast. We can analyze the effects of both thickness and strain-bias variations simultaneously; the strain-bias enters the relationshps below by affecting the birefringence $\overline{\Delta n}$.

In Appendix A we show that an ideal BDC element has an intensity transmission characteristic which can be expressed by $I/I_o = \sin^2(\Delta\phi_p/2)$ where $\Delta\phi_p = (2\pi/\lambda)b\overline{\Delta n}$. We define $\Gamma = b\overline{\Delta n}$ and take I_s as the intensity of scattered and depolarized light always transmitted. Then we can write,

$$I(x,y) = I_s + I_o \sin^2[\tfrac{\pi}{\lambda}\Gamma(x,y)] \quad ,$$

where the x and y dependence of both b and $\overline{\Delta n}$ is indicated by $\Gamma(x,y)$. The optimum contrast is

$$R_o = \frac{I_o + I_s}{I_s}$$

which is achieved for

$$\Gamma_{ON} = \Gamma_1(x,y) = (2m-1)\,\frac{\lambda}{2}\,, \quad m=1, 2, 3, \ldots$$

$$\Gamma_{OFF} = \Gamma_o(x,y) = m'\lambda, \quad m' = 0, 1, 2, \ldots$$

Typically the PLZT is operated with m=1 and m'=1 so that $\Gamma_1 = \lambda/2$ and $\Gamma_o = \lambda$. Suppose that $\Gamma_1 = \lambda/2 + \delta\Gamma$ and $\Gamma_o = \lambda + \delta\Gamma$ where $\delta\Gamma << \lambda/2$ is

a term arising from nonuniformities in b or $\overline{\Delta n}$ or both. Then the modified contrast is

$$R(\delta\Gamma) = \frac{I_o + I_s - \delta I}{I_s + \delta I} = \frac{R_o - \frac{\delta I}{I_s}}{I + \frac{\delta I}{I_s}} \qquad (4\text{-}1)$$

where

$$\delta I = I_o \sin^2\left(\frac{\pi}{\lambda}\delta\Gamma\right) \approx I_o\left(\frac{\pi}{\lambda}\delta\Gamma\right)^2 \quad . \qquad (4\text{-}2)$$

From Equations 4.1 and 4.2 we can obtain,

$$\frac{\delta I}{I_o} = \sin^2\left(\frac{\pi}{\lambda}\delta\Gamma\right) = \frac{(\gamma-1)R}{\gamma R^2 + (\gamma-1)R - 1} \; .$$

We can neglect $(\gamma-1)R-1$ in comparison to γR^2 and get,

$$\delta\Gamma = \frac{\lambda}{\pi R^{1/2}}\left(\frac{\gamma-1}{\gamma}\right)^{1/2} \; . \qquad (4\text{-}3)$$

We first suppose that $b(x,y) = b_o + \delta b(x,y)$ and $\overline{\Delta n}(x,y) = \overline{\Delta n}_o$ with b_o and $\overline{\Delta n}_o$ constant. Then

$$\Gamma(x,y) = b_o\overline{\Delta n}_o + \overline{\Delta n}_o\,\delta b(x,y) = \Gamma_o + \delta\Gamma(x,y)$$

where

$$\Gamma_o = b_o\overline{\Delta n}_o = \lambda$$

$$\delta\Gamma(x,y) = \overline{\Delta n}_o\,\delta b(x,y) = \lambda\frac{\delta\, b(x,y)}{b_o} \; . \qquad (4\text{-}4)$$

We obtain from Equations 4.3 and 4.4 that

$$\frac{\delta b_m}{b_o} = \frac{1}{\pi R^{1/2}} \left(\frac{\gamma-1}{\gamma}\right)^{1/2} , \qquad (4\text{-}5)$$

where δb_m is the maximum allowed value for $\delta b(x,y)$. With b_o = 100 microns, γ = 2, and R = 100 we get $\delta b_m = \pm 2.2$ microns. With b_o = 100 microns, γ = 2, and R = 50 we get $\delta b_m = \pm 3.2$ microns.

With a 32 x 24 device we have experimentally obtained γR = 35 and R = 8 so that γ = 35/8 = 4.38 with b_o = 112 microns. These give $\delta b_m = \pm 11$ microns for the PLZT plate on the 32 x 24 element BDC tested. This result agrees well with the ±10 micron result obtained interferometrically.

These calculations and comparison to experimental data indicate that thickness uniformities required are about ±2 to ±3 microns while those presently being achieved are around ±10 microns.

We can obtain in a similar manner for $b(x,y) = b_o$ and $\overline{\Delta n}(s,y) = \overline{\Delta n}_o + \delta\overline{\Delta n}(x,y)$ that

$$\frac{\delta\overline{\Delta n}_m}{\overline{\Delta n}_o} = \frac{1}{\pi R^{1/2}} \left(\frac{\gamma-1}{\gamma}\right)^{1/2} . \qquad (4\text{-}6)$$

The relationship in Equation 4-6 can be related to strain-bias variations δS_x by considering data such as that presented in Appendix A in Figure A-3. Tolerances on strain-bias variations can be established. More complete data on $\overline{\Delta n}$ versus S_x and on S_x versus position in the BDC area is needed

before accurate determinations of the effects of strain-bias variations on contrast can be determined. Only when the thickness variation problem is solved will such data be accurately obtained.

Two special polishing techniques were tested with PLZT. Neither of these has been more successful than the more conventional approaches normally used in our facilities. The conventional approach with quartz sticky wax as the bonding medium and a variety of standard laps and polishing materails will be discussed later in this section.

One of the special polishing techniques required a vacuum hold-down jig. PLZT plates were polished in this jig without using wax or other bonding agents to hold the PLZT in place. The porous (or sintered) steel plate through which the vacuum was pulled and onto which the PLZT plates were placed proved to be unsatisfactory. In the process of polishing such steel plates to the required flatness, before mounting them in the jig, they often become too clogged with polishing compound to permit sufficient air flow for holding the PLZT plates firmly in place. When an unclogged sintered plate was prepared, the fine grit used for polishing the PLZT again clogged it and permitted the PLZT to slip and sometimes break. This procedure is not considered worthy of pursuing futher.

In another special polishing technique, PLZT plates were bonded with a very thin layer of Lensbond cement to a water soluble sodium chloride (NaCl) substrate. Lensbond forms a thinner and more uniform bond layer than wax, but removal of the thin layer is difficult with normal substrates (such as Pyrex) since solvents must work in from the edges. With the NaCl, the substrate material is dissolved away in water after polishing is complete. Then the Lensbond can be dissolved readily from the face of the PLZT. For reasons that are not presently known, the PLZT has a strong tendency to crack in the final polishing phases or during NaCl removal. Since no satisfactory unbroken plates have results with this approach, we are no longer pursuing it.

The procedure with which we have had the best success involves careful application of conventional polishing techniques. Unpolished PLZT plates at least 0.75 mm thick are bonded with a layer of quartz sticky wax (as thin as possible) to Pyrex or cast iron flats. The first surface is polished with diamond grit (10μ down to 0.25μ average sizes) against grooved tin laps. As little as possible of the initial thickness should be removed during this step. After this surface has been completely polished, the still thick plate is removed, turned over, and bonded again with quartz sticky wax. At this point it is very important that the plate be pressed firmly against the flat while the wax hardens. The layer of wax must be as thin and as uniform as possible since thickness variations in the wax layer will be transferred to the PLZT during the final polishing step. This is the source of most of the thickness variations which have occured in polished PLZT plates. It is also important that the PLZT plate, after one face has been polished, be thick enough to have sufficient rigidity to overcome any unevenness or bumps in the wax when the plate is pressed into the wax and against the polishing flat. If the plate is too thin, it will conform to the wax rather than making the wax conform to it.

The data presented in Figures 4.9, 4.10 and 4.11 in Section 4.3.4 indicate the kind of thickness variation problems which have been encountered. The 20 to 35 micron variations indicate there have been improved to 8 to 15

micron variations over even larger areas. The contrast variation data obtained with the 32 x 24 device have confirmed these results (as noted earlier in this section).

In summary, we have analytically defined the goals required for the desired levels of contrast uniformity and experimental confirmation of this analysis has been obtained with a 32 x 24 device. Thickness variations must be held within about ±2 microns over the BDC area. Special polishing techniques have been tried with little success. The more conventional polishing approach, with attention to certain details, offers the best prospects for achieving the required thickness uniformity characteristics.

4.3.9 Photoresist-Etching Techniques and Other Fabrication Details.— As noted in Section 4.3.3, the electrode patterns for the 128 x 128 device are too fine for depositing through metal masks (as is done for the 32 x 24 devices). The 0.15 mm transparent electrode widths and 0.10 mm gaps are formed on the PLZT by etching the desired pattern from a continuous vacuum deposited Cr-Au film. Several photoresists have been used, including Kodak KMER and KTFR, and Shipley AZ-111 and AZ-1350H. Etchants are C-35 (from Film Microelectronics, Inc) for Au and a proprietary solution for Cr.

The thicker Cr-Au patterns at the ends of the BDC on the PLZT and on the Plexiglas are also formed by photoresist-etching. However, the Au can be electroplated or electrolessly deposited onto these parts; adherence tends to be better with these techniques than with vacuum evaporation.

The thick and thin Cr-Au patterns are formed on the PLZT and on the Plexiglas by contact printing patterns from photographic transparencies onto the photoresist. Following development and baking, the etchants are applied (first for Au, then for Cr). The protective photoresist layer is then removed with acetone or other solvents. Edge definitions of better than 3 microns are typical; better than 1 micron definition can be achieved with AZ-1350H.

Multiple apply, develop, etch, and remove sequences are required for each PLZT plate because of the two faces and the need for two different Cr-Au film thickness (thin for transparent patterns, thick for end tabs and tab extensions). A single sequence is usually adequate for the patterns on the Plexiglas. The large number of process steps has results in considerable PLZT plate breakage. The 100 to 120 micron thick, 40 mm diameter plates are extremely fragile. Some of the plates which survive this process break or crack during the epoxy bonding step, usually because of uneven heating of the bonding jig, nonuniform pressure, or too much pressure. Some of the apparently successful epoxy bonded plates crack when strain or voltage is applied, usually because of a ripple in the epoxy or an imperfection in the PLZT plate or a large dust particle trapped between the PLZT and Plexiglas.

The causes of much of the PLZT breakage, the occassionally poor epoxy bonding, and the sometimes poor Cr-Au film adherence have been isolated and controls have been established. Improvements in all of these areas have been made during the program.

Contact to the electrodes on the PLZT face bonded to the Plexiglas is made to the mating electrodes on the Plexiglas by pressure. If too much epoxy is used, a layer can form between mating PLZT and Plexiglas electrodes and cause poor contact (sometimes forming a capacitive coupler rather than a DC path). An increase in the thickness of the mating electrodes has significantly improved the degree and uniformity of contact typically achieved.

The electrodes on the exposed PLZT face are connected to thick Cr-Au strips on the Plexiglas by 2 to 5 mil gold wires. The gold wires are indium soldered, thermocompression bonded, or ultrasonically bonded to the thick tabs on the PLZT. Indium solder bonds have proven to be reliable and less damaging to the PLZT than thermocompression bonds. Limited data is available with ultrasonic bonds; these appear to be quite satisfactory, based on preliminary tests.

The other ends of the gold wires are indium soldered to the thick strips on the Plexiglas. Neither thermocompression nor ultrasonic bonds work well on Plexiglas (it melts too easily and fouls the bonders).

Alignment of the 32 x 24 patterns with the mating patterns on the Plexiglas is easily done with the unaided eye. Alignment of the 128 x 128 patterns requires a low-level of magnification (such as watchmakers lenses). Alignment aids are provided around the edges of the 128 x 128 pattern to achieve the required perpendicular orientation of patterns on opposite faces.

A photographic mask can be placed at the output face of the BDC to block stray light that is transmitted between active elements. A photographic transparency which is clear where elements are located and is opaque in the interelement spaces can be affixed to the BDC output

face by any of several means. The light which is transmitted in these interelement spaces in the absence of the mask would be projected into the interelement spaces on the PDA. Except for considerations of the holographic K-ratio and the effects on signal-to-noise ratios of light scattered from the PDA interelement spaces, no significant harm is caused by this light.

4.3.10 BDC Electronics. — The BDC electronics provide the interface between the computer and the 128 x 128 element or 32 x 24 element BDC's. This unit consists of an interface logic board and a complement of 256 high voltage driver circuits, as well as power supplies and a cooling fan. The entire unit is housed in a standard rack width chassis with the high voltage drivers accessible through the front panel. Figure 4.17 is a block diagram of the BDC electronics unit.

The interface logic board accepts information from the computer and converts it into a format which is compatible with row and column high voltage driver circuits. Data from the computer is in the form of 12 bit parallel words. Each row of data for the BDC (128 bits) is composed of the first 128 bits of eleven consecutive 12 bit words. This data is loaded by the computer into eleven 12 bit registers located on the interface logic board. Once these registers are full, a command from the computer transfers 128 of these 132 bits into a 128 bit output register. The outputs of this register operate the high voltage column drivers. Each time a new row of data is transferred into the output register, a row counter (modulo 128) is incremented by one count. The state of this counter is then decoded by a 1 of 128 decoder to determine into which row the data will be written. Each of the 128 outputs of the decoder is connected to a separate high voltage row driver.

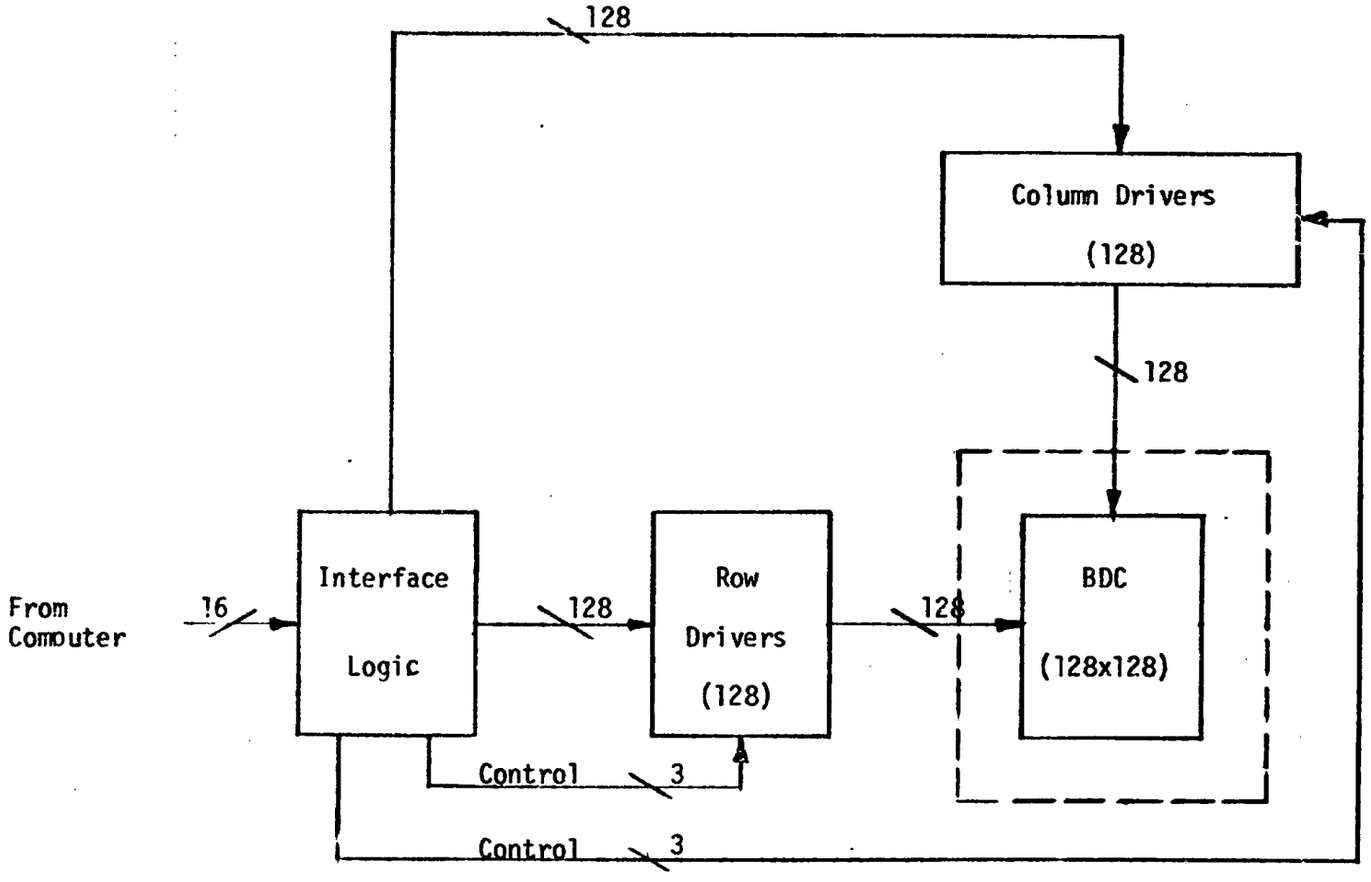

FIGURE 4-17. BLOCK DIAGRAM OF BDC ELECTRONICS.

Once all 128 rows of data are written into the BDC, the writing operation ceases and the interface logic circuitry forces all high voltage driver circuits to a standby status. The standby status is maintained while the hologram is being made. Once the page of data written into the BDC is recorded, the computer commands the interface logic to reset the BDC. This is done by first establishing a common ON state at all positions and then establishing an ERASED state (which is neither ON nor OFF). After this is accomplished the BDC is ready for a new page of data.

In order to switch the high voltages applied to each BDC row and column, upon command from the logic circuitry, high voltage driver circuits are necessary. Each driver circuit (Figure 4.18) employes a common base amplifier stage to provide up to 300 volts output from the 0 to +3 volts logic levels. A complementary emitter follower output stage gives sufficient output current to drive the capacitive BDC lines. Bootstrapping, via capacitor C_1, improves the rise time of the circuit so that both the rise and fall times of the output are less than 10 microseconds. During the erase cycle it is necessary to hold the outputs of all drivers either high or low. This is accomplished with the diodes D_2 and D_3. A logic high on the ERASE HI input forces the driver output high, and a logic low on the ERASE LO input forces the output low. Diode D_1 is used to clamp the output of the circuit to a voltage V_1 in the low state. This allows the output of the circuit to swing between two voltages V_1 and V_2 (where V_2 can be equal to $2V_1$).

The row and column driver circuits are identical in the BDC electronics unit. This allows interchangeable circuit cards to be used. The high voltage driver circuits are constructed on plug-in printed circuit cards with eight circuits per card. The row and column drivers are housed in

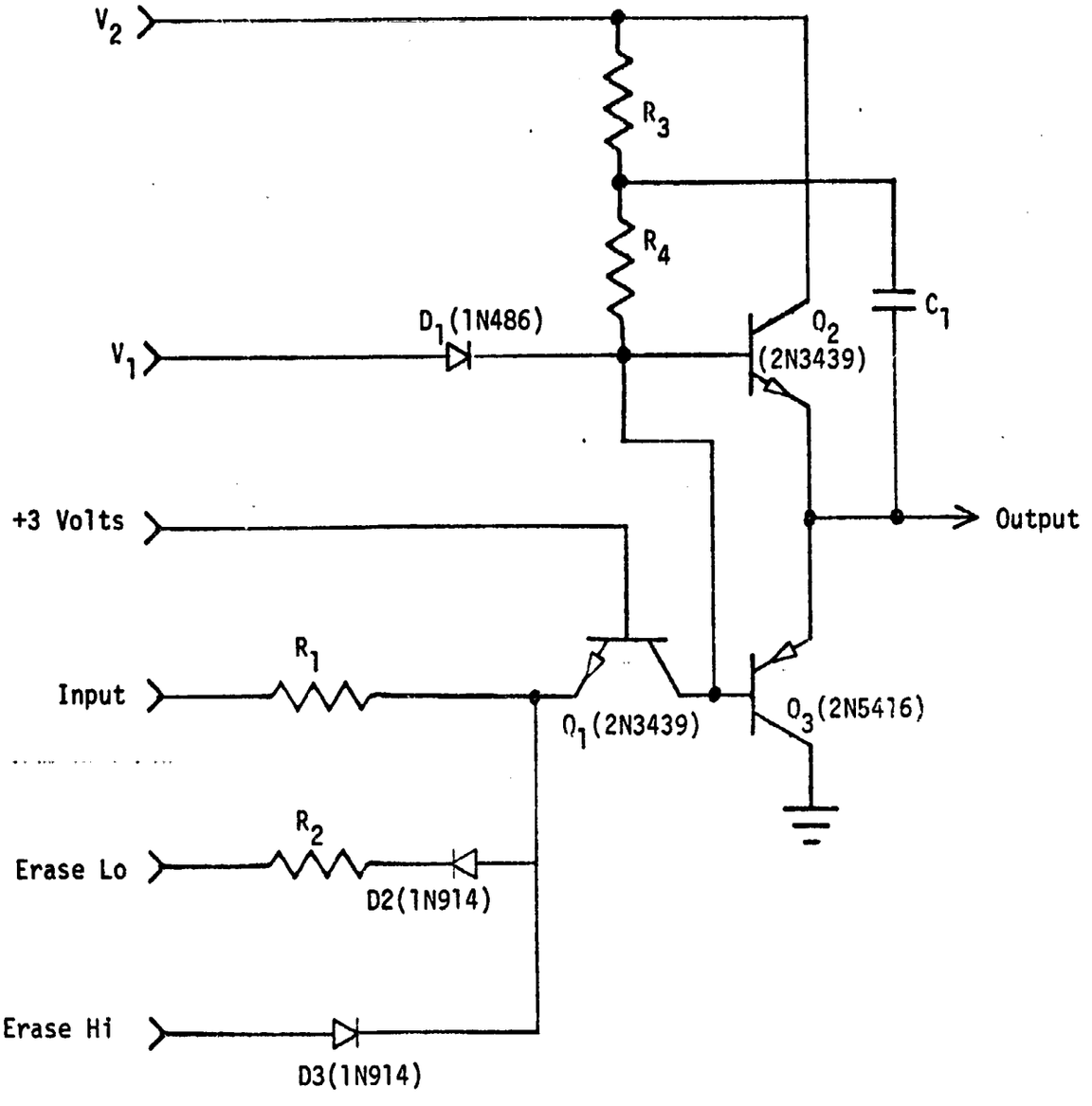

FIGURE 4.18. HIGH VOLTAGE DRIVER CIRCUIT FOR BDC ROWS AND COLUMNS

two separate card files with sixteen cards (128 drivers) in each card file. The two voltage levels are independently adjustable by controls on the front panel. Test terminals are provided on the front panel to monitor these voltages, as well as the logic supply voltage.

4.3.11 Summary of the More Signficant Problems. — The goals for a BDC with PLZT established at the beginning of this program were ambitious. Each goal had been separately achieved in laboratory test devices at Bell Telephone Laboratories, Sandia Laboratories, or in our own facilities (although test devices larger than about 10 mm square had not been reported). All of the goals had not been previously achieved in a single device.

The problem of half-select disturbance effects was considered in detail and solved by using a voltage-controlled excitation mode coupled with a modification of the drive circuitry. Control of thickness variation in thin polished PLZT plates received extensive investigations; improvements were made, but further improvements are required to improve the uniformity of contrast over the full BDC aperture. Although transparent electrode pattern generation with photoresist-etching techniques has been successfully demonstrated on small PLZT samples, fabrication of the full 128 x 128 device with 0.25 mm element center spacings has proved to be more difficult than anticipated because of the extreme fragility of the 50 mm diameter, 100 micron thick plates. Special procedures for handling these plates during processing and techniques for reducing the number of processing steps have been developed.

Electrical contact to transparent electrodes at the PLZT-Plexiglas interface has been improved by using thicker CR-Au tabs at the end of the

transparent electrodes; further improvement is anticipated. Bonding of leads to electrodes on PLZT has been demonstrated with indium solder, thermocompression, and ultrasonic bonding; indium solder bonds are preferred from a reliability viewpoint but are difficult to make to closely spaced electrodes (such as 20 mil center spacings for the 128 x 128 device).

An overall review of the problem areas indicates that improved fabrication techniques are required. It is clear that improvements can be made in all of these areas, but the degree of improvement which can be achieved is not yet known. In particular, thickness uniformities must be improved from the presently achievable ±10 micron levels to the required ±2 micron levels, while simultaneously maintaining uniformity of strain-bias in completed devices.

4.3.12 Conclusions.— The BDC performance goals for bit rate (10^6 bits/sec), switching voltages ($\leq$300 volts), and wavelength range have been demonstrated in a 32 x 24 element BDC. The optical efficiency goal (30 percent) has been exceeded in a 5 x 5 element BDC with In_2O_3:SnO_2 transparent electrodes. The contrast achieved with small test devices has reached 90/1, but 25/1 is a more typical value for the 32 x 24 devices; however, 50/1 contrast ratios are observed for some elements for which the parameters are optimized. The 100/1 contrast goal has not been achieved, but improvements in raw material and in PLZT polishing uniformity are expected to advance the present contrast levels toward this goal.

Fabrication difficulties have prevented the completion of 32 x 24 and 128 x 128 element BDC's which are operable uniformly at every element. Two 32 x 24 devices fully assembled and tested. Electrical access to the electrodes of the PLZT-Plexiglas interface was initially obtained for

21 of 24 lines on one and 17 of 24 lines on the other. Electrical access of all 32 upper lines was obtained. The test data in Figures 4.6, 4.7, and 4.8 were obtained with one of these devices after access to every other underside line had been lost as a result of a crack which formed near an edge of the pattern (transverse to the strain-bias axis).

We conclude that the BDC performance goals are achievable with PLZT with certain improvements in fabrication procedures and in PLZT raw materials. A tradeoff between polishing procedures and BDC contrast exists and should be examined carefully to determine whether the contrast can be reduced (thereby relaxing polishing constraints) without significantly affecting the performance of the system. Implementation of procedures for generating In_2O_3:SnO_2 transparent electrodes will assure that the desired optical efficiencies can be achieved. Refinement of electrical lead bonding procedures will shorten the device fabrication time considerably. Optimization of the thickness of Cr-Au electrodes, which mate at the PLZT-Plexiglas interface, and of the epoxy bonding procedure will improve electrical access to the underside lines. Techniques for improving the PLZT raw materials have been developed at Sandia Laboratories[15,16] and at Bell Telephone Laboratories;[26] our supplier (Honeywell) has improved its process recently and is implementing further improvements paralleling the Sandia process.

4.4 Photoplastic Recording Materials

4.4.1 Introduction. — Photoplastic materials are photoconductive thermoplastic media on which holograms are recorded as surface deformations. The materials are sensitized by a corona discharge to a positive or negative potential, exposed to visible radiation, and developed by heating to the flow temperature. Electrostatic forces produce deformations which are proportional to the light intensity used for exposure, and a stable hologram is formed if the photoplastic is cooled before surface tension of the plastic layer restores the original smooth surface. The hologram can be erased by heating the thermoplastic layer beyond the softening point. The surface forces restore the smooth surface and the materials are ready for a new recording cycle. The features of photoplastic which make it attractive for present holographic memories are (1) read/write/erase capabilities, (2) *in situ* recording, development, and readout, and (3) a virtually real-time recording cycle — typically less than five seconds.

In the sections that follow, we briefly review the mechanism of holographic storage and erasure in photoplastic materials, and consider the details of the materials preparation. We then describe the procedures and results of our investigations in sufficient detail to characterize the performance of photoplastic materials in a holographic memory system. Finally, the 5 x 5 hologram array suitable for use in the read/write mode of the system is described and representative results from such a device are presented.

4.4.2 Photoplastic Holography Process. — Photoplastic recording materials may be made with a number of different configurations on various substrates.[28-35] For the present we shall be concerned only with the configuration shown in Figure 4.19 which can be conveniently prepared. The substrate

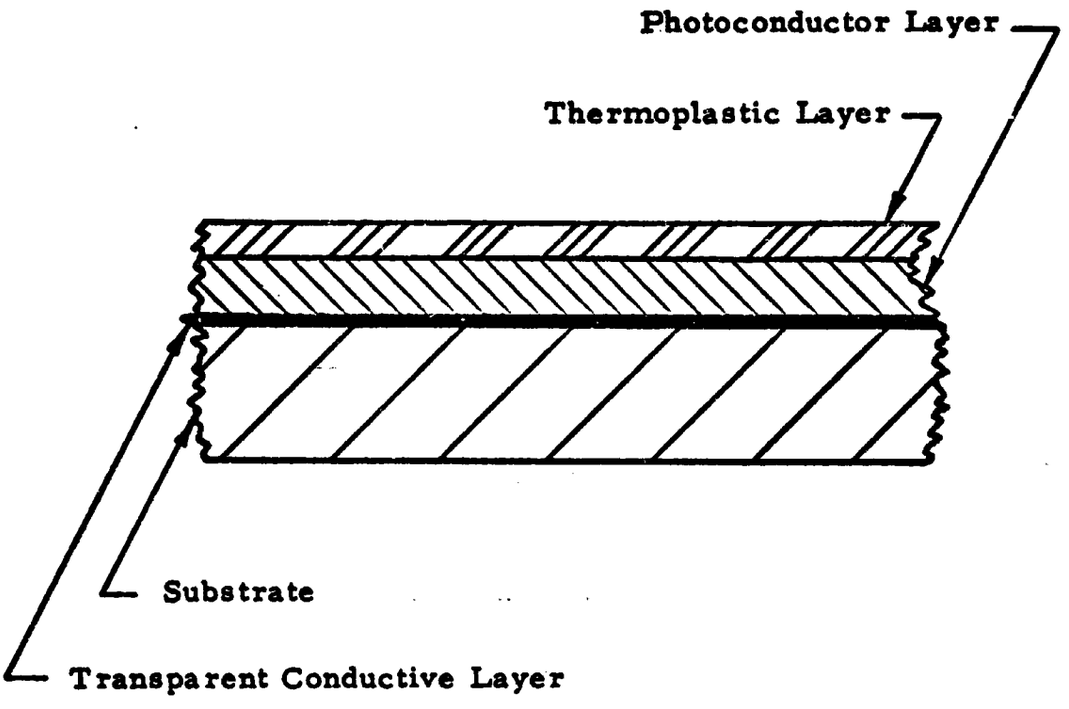

FIGURE 4.19 PHOTOPLASTIC STORAGE MEDIA CONFIGURATION

is an optical grade glass onto which a thin film of transparent conductor (generally tin oxide or indium oxide) has been deposited. The conductive layer is used for electrical heating and also for a ground plane for the charges deposited on the surface of the thermoplastic. An organic photoconductor layer is then coated on the transparent conductor and the top layer consists of a deformable thermoplastic layer.

A hologram is recorded in the photoplastic material as surface deformations corresponding to the spatial variations of the exposure pattern. The photoplastic holography process, which can be described with the aid of Figure 4.20, consists of four basic steps:

1. the recording medium is charged (in the dark) to a uniform potential by a corona discharge device,

2. the medium is exposed to light, causing a variation of the charge pattern on the photoconductor which corresponds with the variation of the illumination, and is recharged at those areas where the exposure has changed the electrostatic surface potential,

3. the medium is developed by raising its temperature to near the plastic point and then rapidly lowering the temperature to the ambient level; surface deformations proportional to the light intensity are produced, and

4. the recording is erased by raising the temperature level to near the melting point to even out the surface deformations.

In the first step the medium is prepared for subsequent recording. The corona discharge device, consisting of a thin wire (approximately 4 mils diameter) at a voltage of 3 to 10 KV and an electrically grounded shield, deposits a uniform charge distribution on the thermoplastic. After this sensitization step the recording material must be handled or stored in the dark. In the second step an exposure is made, and additional surface charge

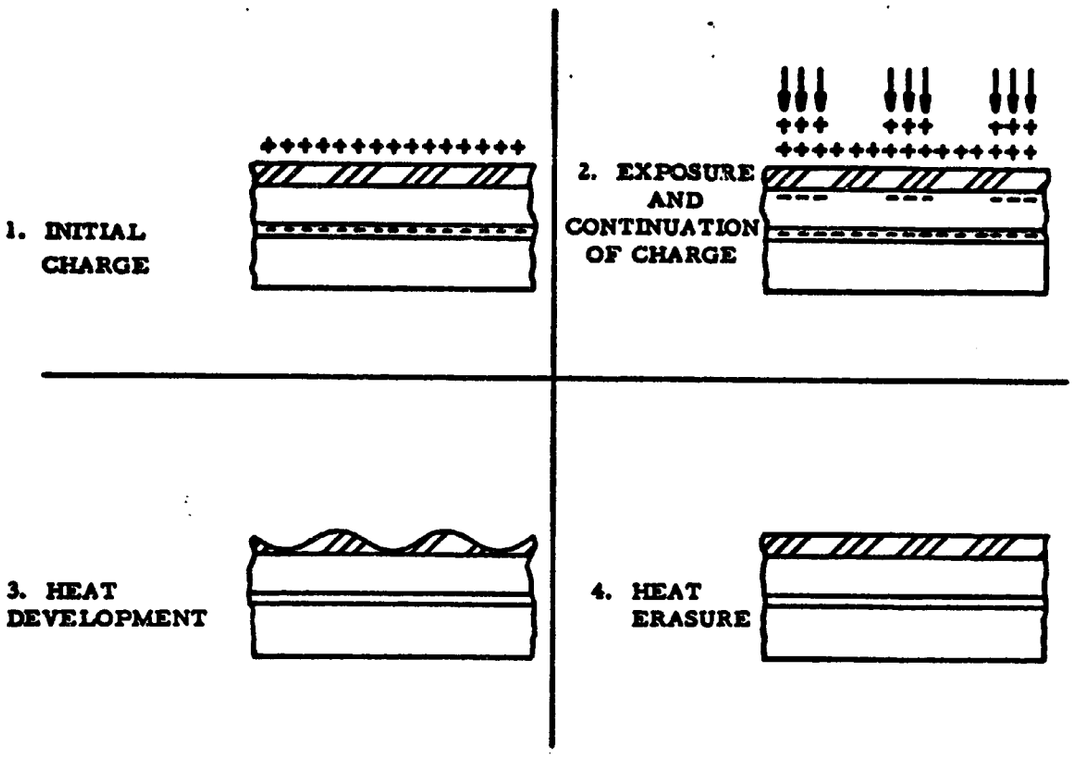

FIGURE 4.20 RECORDING-ERASURE CYCLE

is added to the optically exposed areas only; the amount of the additional charge is proportional to the change in the internal field during exposure and, therefore, to the impinging light pattern. Varying surface charge densities corresponding to the holographic light intensity pattern are thereby formed.

In the third step, the photoplastic medium can be developed, even in ambient light, by lowering the viscosity of the thermoplastic layer. The material then deforms in a manner related to the surface charge density distribution. To lower its viscosity, the temperature is raised to approximately 80°C. Rapid cooling to room temperature will result in a deformation which remains stable until intentional erasure. Heating is achieved by applying a voltage pulse across the conductive layer.

In the fourth step more heat than that used for developing is applied to the thermoplastic either by increasing the current in the pulse or by applying the same pulse for a longer period. Erasure usually neutralizes the electrostatic charges after which the recording process can be repeated.

4.4.3 Material and Sample Preparations. — The holographic technique for recording information places a number of requirements on the photoplastic materials. First, it must be sensitive to laser radiation. Second, it must scatter very little of the laser light. Third, it should have sufficient electrical resistance to prevent dissipation of the electrostatic charges before deformations can occur. Fourth, the transistion temperature must be reasonably low to enable deformation with practical resistive heating but high enough to prevent loss of deformations during storage. Finally, it must be resistant to thermal degradation. One material that satisfies most of these requirements is poly-n-vinyl carbazole (PVK) sensitized with trinitrofluorenone (TNF) photoconductor, used with wood rosin thermoplastics;

most of our experiments have been conducted with this material. In our investigations we used various forms of Staybelite thermoplastics; these included (a) conventionally hydrogenated wood resin, (b) Ester 10, which is a glycerol ester of hydrogenated resin, (c) Foral Ax, which is an acidic resin produced by hydrogenating wood resin to an exceptionally high degree, and (d) Foral 85 and 105, which are highly stabilized ester resins. The Foral resins have very high resistance to oxidation and to discoloration caused by heat and aging. More recently, we have begun testing other thermoplastic materials such as styrene-methacrylate and vinyl-styrene copolymers.

The substrate for the photoplastic device is typically a glass plate, coated with transparent tin oxide having a resistivity of 50 ohms per square. The substrate is etched with zinc powder and hydrochloric acid to leave isolated squares; these squares may range in size from 1 mm x 1 mm to 100 mm x 100 mm. Two silver electrodes along opposite edges of each square are used to connect the tin oxide squares to an electrical source which supplies the necessary current pulses to heat the squares. Development and erasure of a hologram is achieved by resistive heating; a pulsed 60 cycle voltage is applied across each square. We use pulse lengths 150 milliseconds and an average power of 20 watts for developing a 10 mm x 10 mm square area.

After chemical cleaning, the substrate is coated with a layer of organic photoconductor and a layer of thermoplastic; conventional dip coating techniques are used. To obtain a photoconductive solution suitable for coating, we mix the PVK polymer sensitized with TNF in a tetrahydrofuran solvent. The concentration of the solution and the rate of pulling are adjusted to give a coating thickness of 3 microns. The thermoplastic solution is obtained by dissolving the wood resin Stabelite in naphtha; the concentration and pulling rates are adjusted to give thermoplastic layer thicknesses ranging from 0.5 to 2 microns.

The substrate and component layers are then baked in an oven at 60°C for about an hour to evaporate the solvents. The coated plates are removed, cooled, and stored in dust free containers until used. Figure 4.21 is a photograph of a typical simple photoplastic device.

4.4.4 Experimental Procedure and Results. — We performed experiments to determine the exposure sensitivity, spectral response, diffraction efficiency, and signal-to-average noise ratio of various photoplastic samples. We also investigated techniques to extend the number of cycles of the photoplastic devices.

To measure the exposure and spectral sensitivity as well as diffraction efficiency, we recorded simple interference gratings by using plane waves for both the reference and signal beam. The four dominant wavelengths of the krypton laser were used to obtain the desired spectral response. During readout we measured the diffracted laser beam power P_d and the incident beam power P_i for different recording parameters. The diffraction efficiency P_d/P_i was then calculated from these measured values.

To measure the signal-to-average noise ratio we holographically recorded a diffusely illuminated transparency consisting of a bright square surrounding an opaque square center. The recording geometry was arranged so that each hologram contained approximately 10^5 bits per mm^2. In readout a photomultiplier scanner was used to measure the intensity of the signal and noise. The average noise was determined from a scan across the dark square and the average signal was determined from a scan across the bright area of the reconstructed image.

Representative results of these experiments are summarized in Tables 4.4, 4.5, and 4.6. In Table 4.4, we show the exposure sensitivity and diffraction efficiency as a function of wavelength. The results shown in the table were

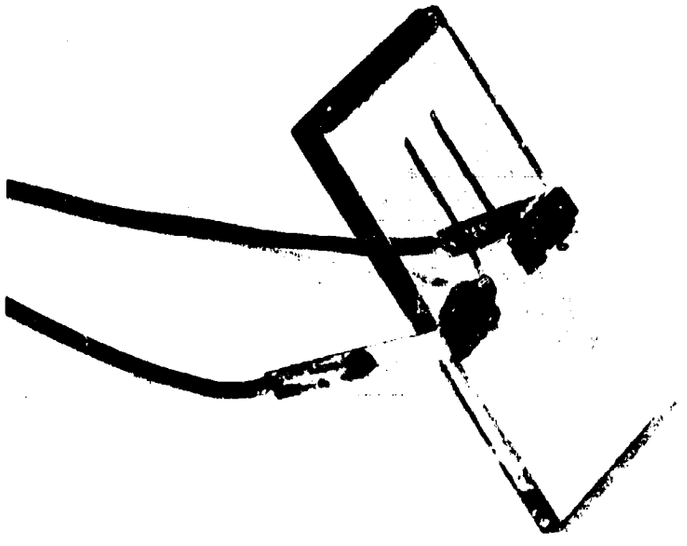

FIGURE 4.21 PHOTOPLASTIC DEVICE SAMPLE

WAVELENGTH	EXPOSURE	DIFFRACTION EFFICIENCY
647.1 nm		20%
568.2 nm		18%
520.8 nm	$75\mu J/cm^2$	16%
482.5 nm		12%

Table 4.4. Exposure and Diffraction Efficiency as a Function of Wavelength

REFERENCE BEAM / SIGNAL BEAM	DIFFRACTION EFFICIENCY	S/N
1:1	20%	16 dB
10:1	16%	15 dB
100:1	7%	14 dB

Table 4.5. Diffraction Efficiency and S/N as a Function of Reference Beam/ Signal Beam Intensity Ratio

SENSITIZER CONCENTRATION	EXPOSURE	DIFFRACTION EFFICIENCY	S/N
100:1	$1000\mu J/cm^2$	22%	16 dB
10:1	$75\mu J/cm^2$	20%	16 dB
2:1	$10\mu J/cm^2$	0.71%	3 dB

Table 4.5. Exposure Sensitivity, Diffraction Efficiency and S/N as a Function of Sensitizer Concentration

obtained with samples having a PVK to TNF concentration ratio of 10:1 and demonstrate that these photoplastic samples are panchromatic. We observed that, although an exposure of 75 $\mu J/cm^2$ is generally optimum, a broad range of exposures can be used. The diffraction efficiency decreases at shorter wavelengths. We believe that the reduction is caused by the TNF sensitizer which absorbs more of the shorter wavelength illumination and consequently reduces the diffraction efficiency.

Table 4.5 shows the diffraction efficiencies and signal-to-average noise ratio S/N as a function of reference beam-to-signal-beam intensities. To obtain these results we used a PVK to TNF concentration ratio of 10:1, exposure values of 75 $\mu J/cm^2$, and the red line of the laser. As shown, the reduction in the diffraction efficiency and S/N is relatively small with increasing reference-to-signal beam ratios. This provides great flexibility in the selection of input signals and recording parameters.

In Table 4.6 we show the effect of the PVK and TNF concentration ratio on exposure, diffraction efficiency, and S/N. Although the diffraction efficiency is somewhat lower, the 10:1 concentration ratio is obviously better for holographic recording because of its increased exposure sensitivity. Furthermore, we noted tht the recycling capabilities are poorer with the 100:1 concentration ratio.

We tested the recycling capabilities of the photoplastic samples and found that all of the samples had limited reusability — some better than others. Although many samples could be reused for over 100 cycles with adequate S/N ratio, some failed completely after only 50 cycles; in all cases the noise characteristics degraded the reconstructions as the number of record-erase cycles increased. We attribute this deterioration primarily to thermal degradation of the thermoplastic materials, and to some extent to dust which is attracted to the surface of the materials during the

development and erasure processes. The thermoplastic undergoes cross-linking as the number of cycles increase and causes the recording characteristics to become progressively more sluggish to the point of no response.

We also noted that erasure does not completely neutralize the electrostatic charges so that a latent image of an earlier recording appears in subsequent holographic recordings. This latent image tends to obscure the desired information and degrade the S/N of the reconstructed image. Furthermore, the latent image is particularly intense after the photoplastic material was reused a number of times, typically after 10 recordings. We have determined that the intensity of the latent image can be reduced with several erasure pulses rather than just one pulse. This technique, however, is not satisfactory because it extends the duration of the record-erase cycle, and is useful only for a limited number of cycles.

A better solution for the elimination of the latent image is to charge the photoplastic during application of the erasure pulse. We hypothesize that this addition of charges during erasure eliminates the residual surface charge from earlier recordings and leaves a uniform charge distribution at the surface. We also determined that this technique produces more consistent results when the erasure is made using a longer pulse with the same voltage as the development pulse rather than at a higher peak voltage. This erasure technique was tested with several photoplastic materials. The testing sequence for recording and checking for latent image was to expose-develop-erase-develop, measure the intensity of the image, and then repeat the cycle. We found that with this technique no latent image could be observed even after 100 recordings.

We determined that a stationary corona device can uniformly charge the surface of the thermoplastic and be active during the entire sequence of exposure-development without adversely affecting the holographic recordings. The amount of surface charge is controlled either by varying the spacing between the corona device and the photoplastic surface or by varying the

voltage applied to the corona device. A simultaneous, rather than sequential, charge-exposure-recharge mode eliminates the need for switching networks to control the charging mechanism and simplifies the recording procedure.

We also observed that the exposure sensitivity is a nonlinear function of the surface charge deposited by the corona device. In particular, by increasing the surface charge by 50 percent, the exposure sensitivity was increased by a factor of 5. However, an increase of the surface charge corresponds to an increase of the scattering noise. Because the noise is generally a more serious problem than sensitivity, the surface charge should be kept at a relatively low level.

Finally, we determined that a practical operating sequence for recording each hologram is to (a) energize the corona discharge device, (b) apply an erasure heat pulse for 500 milliseconds, (c) pause to allow cooling of the substrate, (d) expose, (e) pause to allow recharging of the photoplastic surface, and (f) apply a development heat pulse for 150 milliseconds. The duration for the entire sequence is about 5 seconds.

4.4.5 Hologram Array and Mounting Fixture. — The array for recording 25 independent holograms is shown in Figure 4.22. The storage geometry is a 5 x 5 array of independent holograms, each capable of storing 1.6×10^4 bits for a total capacity 4×10^5 bits. Each hologram pad is electrically isolated from all other pads to allow for thermal development and erasure of each hologram without adversely affecting its neighbor.

The substrate for the array is a glass plate with a transparent conductive coating of indium oxide. The substrate is etched with zinc powder and hydrochloric acid to leave a 5 x 5 array of isolated 4 mm by 3 mm rectangular pads. The center spacing between adjacent pads is 5.5 mm. Aluminum electrodes are deposited through a mask, forming the electrode

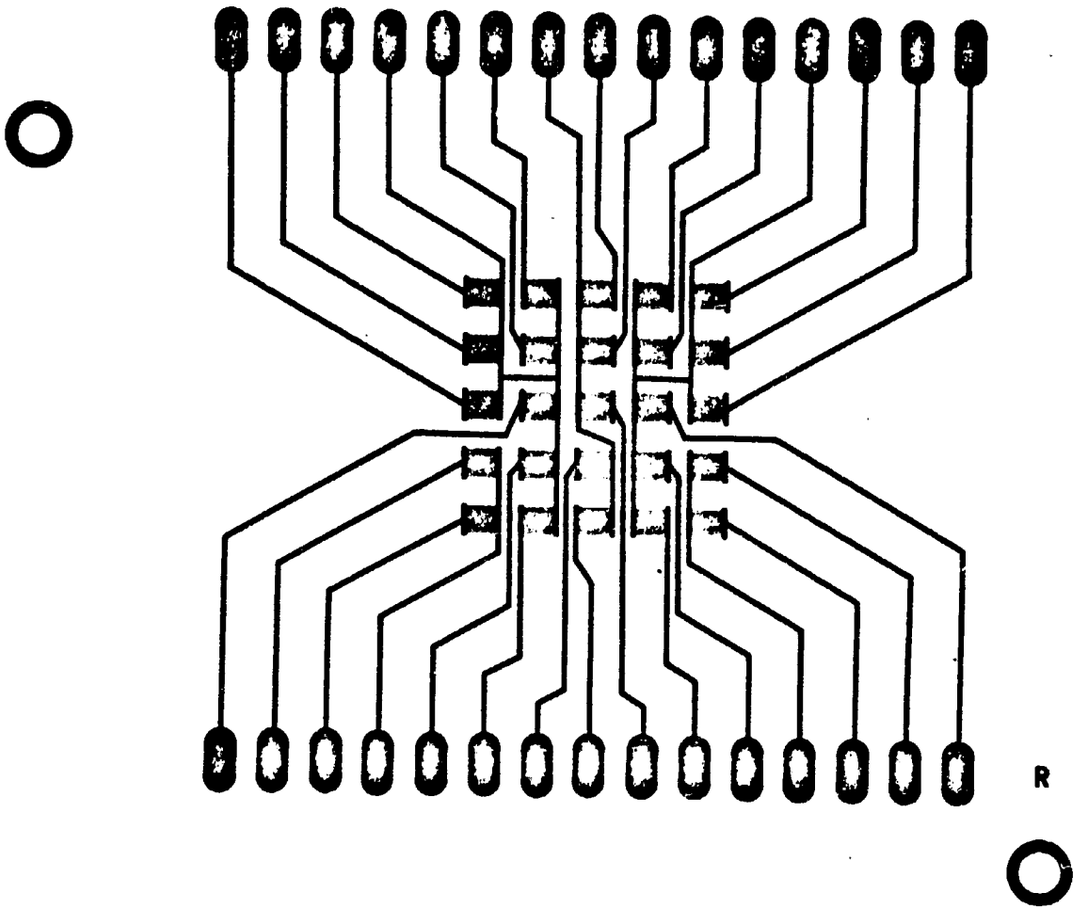

FIGURE 4-22. GEOMETRY OF HOLOGRAM ARRAY

structure shown in Figure 4.22. There is one electrode common to each row of pads and 25 independent electrodes for controlling each pad separately. The width of each electrode is 0.5 mm, leaving a workable aperture of 3 mm x 3 mm, larger than the required hologram aperture. The electrodes are wired to a 25 position selecting switch for electrically addressing each pad. The prepared substrate is coated with a photoconductive layer of 2 microns and a thermoplastic layer of .7 micron.

We initially tested the performance of the array with the experimental setup shown in Figure 4.23; the setup and input data are similar to those of the final memory system. In this recording arrangement a modified near-Fourier transform approach is used. The signal beam is modulated by an input data transparency consisting of an array of dots on a black background. The lens system is used both as an imaging lens and a transform lens. As an imaging lens it projects an image of the original input onto a plane where a photodetector array may be located. As a transform lens it forms the Fourier transform of the input data in the vicinity of the recording medium. The pattern created by the interference of the transformed signal beam with the reference beam, both derived from the same laser, is recorded to form a hologram. In readout, the hologram is illuminated with a replica of the reference beam. Representative samples of our results are shown in Figure 4.24. The upper left photograph shows a magnified portion of the original input transparency. The upper right photograph shows the reconstructed image after 15 cycles, the lower left shows the reconstructed image after 55 cycles, and the lower right shows the reconstruction after 105 cycles. As is evident from these results, the S/N decreases significantly as the number of cycles increases.

We also demonstrated that it is possible to record and readout successive holograms with little or no interaction between them. Figure 4.25 shows successive reconstructed images from one sample. These images were obtained from the 14, 15 and 16 cycles. As is evident, the effect of latent imagery is negligible.

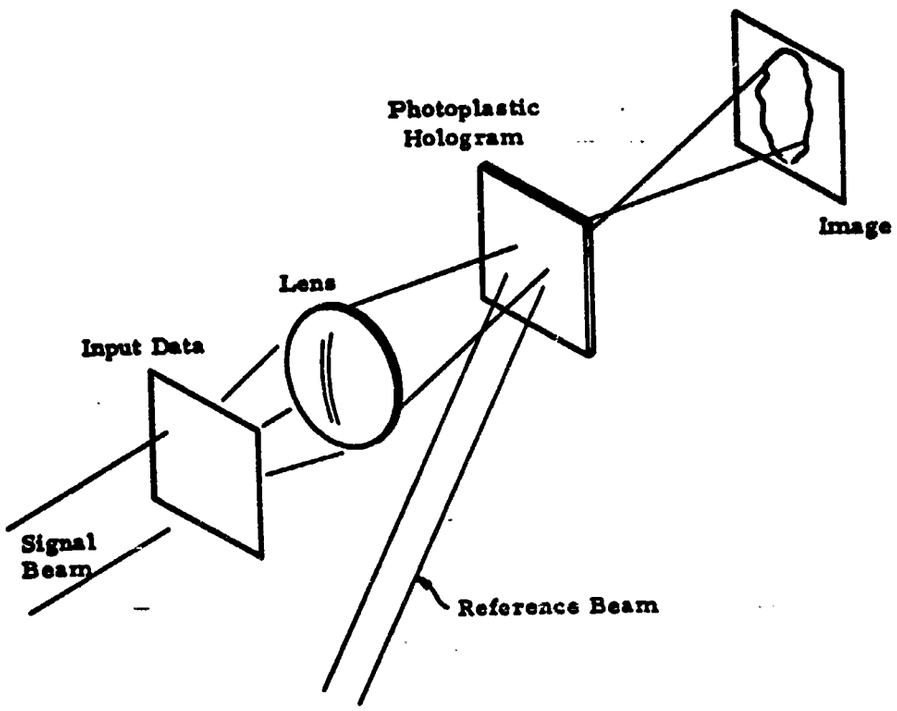

FIGURE 4.23 HOLOGRAM RECORDING ARRANGEMENT

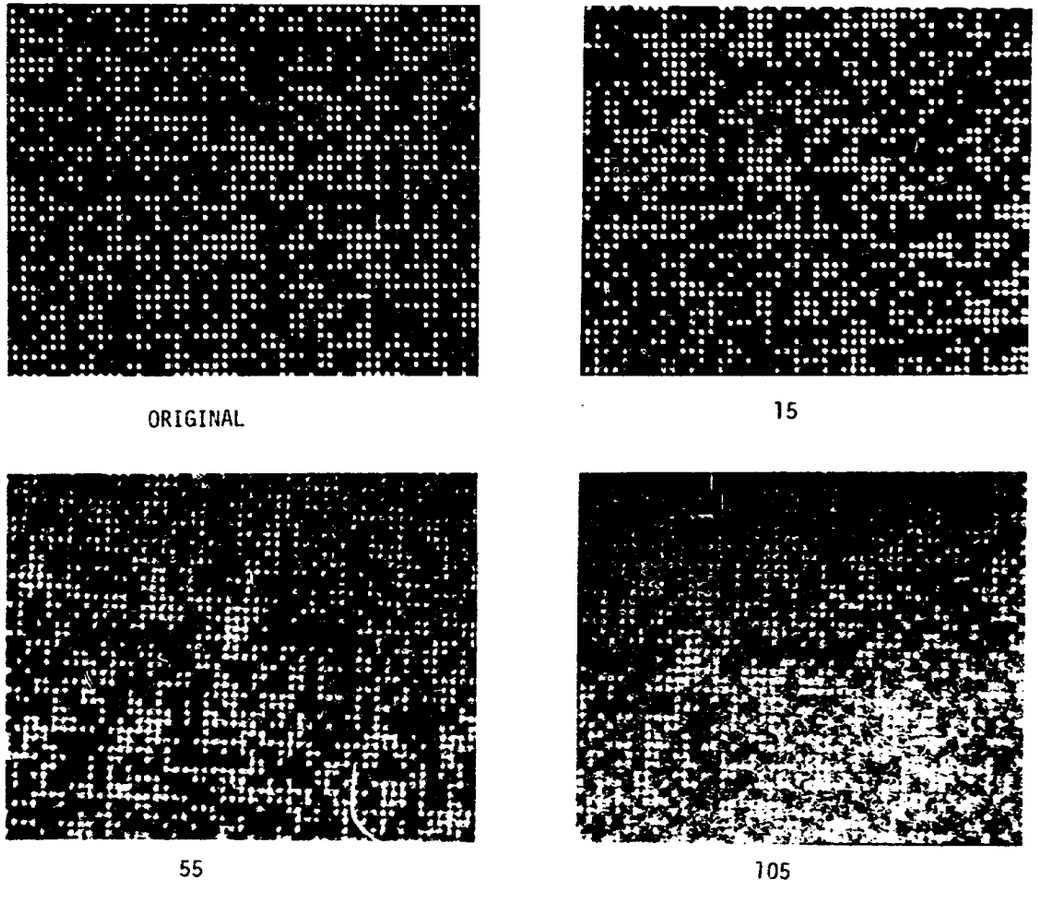

FIGURE 4.24. PHOTOGRAPHS OF ORIGINAL AND RECONSTRUCTED IMAGES FROM HOLOGRAMS AFTER 15, 55, and 105 CYCLES

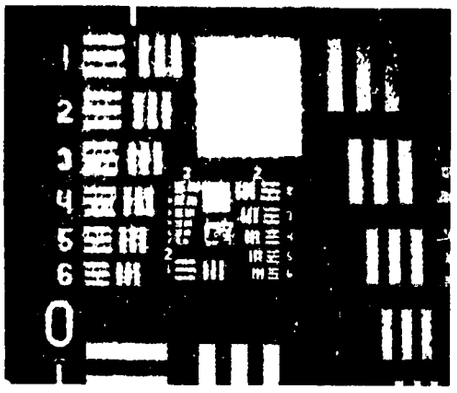

14

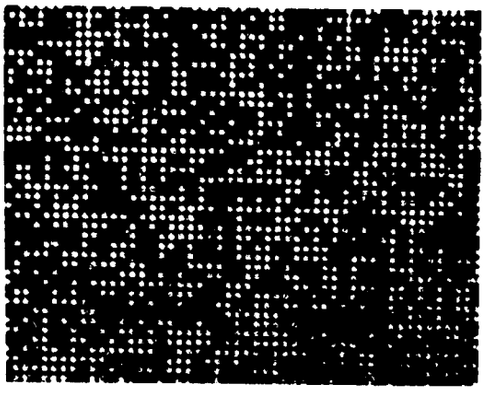

15

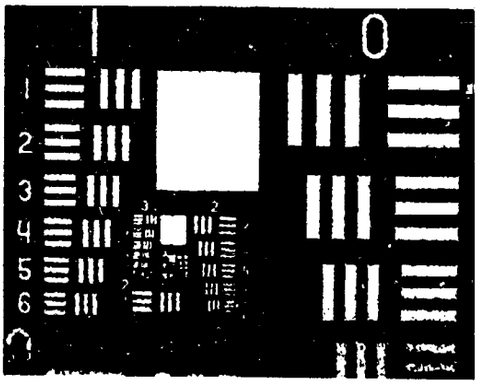

16

FIGURE 4.25. PHOTOGRAPHS OF RECONSTRUCTED IMAGES FROM HOLOGRAMS AFTER 14, 15, and 16 CYCLES.

The design of the mounting fixture is described with the aid of the line drawing shown in Figure 4.26. The major parts of the fixture were machined from polycarbonate, a translucent dielectric material. The holographic recording plate, inserted into the rear of the fixture, is accurately located with three registration pins and is secured to the fixture body with the two large clamps. The clamps also apply pressure on the recording plate for better contact with the beryllium copper prings which are used to connect the heating voltage to the hologram array electrodes.

The corona discharge device, consisting of a single loop of 4 mil diameter wire and an electrically grounded shield, is mounted in the front part of the fixture. It is secured in place with a front plate and 6 screws.

Photographs of the front and rear of the finished mounting fixture and hologram array are shown in Figure 4.27. The wires along the top and bottom of the fixture are used to connect the hologram array to an a.c. power source. The two heavy wires protruding from the center of the fixture are used to connect the corona discharge device to a 7KV d.c. power supply.

During the last part of the contract period we tested the performance of the photoplastic array and mounting fixture in the deliverable test bed. Although the results of these tests are generally similar to those shown in Tables 4.4, 4.5, and 4.6 and Figures 4.24 and 4.25, we encountered a number of difficulties. In particular, we found that the charge distribution over the entire array is not uniform and that the resistance and size of some pads differ significantly. To overcome these difficulties and to optimize the holographic performance of every component holograms, each pad of the array should be calibrated in terms of charge, exposure, and heating voltage. We have gone through a calibration routine with one array and successfully recorded good holograms on each pad. Typical diffraction efficiencies were in the range of 1 to 3 percent with S/N ratio around 10 dB.

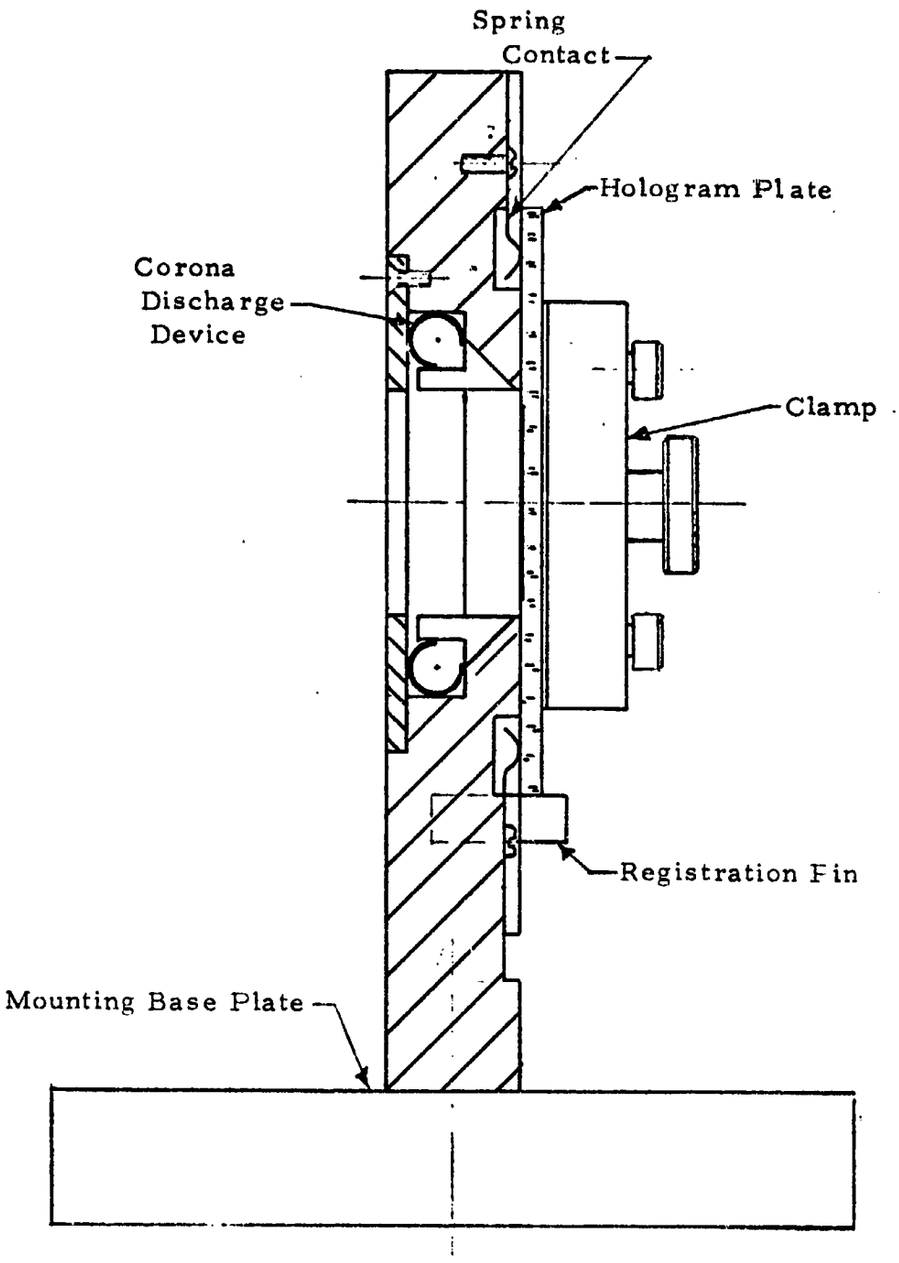

FIGURE 4.26: MOUNTING FIXTURE FOR HOLOGRAPHIC STORAGE MATERIAL

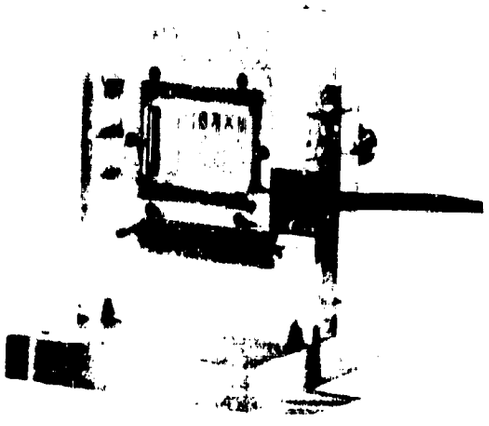

(a)

Front View

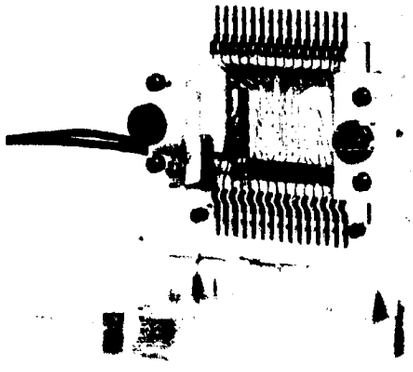

(b)

Rear View

FIGURE 4.27. MOUNTING FIXTURE & HOLOGRAM ARRAY

4.4.6 Photoplastic Array Drive Electronics. — When recording holograms on the photoplastic material we require charging of the surface and heating of the resistive pads to develop the surface relief. Erasure of a hologram requires heating the pad to a temperature which allows the charge to dissipate and eliminate the surface relief. Cooling after recording or erasing fixes the recording. We discuss the sequence of operations for the array by referring to Figure 4.28 which shows the block diagram of the array circuits.

The initiation and duration of the charging and heating cycles are controlled from the operator console (TTY). Charging is initiated and terminated under control of a set/reset flip flop in the controller. The flip flop (through a buffer) controls the gating on of a triac which is a bidirectional alternating current switch. The switch is in the primary circuit of a high voltage transformer which is, in turn, connected to the charging wire encircling the array. The voltage amplitude is controlled by a variac in the primary circuit. The primary charging voltage is adjusted to the recommended voltage for the array using the panel meter. Setting the primary voltage to 50 volts rms provides approximately 5000 volts rms at the array. When operating properly, a dull blue glow can be observed around the array charging wire.

A fuse in the primary circuit protects against overload and damage to the circuits. Dust particles in the air can occassionally cause flashovers to the array which cause no damage. Extreme caution should be used when touching the array since the charging voltage is at 5000 volts. It is recommended that the primary voltage leads be disconnected from the charging control box when changing the array.

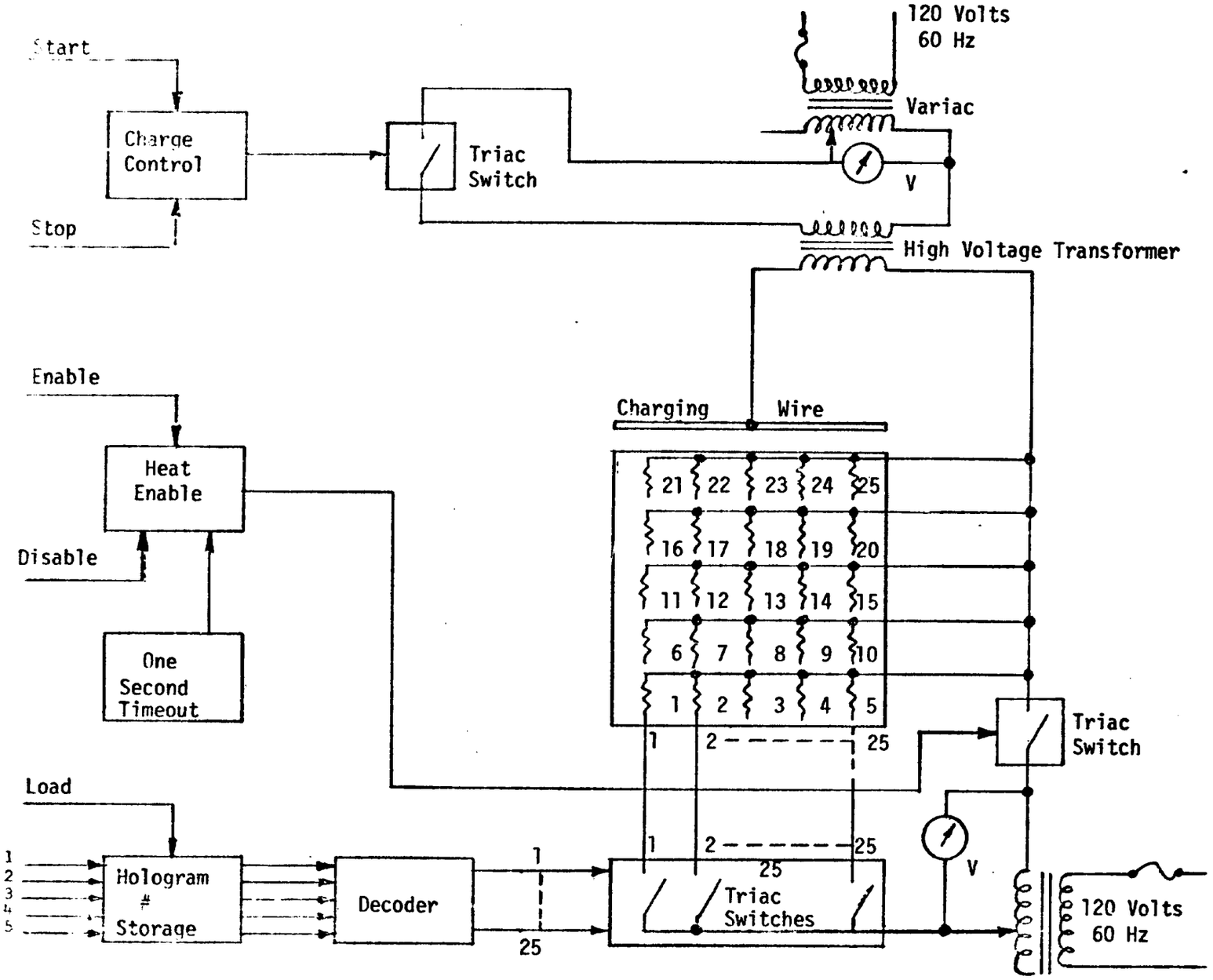

4.28. PHOTOPLASTIC ARRAY CONTROL

Each of the 25 hologram positions on the photoplastic array has an underlying resistive pad. Twenty-five triac switches provide an alternating current connection to one end of each pad. The other ends of the pads are all interconnected to the alternating current return through a single triac switch, which enables the heating operation.

The hologram number, between one and twenty-five, selected by the operator is stored as a binary number in the controller. After decoding the binary number, the triac associated with the proper pad is selected and gated on. The start and duration of the heating is controlled by an enabling flip flop which gates on the triac in the a.c. return. The voltage is controlled by a variac which is adjusted using the panel meter to the recommended voltage for the array. An array with 300 to 400 ohm resistive pads is heated with approximately 30 volts rms. An automatic disable of the heating after 1 second, through the use of a one shot multivibrator, prevents the operator from overheating pads on the array and destroying them. A fuse is provided in the primary circuit to protect the circuits against overloads.

4.4.7 Recording Materials for Read-Only Memory. — In the early part of the current contract we investigated the recording of composite holograms in thick materials. A composite hologram is comprised of two incoherently added holograms, each of which is recorded and independently retrieved with a different illumination wavelength. As the work on the contract progressed it became apparent that the available photodetector sensitivity is inadequate to detect the various bits in the holographically reconstructed imagery from the composite holograms.

To overcome this deficiency we decided that in addition to the composite holograms, whose diffraction efficiency is inherently low, we should also deliver simpler holographic arrays. In the simpler arrays only one hologram is recorded per storage location so that more efficient recording materials such as dichromated gelatin can be used. Some of

the more efficient arrays can be used with the available photodetectors for readout whereas the composite hologram arrays require more sensitive photodetectors which will be available in the future.

4.4.7.1 Thick Recording Materials. — For holograms recorded in thin media, a change in the readout beam angle or wavelength generally results in aberrations, distortions, and a displacement of the reconstructed image. The intensity of a diffracted image is relatively constant over a wide range of angular orientations and illumination wavelength changes. Thus, when a multiplicity of images are holographically stored in one location, we cannot selectively readout one hologram without interacting with the others. Such interacting causes degradation of the SNR of any one reconstructed image.

For holograms recorded in thick media, however, a change in the direction or wavelength of the readout beam also produces a change in the diffracted intensity from the hologram. These parameters can therefore be used to construct a composite hologram which stores a multiplicity of images, each image stored uniformly throughout the recording medium. We have favored wavelength discrimination techniques over angular discrimination techniques for multiple storage of holograms in the memory because they lead to relatively simpler addressing schemes.

A measure of the wavelength discrimination is the wavelength bandwidth between the half-power points on the curve of the diffracted intensity versus readout wavelength. An expression for this bandwidth was derived by adopting X-ray diffraction and is given[36]

$$\Delta\lambda_{1/2} = \frac{\left(\frac{\ln 2}{\pi}\right)^{1/2} \lambda^2 (n^2 - \sin^2 \theta_s)^{1/2}}{t_o \left[n^2 - (n^2 - \sin \theta_s)^{1/2} (n^2 - \sin^2 \theta_r)^{1/2} + \sin \theta_s \sin \theta_r\right]}$$

where n is the average index of refraction of the recording medium, t_o is the thickness, λ is the wavelength of the illumination, and the incidence angles of the reference and signal beams relative to the hologram are denoted by θ_r and θ_s, respectively. This equation can be used to calculate the wavelength discrimination and as a function of reference beam and signal beam orientations.

As an illustration, consider the following parameters which were used in recording two superimposed holograms, one recorded at 488 nm and the other at 647.1 nm:

$$n = 1.49$$
$$\theta_s = 0$$
$$\theta_r = 30°$$
$$t_o = 35 \text{ microns}$$

By inserting these values into the wavelength discrimination equation, we find that $\Delta\lambda_{1/2} = 37$ nm for $\lambda = 488$ nm and $\Delta\lambda_{1/2} = 65$ nm for $\lambda = 647.1$ nm. These values imply that, with an emulsion thickness of 35 microns, there should be adequate suppression to discriminate between the two holograms. If the emulsion thickness were 15 microns (a typical value for a thin emulsion), the corresponding wavelength discrimination would be $\Delta\lambda_{1/2} = 86.33$ nm for $\lambda = 488$ nm and $\Delta\lambda_{1/2} = 151.67$ nm for $\lambda = 647.1$ nm. Note that these wavelength discrimination values are comparable to the difference between the two recording wavelengths; this confirms the statement that the wavelength discrimination is not adequate for thin emulsions.

To demonstrate how the effective memory capacity is increased and to simulate the readout characteristics of storage materials that we expect to use in more advanced system, we are delivering hologram arrays which are recorded in thick (35 microns) nonerasable materials. Specifically, each array has 20 x 20 storage locations, each of which is comprised of two incoherently added holograms, for a total of 800 holograms.

The hologram arrays were recorded on the feasibility test bed system. Before recording these arrays the 5 x 5 lenslet array used in the signal path for read/write operation was replaced with a 20 x 20 lenslet array and the reference beam was expanded to cover all 20 x 20 hologram locations simultaneously. The size of each hologram is approximately 1 mm square; their separation is approximately 1.5 mm. One of the holograms at each storage location was recorded with the 488 nm wavelength derived from the argon laser and the other hologram was recorded with the 647.1 nm wavelength derived from the krypton laser. To distinguish between the reconstructed images from the two holograms, we have purposely blocked a few bits in one corner of the input signal prior to recording the component hologram with the 488 nm wavelength. Otherwise the reconstructed patterns from all the holograms in the array are identical.

To cover a wide range of quality and bit densities in the reconstructed patterns, we have recorded several hologram arrays in both thick absorptive and thick phase materials. Two input data masks were used; in one mask 10% of the bits in a 128 x 128 data mask were activated and in the other mask 50% of the bits in a 128 x 128 data mask were activated. All holograms were recorded on special Kodak 649F photographic plates with an emulsion thickness of 35 microns; subsequently some of these hologram

arrays were bleached to provide greater diffraction efficiencies from the holograms. The diffraction efficiencies range from 0.1 percent to 4 percent and the S/N ratio ranges from 5 dB to 20 dB.

4.4.7.2 Thin Recording Materials. — To more adequately test the various components of the test bed system by providing greater diffraction efficiencies and better S/N ratios, we have also recorded a series of simple 20 x 20 hologram arrays, each with only one hologram per storage location. The recording arrangement was identical to that described in the previous section, except that only one wavelength was used to record each hologram array.

Several hologram arrays were recorded in both absorptive and phase materials; for the absorptive holograms we used conventional Kodak and Agfa photographic emulsions with 15 micron thicknesses, and for the phase holograms we used either bleached photographic emulsions or dichromated gelatin materials. The holograms recorded in dichromated gelatin materials were of the highest quality in terms of their diffraction efficiencies and S/N ratios. Since dichromated gelatin is only sensitive to 488 nm illumination wavelength we used the less efficient photographic emulsions when recording at 647.1 nm.

Three input data masks were used; in one mask 32 x 24 bits correspond to a completely active photodetector array, in the second mask only 10% of the bits of the 128 x 128 random array were activated, and in the third mask 50% of the bits in the 128 x 128 array were activated, The diffraction efficiencies and S/N ratios of reconstructed patterns from the absorptive and bleached photographic emulsions ranged from 0.1 percent to 8 percent and from 5 dB to 20 dB, respectively. The

diffraction efficiencies and S/N ratios of reconstructed imagery from the dichromated gelatin holograms ranged from 1 percent to 15 percent and from 8 dB to 20 dB, respectively.

The various hologram arrays in this series could be used to test the registration accuracy of each reconstruction with the photodetector array as a function of hologram positions. Furthermore, these arrays could be used to test the sensitivity of the photodetector array as a function of holographic efficiency and S/N ratio in the output. Finally, these arrays could be used to determine the read-only error rates of the overall system.

4.5 Photodetector Array

The photodetector array (PDA) detects the optical bit pattern reconstructed from a hologram and generates an electrical signal that represents the original stored data. Since fully populated arrays (128 x 128 elements) having approximately 250μ center spacings are not commercially available, the contract requirements are to supply a partially populated array that can be used to test the performance of the memory.

The photodetector array originally specified for use in the memory became unavailable due to a reorganization at Fairchild Semiconductor. During the first quarter of this contract we tested a beam lead PDA manufactured by Texas Instruments. The partial array used in these tests consisted of a single column of phototransistors which had all collectors connected in common to a positive voltage supply through a load resistor of 1.3 KΩ. Each phototransistor was addressed by grounding the emitter.

Each photodetector was illuminated with 20 nanowatts of laser power at 6328Å which corresponds to the power available if we assume a hologram efficiency of 1% and a laser power of 30 mw. Each device was allowed to store charge for 1024 μsec before being read out. With a load resistance of 1.3KΩ a minimum discharge time of 32 μsec was obtained. Typical photosignals are 40 to 80 mv for 20 nanowatts/bit of optical power. These are adequate signal levels for detection using standard core memory sense amplifiers.

Based on the results of these tests, we ordered a two-dimensional PDA in a 32 x 24 element format. The photodetector array consists of 32 rows x 24 columns of photosensitive transistors connected as shown in Figure 4.29. The collectors are connected by columns and the emitters by rows; the bases are not accessable. The common emitter rows are spaced at 0.040", the common collector columns at 0.050", and the whole array is covered with a

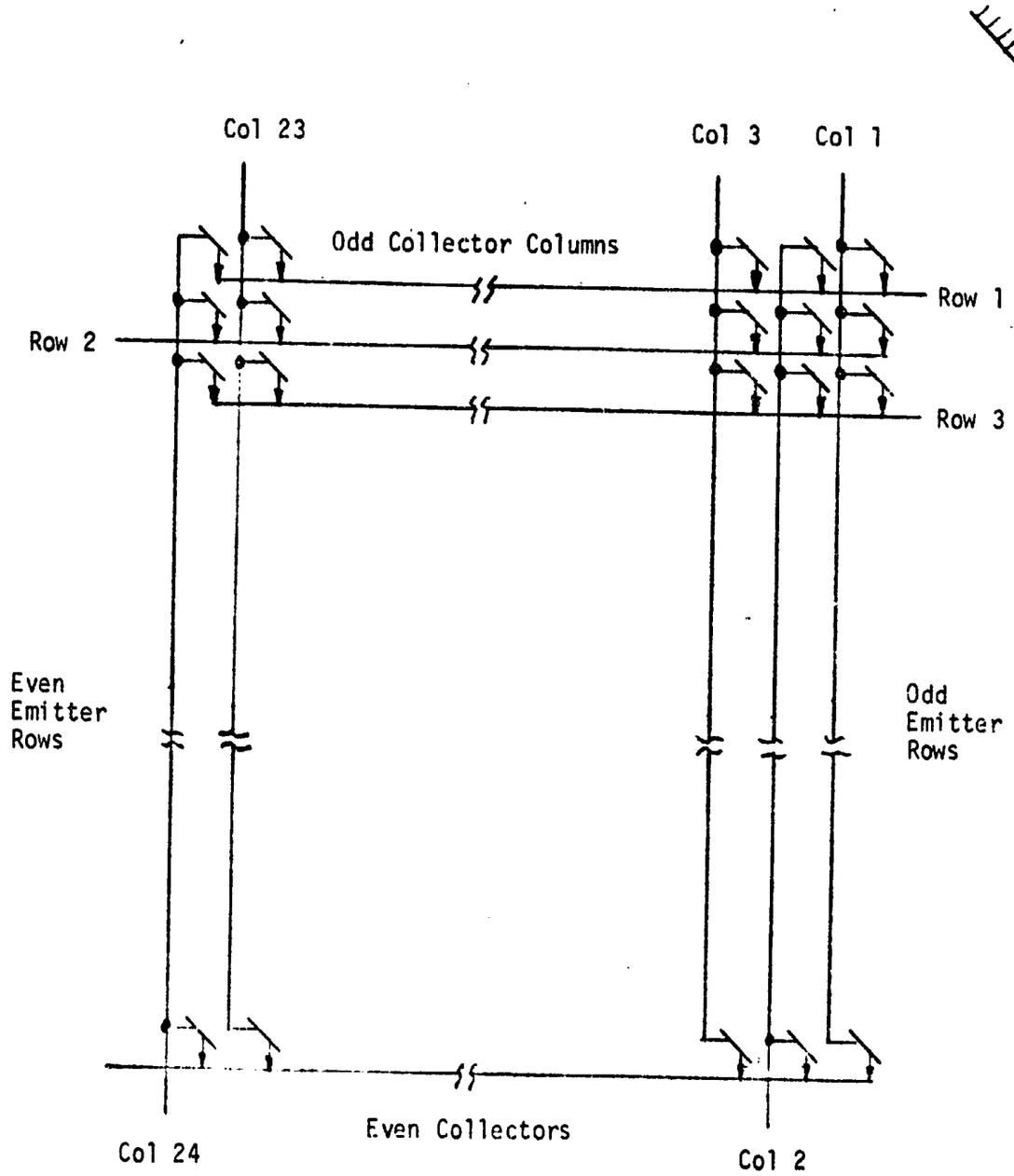

FIGURE 4.29. PDA INTERNAL CONNECTIONS

silvered mask. The mask has 6 mil diameter holes placed at the transistor centers and has the effect of selecting every fourth bit in one direction and every fifth bit in the other direction in a 128 x 128 bit array. The whole array is mounted on an x-y adjustable stand, where x and y are both at 45° to the plane of the optical bench. The array can thus be finely positioned in the hologram image plane to read out any group of 32 x 24 bits defined by the PDA mask. Figure 4.30 shows the array.

4.5.1. Mode of Operation. — The photosensitive transistors (PST's) in the PDA are used in their charge storage mode. In this mode the transistors are illuminated for a relatively long period of time, called the integration time (T_i), and then charged during a much shorter time, called the charge time (T_c). Only during the charge time are the transistor circuits complete, so that during the integration period all light falling on the PST's is integrated. The ratio of these times gives a gain figure G_T which enables very low light levels to be observed.

The associated electronics provides the sequencing of T_i and T_c pulses to the emitter rows and senses the resulting outputs from the collector columns. Each common collector column will exhibit 32 bits of information during a complete read-out period corresponding to the illumination on the 32 transistors in that column. This timing sequence is shown in Figure 4.34. The result is 32, 24-bit words corresponding to the 32 x 24 bit-pattern illumination on the PDA.

4.5.2 Performance. — The performance of the array has fallen short of that predicted from the original test samples. The level of sensitivity required has always been defined from the requirement that a 20 nw signal can be detected with a 30:1 signal-to-noise ratio. In practice, this level of signal will generate a waveform such as that illustrated in Figure 4.31, where it can be seen that at least 50 mV of signal is available for detection.

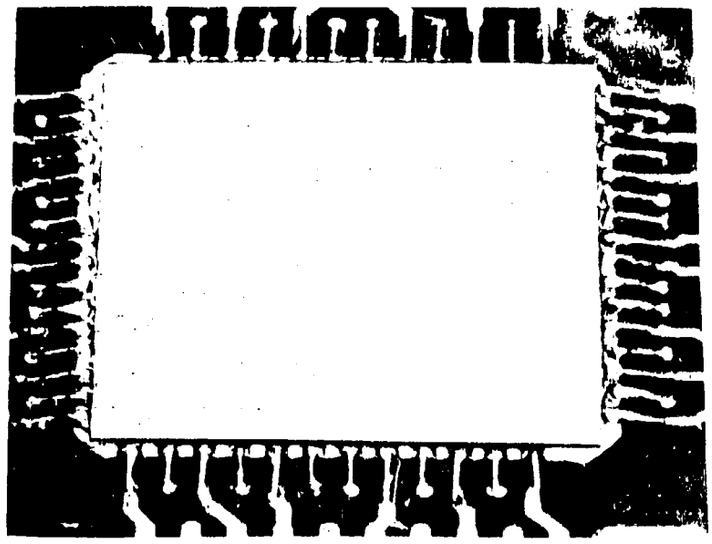

FIGURE 4.30. PDA

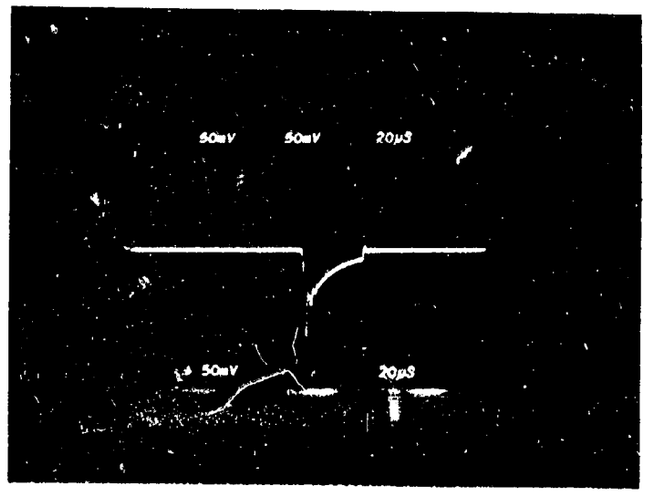

FIGURE 4.31. COLLECTOR OUTPUT OF SINGLE PHOTOSENSITIVE TRANSISTOR; TOTAL ILLUMINATION = 20 nw, INTEGRATION TIME = 1 mS, λ = 6328. (ORIGINAL T.I. SAMPLE)

The full 32 x 24 array has fallen far short of this specification. To obtain such a waveform an illumination of at least 200 nw and an integration time of 10 ms is required. Any attempt to increase the integration time beyond 10 ms results in an inordinately large level of system noise. This noise is not thermal dark current in the normal sense but integrated leakage current. Operating at 20 nw, virtually no signal is apparent and any attempts to amplify these small signals would give rise to poor signal-to-noise ratios. There is no way of artifically increasing the sensitivity of the array. Also the DC response of the new array is vastly different from the DC response of the original samples (Figure 4.32).

This failure to meet specification would not have occurred if the transistors used in the array were identical to those original samples. Evidently some important differences exist between the two sets of PST's as indicated by the DC response, but the critical difference must be a difference in C_{BC} and C_{BE} between the samples. The addition of other common collector columns may have some effect also.

4.5.3 Photosensitive Transistor Analysis. — Each transistor in the array may be modeled as follows:

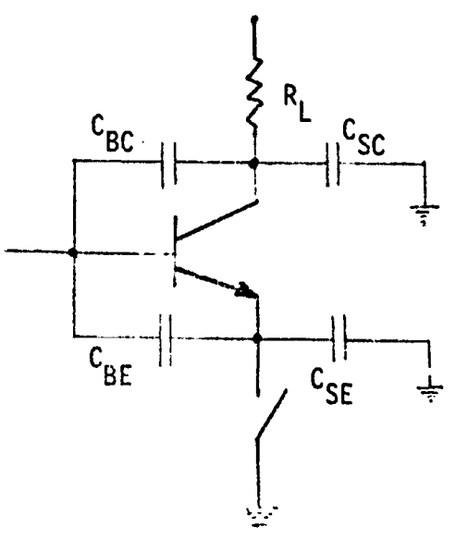

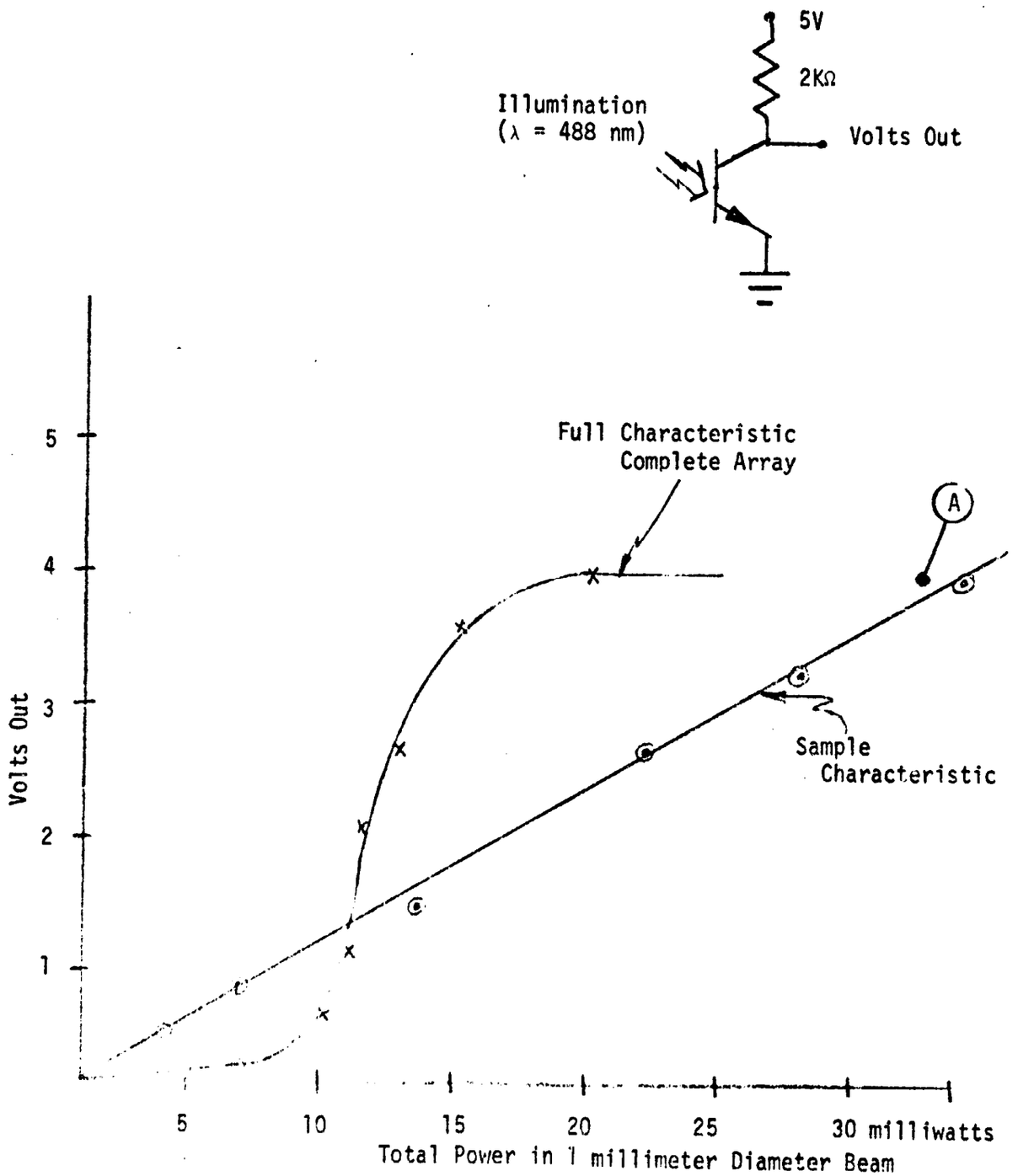

FIGURE 4.32. D.C. CHARACTERISTICS OF SAMPLE AND COMPLETE ARRAY

where C_{BC} is the depletion layer capacitance between collector and base,
C_{BE} is the depletion layer capacitance between base and emitter,
C_{SC} and C_{SE} are stray capacitance to other transistors, and
R_L is the external load resistor.

4.5.3.1. DC Mode. — If light falls on the base area of the transistor, a charge is produced proportional to the illumination. If the switch is closed to the ground position a current will flow through R_L. This is the DC mode of operation, as shown in Figure 4.32, for both the original TI sample and the final array. The graphs are a plot of I_{CEO} (base open-circuit) for both transistors and are seen to be linear for the original sample only. In general I_{CEO} is a difficult parameter to control which is one reason for not using the DC mode of operation. As a first approximation

$$I_{CEO} = \beta I_{CBO}$$

$$I_{CBO} = KI_{\ell}$$

where K is a constant of proportionality. The output voltage is

$$V = \beta K I_{\ell} R_L \ . \qquad (4\text{-}7)$$

If β is constant, the relationship between illumination and voltage should be linear. However, β can vary significantly with the level of illumination since β is itself a function of collector current I_c. Therefore, graphs such as those shown in Figure 4.32 can be expected for the complete array where low illumination levels result in low β's.

The only sensitivity figure given for the transistors used in the full array is a single point on the DC characteristic. Texas Instruments specified that, for an illumination of 20 mw/cm^2, the unmasked transistors should exhibit a collector current of 2mA with illumination from 2400°K tungsten source. This point is plotted as point A on Figure 4.32 and shows that, in terms of its DC response, the delivered array is equal to the test array. However, since the array is operated in a pulsed mode, the DC response is not the most important parameter.

4.5.3.2. Pulsed Mode.[37] — In this mode of operation the array is less dependent on I_{CEO} and greater sensitivity should be obtained. Figure 4.31 shows a typical discharge voltage waveform appearing across the load resistor R_L. This occurs after an integration period of 1 ms with a load resistance of 2KΩ and an illumination level of 20 nw.

The operation in this mode is best described with reference to Figure 4.33 which describes the voltage waveforms appearing on the various junctions of a single transistor. The waveforms with respect to the base cannot be observed but can be inferred. During the integration period the capactance C_{BC} discharges by an amount Q where

$$Q = \int_0^{T_i} I_{CBO}\, dt = I_{CBO} \times T_i$$

At the end of the integration period therefore, V_{CB} has fallen by an amount $Q/C = (I_{CBO} \times T_i)/C_{BC} = \Delta V_{CB}$ so that

$$\Delta V_{CB} = \frac{K I_\ell T_i}{C_{BC}} \qquad (4\text{-}8)$$

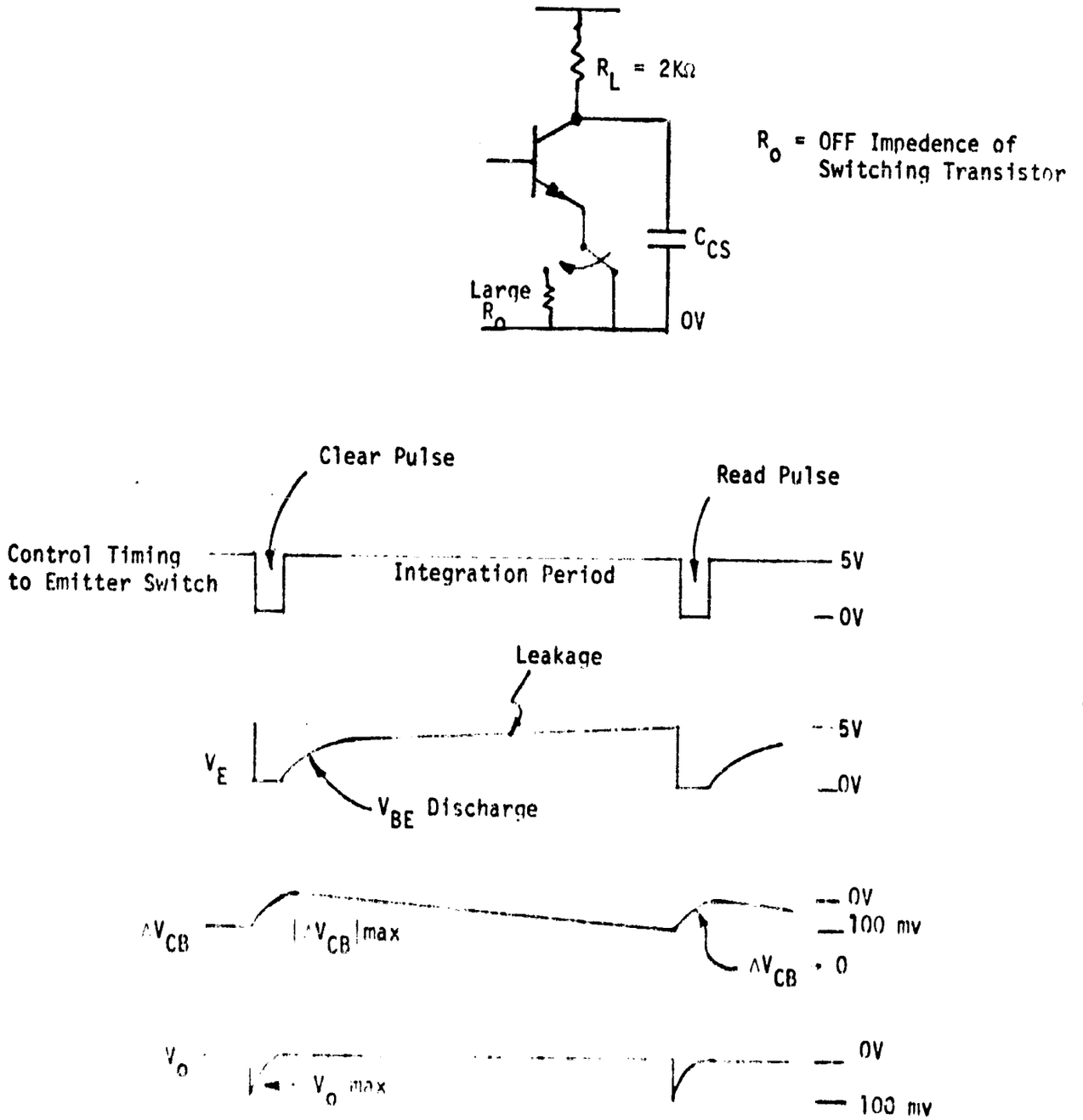

FIGURE 4.33. TIMING WAVEFORMS FOR SINGLE PHOTOSENSITIVE TRANSISTOR

Now as soon as the circuit is completed with the closure of the switch, corresponding to the start of the charge period, the capacitance C_{BC} will charge back to $V_{CC} - V_{BE}$, i.e., $\Delta V_{CB} \rightarrow 0$. However, C_{BC} can only charge through the external circuitry through an effective resistance equal to βR_L, giving a charging time constant of

$$T_f = \beta R_L C_{BC} \tag{4-9}$$

The above simple model and analysis does not include the external stray capacitors associated with the large array and leads to the conclusion that β has no effect on the output voltage peak value. It is shown below, however, that for high β's, the external capacitance has little effect on the peak output voltage, but for low β's the capacitance severely attenuates the output signal.

From Equation (4-8) ΔV_{CB} is given by $\Delta V_{CB} = (I_{CBO}\, T_f\, I_\ell)/C_{CB}$ just before the moment of switch-on. At the moment of switch-on some of the charge will be lost in charging the stray capacity C_{CS} through the transistor. If we consider an ideal transistor (constant β) conducting in the linear mode, ΔV_{CB} will be reduced to

$$\Delta V_{CB} = \frac{C_{CB}}{C_{CB} + \frac{C_{CS}}{\beta}} \Delta V_{CB} \tag{4-10}$$

where ΔV_{CB} is the peak value without stray capacity. We can rewrite Equation (4-10) as

$$\Delta V_{CB} = \Delta V_{CB} \frac{1}{1 + \frac{C_{CS}}{\beta C_{CB}}} \tag{4-11}$$

Thus, for large β, ΔV_{CB} is approximately equal to $\Delta \tilde{V}_{CB}$, independently of the value of C_{CS}. But for a combination of low β, low C_{CB}, and high C_{CS}, we have

$$\Delta V_{CB} \simeq \Delta \tilde{V}_{CB} \frac{\beta C_{CB}}{C_S} \qquad (4\text{-}12)$$

No values are available for the present array for C_{CS}, C_{CB} or β, but values of 10 pf and 1 pf may be assumed for C_{CS} and C_{CB}, and β may be inferred from the D.C. mode (Figure 4.32). β is given by the slope of the curve and, at 50 mV output, the slope is of the order of 2. This gives $\Delta V_{CB} = \Delta \hat{V}_{CB}/5$ which represents an 80% reduction in output voltage.

The following observations may be made regarding the above analysis:

1. Providing β is large, the output voltage is a function of illumination and integration time only.

2. For low β values the stray capacitances serve to reduce the output voltage drastically.

In the present PDA, the low light level value for β is clearly low, so that low voltage outputs in the pulsed mode can be expected.

Although no exact quantitative analysis has been made of the transistor used in the array, it is apparent that the sensitivity of a phototransistor is a complex function of the various transistor parameters and associated stray capacitors. These parameters must be very carefully controlled in manufacture if successful low level operation is to be achieved.

4.5.4. Electronics. — The PDA electronics has the function of reading out the optical information presented to the PDA array, quantizing the signals into logical ones and zeros, and presenting the information

to the computer in the form of 32, 24-bit words. Figure 4.34 is a block diagram of the electronics and shows the basic timing sequence.

Two groups of 32 clock pulses are received by the electronics from the computer/controller. The first group is used to clear the PDA and the second to read out the array. The leading edge of each clock pulse is used to switch successive emitter rows so that 32 pulses clears the whole array. On the trailing edge of each clock pulse, each common collector output line is sampled 32 times. Twenty-four outputs, sampled in this manner, are transfered as 32, 24-bit words to the computer.

Referring to the block diagram (Figure 4.34), outputs from the PDA array are first quantized in sense-amplifiers before sampling. The reference level determines whether the analog level corresponds to an illuminated bit or a dark bit and is variable over the range 40 mv to 60 mv. An analog level greater than the reference level gives a logical '1', whereas a level less than the reference level gives a logical '0'. The sample-and-hold stages are D-type edge-triggered flip-flops which sample on the trailing edge of the clock from the controller. The computer/controller interrogates the sensed-output lines shortly after the D-types have clocked.

The sequencing of the 32 common emitter lines is controlled by a 32-bit shift-register which is clocked on the leading clock-pulse edges from the controller. Each common emitter line is switched for a whole clock pulse period and not for just the clock-pulse width. This makes sure that each collector has time to full discharge after its sampling edge. The emitters are driven from open-collector gates which slightly improves the signal-to-noise ratio over normal T^2L gates.

Some severe noise problems were incurred in the PDA electronics due to the fact that the cables to the controller are 12 feet long. Pick-up

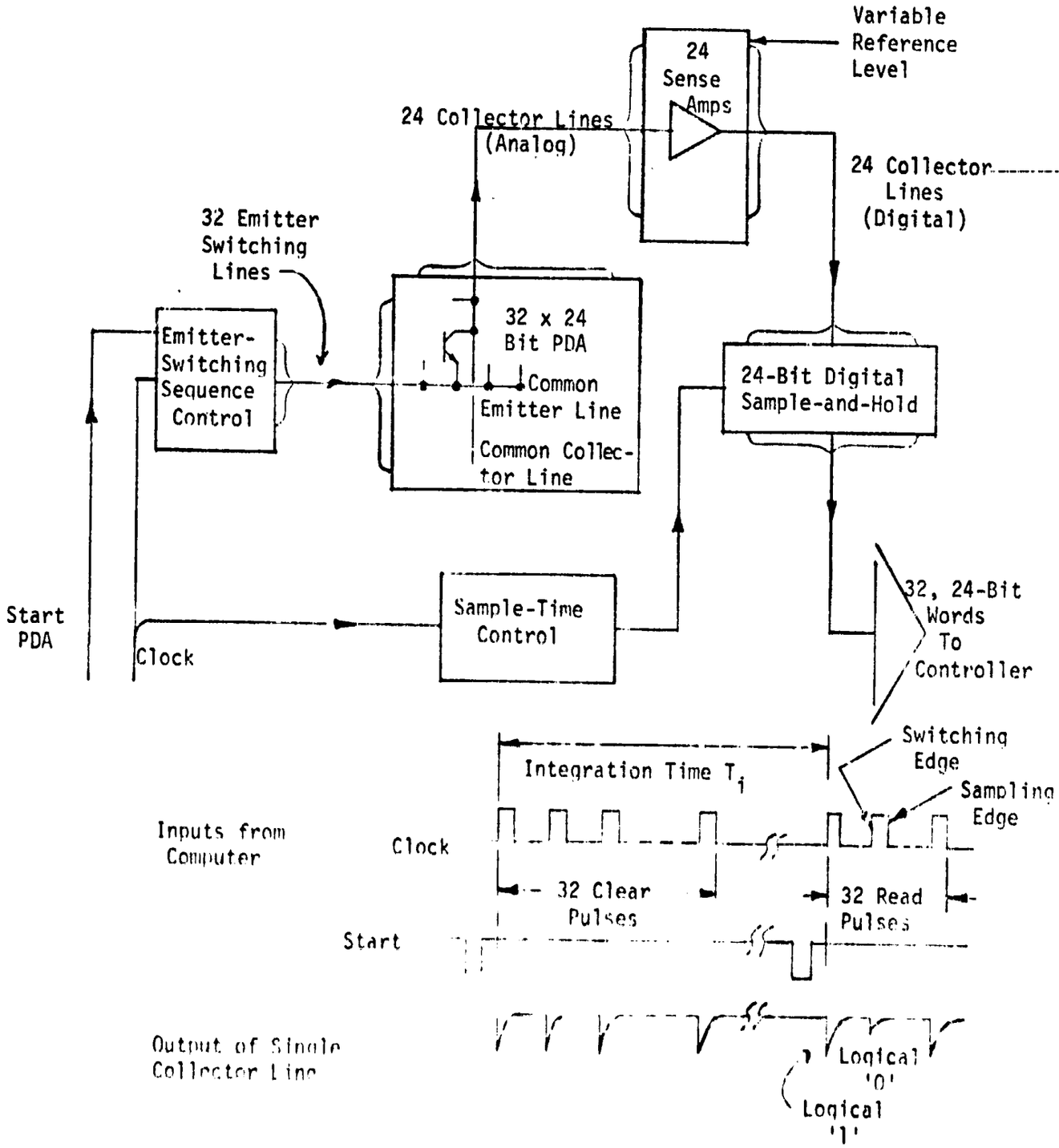

FIGURE 4.34. PDA ELECTRONICS

within the interconnecting flat cables has been reduced by running separate coaxial connections, and the electronics are grounded to the bench to reduce pick-up from the lasers.

4.5.6. Conclusions. — The array works only at greatly increased integration times and signal levels. As we have noted, the main reason for the reduced performance is a combination of low gain at low illumination levels, and excessive stray capacitance and leakage current. During the fourth quarter we discussed this problem in greater detail and other supeliers of photodetector arrays. It appears that PDA's having increased sensitivities and signal-to-noise ratios can be fabricated from either photodiodes or phototransistors if the operating characteristics of the array are carefully specified rather than specifying the operating characteristics of single elements in the array.

4.6 Controller

The electronic control system for the holographic memory controls all the system components. These components are the lasers, the beam deflectors, the block data composer, the hologram array, and the photo-detector array. The controller coordinates these systems to generate memory read, write, and erase cycles. The controller consists of a Digital Equipment Corporation PDP 8/e and a set of interface circuits. The computer system has 8K words of core (12-bit words), a high speed paper tape reader and punch, a console teletype, a 10 bit A/D converter and the necessary subsystems for interfacing to the controllers for the individual components.

The controller software program is written in a standard PDP/8 mnemonic language and is converted to a binary language with the PAL assembler program. The program listing is included in the equipment operator manual and a binary tape is provided to load the program into the PDP-8/e. The controller interfaces the PDP-8/e computer with the electro-optic devices on the memory system breadboard. Information is transferred between these devices and the PDP-8/e by two methods: programmed transfers and data break. The first method uses the accumulator as the buffer and one 12 bit word is transferred in or out at one time under control of the program. Data break allows direct exchange of information between the device and the PDP-8/e memory.

Large quantities of data can be transferred in the minimum time using a one cycle data break. The data break transfer is initiated and controlled by the hardware. The basic blocks of the controller hardware are discussed briefly in the following paragraphs. A detailed description of each is given in the operators manual.

4.6.1 BDC. — The BDC controller accepts 12-bit bytes from the computer and signals the computer when the eleventh byte has been received. The signal sets the computer into a data loading loop from which it automatically exits when the BDC controller signals that it is full. This saves about one third the time that it would take to load the BDC buffer if the computer were used to count the number of byte transfers.

Data is transferred from the accumulator (AC) of the computer to the BDC intermediate buffer and the AC is automatically cleared upon transfer, avoiding the need for software to clear the AC after each transfer. When 128 bits are accummulated in the intermediate buffer, all 128 bits are transferred simulataneously to the output buffer. Thus, the output buffer remains static most of the time.

The BDC buffer can be loaded with 128 bits in approximately 118μmsec for a data transfer rate of 1.075 megabits per sec. A system based on direct transfer from the core memory of the computer (i.e., not through the AC) could operate at rates up to 6 megabits per second. The controller has been tested by simulated signals at transfer rates of over 8 megabits/sec.

4.6.2 PDA. — The PDA control allows software determination of the discharge and charge cycle times of the PDA which operate in a charge storage mode. The charge cycle times are set by loading appropriate counter-buffers from the AC. The counters count the output of the one MHz clock which runs continuously.

Data is transferred from the PDA controller directly into core memory. The starting time of the block of 64 core words used for this storage can be set by the software.

4.6.3 AOBD. — The acousto-optic beam deflector controller converts two eleven-bit digital words to frequency modulated signals which drive the AOBD x and y transducers deflecting the laser beam to the proper position. The x and y words are loaded from a common storage register in the controller. The computer can be overriden by a manual deflection control on the AOBD electronic rack.

4.6.4 K-Radio. — The K-ratio controller accepts, from the AC, a 12-bit word to be used as the input to a digital to analog converter. A read/write mode line is provided to indicate when a read operation is to be performed. In this case the signal beam intensity is set to as near zero as possible.

4.6.5 Recording Control. — This controller accepts, from the AC, a 4-bit word used to control the operation of the shutters in the optical system, and the charging and heating functions for the thermoplastic recording material.

5
STORAGE MEDIA OPTIMIZATION

The long range goal of the storage media optimization program is to develop a read/write/erase memory material suitable for use in the 10^{10} to 10^{12} bit NASA optical memory system. The first phase of this program will be discussed in this report. Its goal has been to isolate several physical phenomena or material classes which appear to have the potential of being acceptable storage media. Throughout the course of this work, an attempt was made to think in terms of the physical phenomena which are capable of exhibiting an optically induced index of refraction change, as opposed to considering only those specific materials in which such behavior had previously been observed. This approach was deliberately adopted to insure that the potential of a general writing phenomenon rather than a specific material would be evaluated. It was, of course, necessary to resort to data on specific materials to determine realistic ranges of values of certain parameters.

The work described in this report was mostly conceptual and computational, although some laboratory work was required in order to establish the feasibility of a Battelle conceived scheme involving a reversible photochemical system. In addition, a preliminary holographic test set up for the evaluation of potential memory materials was assembled.

The following section of this report discusses the criteria which were used to evaluate potential storage media. The main body of this report deals with the material evaluations. In each case an attempt was made to show why a particular material class or recording phenomenon was rejected or retained for further consideration by comparing its characteristics to these criteria. Finally these results are summarized and suggestions for future work are presented.

5.1 Material Selection Criteria

The initial criteria for the selection of the recording media were derived on the basis of system considerations and are discussed in detail in "Investigation of Optical Memory Techniques", Final Report to NASA by Electro-Optics Center under Contract No. NAS 12-2200 (October 1970). Since these criteria influenced all phases of the material optimization program they will be summarized below.

5.1.2 Initial Criteria

1. Phase Material - Phase rather than absorption processes are favored because of the possibility of higher diffraction efficiencies and lower noise. The material should be capable of an optically induced index of refraction change Δn of at least 10^{-3}.

2. Linearity - The induced Δn should be linearly related to the writing light intensity over a range of $\Delta n = 10^{-3}$.

3. Thickness - To achieve high angular resolution in the reconstructed image and thereby allow multiple hologram recording, a minimum thickness of 1 mm is required.

4. Resolution - The material should respond uniformly to spatial variation of intensity over the range 100 to 2200 lines/mm.

5. Exposure and Erasure Sensitivity - On exposure to laser illumination of 100 milliwatts/mm^2 for a 0.1 millisecond duration, the material should change its index of refraction by $\Delta n = 10^{-3}$.

6. Spectral Response - The spectral response should be uniform to within ±10% over a range of 200 nm. The center of the range should be between 500 nm and 640 nm.

7. Noise Characteristics - At any index value within the operating range, the scatter should be less than 10^{-8} of the incident intensity.

8. Reversibility - The material should operate through repeated record/erase cycles, with no significant degradation between recordings, for a period of several years. The number of record/erase cycles is dependent on the exact function of the optical memory and whether the storage material can be periodically replaced.

9. Nondestructive Readout - The material should be capable of nondestructive readout of the recorded information with any wavelength in the wavelength range 4000Å to 7500Å. Degradation of the recorded fluctuations of the refractive index should not exceed 10%.

10. Multiple Recordings - Superposition of twenty independent recordings should be possible. Later recordings in a sequence shall not adversely affect earlier recordings.

11. Localized Recording and Erasing - The material should have the capabilities for effectively partitioning it into independent cubes having 1 mm sides. Reading and erasure of the recorded information in each of these component cubes should not affect the recordings in adjacent cubes. The spacing between the centers of these cubes should not exceed 2 mm.

12. Environmental Effects - Limited environmental changes should have negligible effect on the dimensional stability of the material. Specifically, the thermal coefficient of linear expansion should not exceed 1×10^{-6} cm/cm/°C, and the humidity coefficient of linear expansion should not exceed 10^{-6} cm/cm/1% change in relative humidity.

5.1.2 Revised Criteria

The above criteria were set down as a means of defining the ideal recording medium from the system viewpoint. In order to use them as guidelines for selecting candidate material classes, the criteria had

to be ordered according to their importance and relaxed whenever possible. The phase material, linearity, thickness, resolution and noise criteria were considered to be essential. The following modifications were made in the remaining criteria.

Exposure Sensitivity - The availability of a 1 watt average power tunable laser is assumed along with overall page composer and optical system efficiencies of 5%. If 1000 holograms are written per second, then 5×10^{-5} joules are available at the surface of the storage material to write each 1 mm hologram. For this hologram to have unit diffraction efficiency a Δn of 2×10^{-4} is required. The allowable writing time is 0.1 m sec, allowing 0.9 m sec for cycling of the page composer. The sensitivity requirements are therefore; a Δn of 2×10^{-4} shall be effected with a laser energy density of 5×10^{-5} joules/mm^2 or a laser power density of 0.5 watts/mm^2 delivered for 10^{-4} sec.

The erasing process is not as critical since, because of the multiple hologram storage technique, a single erase operation will erase a multitude of holograms. Also, the memory could be managed so that erasure was an operation which was performed during slack times. The most stringent erase requirements therefore allow at least an order of magnitude more energy than the write requirements.

Spectral Response - The limitation on the center of the response band was removed since a trade off with the characteristics of the other optical components is possible.

Reversibility and Nondestructive Readout - The phenomenon of reversibility is, for most physical systems, to some degree incompatible with long storage times and nondestructive readout. In an attempt to resolve this conflict, it was assumed that it would be reasonable to rewrite the entire memory periodically if this took no more than 1% of the available time. Since we are assuming a writing rate of

$(256)^2$ bits/msec or 6×10^7 bits/sec, a 10^{10} bit memory can be rewritten in 150 sec. Therefore, storage time for a 10^{10} bit memory should be $\sim 1.5 \times 10^4$ sec or 4.3 days. For a 10^{11} bit memory, a storage time of 43 days is required.

Multiple Recording - This is the major reason for the linearity requirement. It is assumed that any material which is linear and has a dynamic range of $\Delta n = 10^{-3}$ can support at least 10 holograms each of which involved a maximum Δn of 10^{-4}.

Localized Record and Erase - This is not foreseen as a problem for any storage material.

Environmental Effects - These criteria are very severe. It is assumed that a constant environment enclosure can be employed.

5.2 Survey of Storage Media

There are about twenty material classes or phenomena which have been suggested for various holographic recording applications. A large number of these must be rejected immediately for the present application since they do not satisfy one or more of the criteria discussed in the preceding section. These are listed in Table 5.1.

The use of most of the materials listed in Table 5.1 for holographic recording has been well known for a number of years. Representative references to papers which discuss their properties in detail are listed in the Recording Media Bibliography which is appended to this report. A few less well known techniques have also been suggested in the literature. These will be discussed briefly to indicate how their characteristics compare to those desired for the memory medium.

TABLE 5.1. MATERIALS REJECTED DUE TO INHERENT INABILITY TO SATISFY IMPORTANT CRITERIA

Material	Comments
Silver Halide films	Not reversible
Dichromated gelatin	Not reversible
Photopolymers*	Not reversible
Photoresists	Not reversible, thin
Thermoplastics**	Thin
Liquid crystals	Poor resolution, true thick hologram not possible***
Magnetic materials**** (Curie point writing)	Thin, nonlinear, absorption

*An exception to the general rule that photopolymerization is irreversible is a particular form of photodimerization. This will be discussed below.

**Although not suited for the high capacity memory material, thermoplastics are considered to be quite promising for use in a smaller memory in which volume recording of holograms is not required. They will therefore be briefly discussed below.

***These materials must be used ton conjunction with a photoconductive layer. A projection of the optical pattern on the layer is recorded in the liquid crystal medium.

****Thin phase holograms have been recorded in MnBi, which has adequate resolution, but is metallic and, of course, very absorptive. Most of the other magnetic materials that might be considered (EuO, garnets, etc.) tend to transmit only in the red. FeF_3 and $feBO_3$ transmit in the green and might have adequately small domains, but are difficult to prepare and have the additional complication of being birefringent. In any case, obtaining small domains and high resolution depends on using thin films; so to obtain a thick phase hologram one is required to use a stack of such films with nonmagnetic separators. Making such stacks has been found to be extraordinarily difficult because of the formation of magnetic bridges coupling the films.

Silicon - Several methods have been used to record optically on the surface of n-type silicon single crystal wafers.[1,2] These processes depend upon the fact that the impinging light produces electron-hole pairs. The free carriers thus produced at the surface control the formation of an anodic film or an etching process which results in an engraved pattern in the semiconductor surface. The photoanodic method is capable of producing very high resolution (over 2000 lines/mm) holographic gratings with moderately high efficiencies (14% for a 1000 line/mm grating). The silicon holograms are not erasable and therefore not suited for the present application. However, due to their high resolution and durability, they may be useful in a read only memory system.

Arsenic-Sulfur Glass - There have been several recent reports[3,4] of successful hologram formation in arsnic-sulfur glasses of various compositions. Phase gratings with diffraction efficiencies as high as 80% have been reported and holograms as fine as 2860 lines/mm have been recorded. Both thin (1 micron) and thick (0.5 mm) holograms have been formed. The sensitivity of the process is reported to be about 0.5 joules/mm^2 for a diffraction efficiency of 10%.

The mechanism for hologram formation is not yet known. A variety of explanations including devitrification, crystalline phase change, and photochemical effects have been suggested. Erasure of the stored hologram has been accomplished but it is not clear that the erasure procedure returns the material to its original state. Fatigue may therefore be a problem.

Currently, there is not enough known about the use of arsenic-sulfur glasses as holographic recording media to be able to predict if the required increase in sensitivity and the ability to be erased repeatedly will become available in these materials.

5.3 Detailed Material Considerations

With the singl_ exception of the glasses about which very little is currently known, the preceding section dealt with materials which were rejected because of an inability to satisfy, even qualitatively, one or more of the criteria for the recording medium. This section will be concerned with material classes and phenomena which satisfy the qualitative requirements (e.g., thickness, reversibility) but which have not yet been perfected to the point that they satisfy the quantitative requirements. An effort will be made to discuss these materials in such a way that their potential for satisfying these criteria can be estimated.

For a class of materials to qualify for serious consideration, the potential for exhibiting an index change of at least 10^{-3} must exist. Also, the index change mechanism must be approximately linear in order to allow the superposition of a number of holograms. Therefore, processes which have a threshold or which involve the switching of domains whose size is comparable to the resolution element cannot be considered for the memory material. The major criteria which remain are those relating to noise and sensitivity. Noise is expected to result largely from light scattering at the surface and in the volume of the recording material. In most materials, the amount of scatter will be determined by the purity and perfection of the material and by the details of the material preparation procedure. It is therefore not possible to predict the noise characteristics of a given class of materials until a detailed experimental study of the results of various preparative procedures has been made.

It will be shown that, with the exception of the noise characteristics which have been largely ignored, there are a number of classes

of materials which satisfy all of the requirements for a successful recording material but that of sensitivity. This is a difficulty which might be overcome by considering writing schemes which involve sources of energy other than the writing beam itself. An example of such a scheme is the normal photographic process in which the incident photons merely prepare the site for future chemical reactions. The photographic process suffers from a lack of speed and reversibility. Other fast processes for introducing energy over and above that found in the original writing beams are possible. For example, a laser amplifier could be employed to allow the use of less sensitive recording media. Other approaches such as synthesizing a "thick" recording material by stacking thin recording layers may also be possible. However, these types of considerations involve major revisions of the system concept and were therefore judged to be outside of the mainstream effort of this program. Detailed consideration was given only to writing phenomena in homogeneous thick materials in which the only energy source is the original one-watt average power laser beam.

These writing phenomena, which will be discussed below, fall naturally into two categories. The first category consists of several classes of materials in which the writing takes place by the promotion of an electron from a trap into the conduction band. The electron then migrates to another site where it is again trapped. The result is two new ions which, via one of several mechanisms, exhibit an index of refraction which differs from that of the original material. These photoionization phenomena are characteristic of many classes of inorganic materials.

The second category of writing phenomena involves several classes of organic materials in which the absorption of a photon

causes a chemical reaction which results in the formation of a new chemical species. The desired index of refraction change is due to the differing electronic structures of the original organic molecule and the photochemically formed species.

5.3.1 Photoionization of Inorganic Materials

General Comments - Before discussing specific read/write/erase phenomena in inorganic materials, a few general comments will be made which will help to establish the order of magnitude of the effects which are required to satisfy the previously established cirteria.

In the desired material, it should be possible to effect a change of index of refraction of 2×10^{-4} in a 1 mm^3 volume with an incident writing energy of 5×10^{-5} joules. To write a reasonably uniform thick hologram, not more than half of the writing light should be absorbed in the 1 mm thickness. Therefore, 2.5×10^{-5} joules, or assuming green writing light, about 7×10^{13} photons/mm^3 are available to effect the required index change.

In any material, the index change must be associated with a change in the electronic structure of some basic structural element. Assuming either a molecule with a molecular weight of 100, or a unit cell with a volume of 100Å^3 as the basic structural unit, we find that there are about 10^{19} such units in the 1 mm^3 hologram volume. Since the number of structural units is about 10^5 times larger than the number of available photons, it is immediately obvious that each photon must either initiate an event which causes an extremely large local index of refraction change, or there must be some effect which allows a single photon to cause an index change to occur in a volume which is much larger than that of the specific structural unit in which the ionization took place. The magnitude of the sensitivity problem

which results from the disparity between the numbers of structural units and available photons will be discussed in detail in the following sections.

Anamalous Dispersion of Inorganic Photochromics - Photochromism is observed in a variety of crystalline and glassy solids, generally as the result of the photoionization of an impurity transition metal or rare-earth ion, or a defect color center. The properties of these materials have recently been reviewed by Faughman, Staebler and Kiss.[5] Typically, they are switched to a state of higher optical density by exposure to blue light, and reversed to their original state by longer wavelength visible light. In the ideal case, one would hope to find a band of wavelengths between the darkening and bleaching bands which causes neither reaction and can therefore be used to nondestructively read the photochromic material.

The primary optical effect in these materials is, of course, the optical density change associated with the photochromic reaction. This effect has been used to record thick absorption holograms of reasonable quality in a number of materials[6] with grating spacings of over 1000 lines/mm. Because of simultaneous phase effects, these holograms are not as severely limited in readout efficiency as most thick absorption holograms.

The change in absorption exhibited by photochromics is accompanied by a change in index of refraction due to the anamalous dispersion associated with the absorption lines. This index change has been observed by J. M. Hammer[7] in $SrTiO_3$:Fe, Mo. His results, which are in good agreement with a calculation based upon fitting the measured absorption curve by a sum of Lorentzian lines, indicate a maximum Δn on the order of 5×10^{-5} per change in optical density per centimeter

of thickness. For a 1 mm sample we could therefore expect $\Delta n \approx 5 \times 10^{-4}$/OD so a Δn of 2×10^{-4} would be accompanied by an optical density change of 0.4, limiting the reconstruction efficiency to a maximum of 40%. Multiple hologram recording would soon reduce the efficiency to very low values, ten holograms producing density of 4 or a maximum efficiency of 0.01%. A naive approach to this problem indicates that a small increase in the variation of Δn with OD can lead to large improvements in readout efficiency. For example, if $\Delta n = 10^{-3}$/OD, a single hologram involving $\Delta n = 2 \times 10^{-4}$ could be expected to reconstruct with an efficiency of 62% and ten holograms would involve an OD change of 2 or a maximum of 1% efficiency. Kermisch[8] performed a more sophisticated derivation which accounts for the nonuniform exposure through the depth of the material, as well as the interaction of the writing light with the hologram it is forming. Based on Hammer's data, Kermisch concluded that a maximum reconstruction efficiency of 10% was possible for a single hologram. Again, multiple hologram recording is expected to reduce the readout efficiency of each hologram.

These limits on efficiency are quite severe. Since they are based upon a specific absorption lineshape, there is some hope that slightly larger Δn/OD values may be obtained, but a significant improvement should not be expected.

Another potential problem with inorganic photochromics is their thermal instability which will limit storage times unless the material is cooled.

Sensitivity is not as severe a problem in these materials as in most of the read/write/erase candidates. Bosomworth[6] reports an OD change of 0.2 in $SrTiO_3$:Ni-Mo with an exposure of 4×10^{-4}/OD/mm, we

expect Δn to be almost 10^{-4} in this case, so a high efficiency is expected. The sensitivity reported by Bosomworth is somewhat less than the value of 5×10^{-4} joules/mm^2 for an OD change of one reported by Kiss[9]. Sensitivities much greater than Kiss' value are not likely without quantum multiplication.

The fact that photochromics are combined phase and amplitude materials severely complicates considerations of their capabilities, especially since the ratio of phase to amplitude effects is a function of the read wavelength. The use of these materials is also complicated by the fact that there are two available methods of hologram formation. Either the hologram can be written by exposure to blue light which is a darkening process, or the material can be uniformly darkened and information can be written by bleaching with red light. In the former case both the sensitivity and diffraction efficiency decrease with the addition of each successive hologram. Superposition of ten holograms would probably lead to a reconstruction efficiency of considerably less than 1%! Also, the effective thickness of the hologram decreases as the density increases. Inverse effects will accompany the formation of successive holograms by bleaching.

Photochromic-Faraday Effect Holograms

Another possible effect of the photochromic process in inorganic materials is that the new centers created by the carrier transfer may, in the presence of a magnetic field, rotate the plane of polarization of light incident along the field direction (Faraday effect) by an amount which differs from that of the original material. It should be possible to use this change to create a phase hologram which is

read out using circularly polarized light. The following section describes how this can be done, and outlines a calculation of the magnitude of the effect. The calculation shows that, although the required index change can be attained, high magnetic fields and low temperatures are involved, and the writing sensitivity is very low.

The Faraday effect is usually described in terms of the rotation of the plane of polarization of plane-polarized light as it passes through a Faraday rotater. The angle of rotation θ, is related to the magnetic field along the direction of light propagation H, and the path length through the material d, by the Verdet constant V through the equation

$$\theta = VHd \quad . \qquad (5.1)$$

The rotation is due to the fact that the normal modes of propagation in the medium are the two oppositely polarized circular modes and, due to the magnetically induced dichroism, these propagate at different velocities v_+ and v_-. The medium therefore has a different index of refraction for right (+) and left (-) circularly polarized light. Photoionization can transform the material from a state of low, or even zero, Verdet constant to a state with a relatively high Verdet constant. To evaluate this phenomenon for holographic recording, we need a relationship between the effective index change and θ or V.

We start with a medium for which V = 0, so $n_+ = n_- = n_0$. A hologram is then written with light of any polarization which transforms the material to a Faraday rotater with indices n_+ and n_-, in proportion to the local light intensity. The hologram is then read

with either + or - circularly polarized light, so the required Δn is either $|n_+ - n_o|$ or $|n_- - n_o|$. The angle of rotation is

$$\theta(d) = \frac{\psi_+(d) - \psi_-(d)}{2} , \qquad (5.2)$$

where $\psi_\pm(d)$ are the phase differences for the $\pm$ polarizations between two faces of the material. These are related to the indices of refraction $n\pm$ by

$$\psi_\pm = 2\pi\, n_\pm \frac{d}{\lambda} , \qquad (5.3)$$

where λ is the free space wavelength of the light expressed in cm. Therefore,

$$\theta = VHd = \frac{\pi d}{\lambda}(n_+ - n_-) , \qquad (5.4)$$

where V has dimensions of rad/Oe-cm. For hologram reconstruction we will use light of a single circular polarization, for example the + polarization. Then

$$\Delta n = n_+ - n_o . \qquad (5.5)$$

To express Δn in terms of θ or V, we make the assumption that for a given material the + and - indices are symmetric about n_o.

$$\begin{aligned} n_+ &= n_o + \alpha \\ n_- &= n_o - \alpha \end{aligned} \qquad (5.7)$$

where α is a function of H,T and writing exposure. This assumption is certainly valid for this order-of-magnitude calculation. The result of this assumption is

$$\theta = VHd = \frac{2\pi d}{\lambda} \Delta n \quad . \qquad (5.7)$$

We want a material which is capable of being optically switched in and out of a state with a high Verdet constant, which, in a reasonable magnetic field, will lead to a maximum Δn of at least 10^{-3}. The europium ion has a high Verdet constant in the divalent state and a zero Verdet constant in the trivalent state.[10] Therefore, a material such as CaF_2:Eu, Sm which exhibits the photochromic reactions[5]

$$Eu^{2+} + Sm^{3+} \frac{h\nu_1}{h\nu_2} Eu^{3+} + Sm^{2+} \quad , \qquad (5.8)$$

may be a suitable candidate.

A reasonable amount of Faraday rotation data is available for Eu^{2+} in various hosts. We will assume the cahnge of valence of the Sm ion causes a negligible Δn.

The Verdet constant for Eu^{2+} in CaF_2 is reported by Shen[11] to be 10 deg/kOe - mm - % Eu for T = 4.2 K and λ = 4500Å. In the dimensions required by Eq. 3, V = 1.7×10^{-3} rad/Oe - cm - % Eu. For a 1 mm thick crystal containing 5% Eu^{2+} in a 5 kOe field we have, from Eq. (5.7)

$$\Delta n_{max} = 3 \times 10^{-4} \quad , \qquad (5.9)$$

which is close to the desired value of 10^{-3}. This value could be reached by increasing the magnetic field to 25 kOe. (The field dependence of the effect is not linear, but follows a Brillouin function.)

Assuming the 25 kOe field, 10% of the Eu^{3+} ions would have to be switched to the divalent state to produce a Δn of 10^{-4}. The lattice parameter for CaF_2 is 5.462Å with 4 possible Eu sites per unit cell. We wish to switch 0.5% of those or $1.2 \times 10^{17}/mm^3$. Using visible light, this would require at least $.5 \times 10^{-2}$ joules which is about three orders of magnitude more than we wish to use. This method of holographic storage is therefore considered to be unsuitable for the present purpose.

Ferroelectrics - In terms of the requirements imposed on the holographic memory system in question ferroelectrics represent one class of materials which show a relatively high degree of promise for the holographic storage medium. With the exception of writing sensitivity, and possibly long storage time (if low temperature storage cannot be employed), current state of the art ferroelectrics satisfy all of the "revised selection criteria" which have been enunciated in the introduction of this report. Therefore, this section is devoted primarily to a discussion of writing sensitivity with only brief comments about the remaining criteria. Following a general description of two possible writing mechanisms in ferroelectrics, the current capabilities of $LiNbO_3$ and several related materials are reviewed. It will be seen that further improvements in materials must be forthcoming in order to satisfy the system requirements in this program. Although a purely empirical approach might be undertaken in order to achieve such improvements, we believe that the key to improved recording properties in ferroelectrics is a better understanding of the writing process. Thus, this section is concluded with a few comments on

experiments which might provide insights to a more detailed description of the recording mechanism.

One successful method of writing in a ferroelectric material is by direct electric field switching of the spontaneous polarization.[12] In this method an illuminated photoconductor-poled ferroelectric sandwich is subjected to an applied voltage which is not quite sufficient to produce the electric field that is required for switching the spontaneous polarization. Upon exposure to light the photoconductor becomes conducting, and the electric field in the ferroelectric rises above threshold causing a reversal of the spontaneous polarization. Since this process is restricted to the illuminated region, at least to the extent that the photo carriers drift only in the direction of the imposed electric field, the index change in the ferroelectric provides a permanent record of the spatial distribution which the incoming beam has at the position of the photoconductor layer.

The hologram formed by this process is not a true thick hologram since the index variation occurs in a pattern which is a projection of the two-dimensional pattern on the photoconductor surface. In contrast to this "quasi-thick" hologram, a true thick hologram is characterized by index variations which reproduce the variations of the optical field over the full depth of the recording medium. It is expected that there will be differences in the optical properties of the true- and quasi-thick holograms which will effect the quality of the holographic reconstruction. Until these effects are explored theoretically, it is not possible to evaluate the ability of the photoconductor-ferroelectric sandwich to satisfy the criteria for a satisfactory storage material.

A second, and more promising, method for writing in ferroelectrics is by optical damage. Although the details of this writing process are not well understood, a general description of the method is reasonably agreed upon. Exposure of the material to a nonuniform light field results in optical excitation of free carriers from donors in the bright region. These carriers migrate to the dark regions where they fall into rather deep traps. The resulting charge distribution leads to a spatial variation in the electric polarization and/or local electric field which, via the large electrooptic effect in the ferroelectrics, causes a corresponding spatial variation of the index of refraction which can be used as a phase hologram.

Several attempts have been made to describe the recording process in more detail, but there is not yet a single selfconsistent description which accounts for all of the observed facts. The first experiments done to provide an explanation of the damage mechanism were performed by Chen.[13] He assumed that the original material consisted of a crystal with a uniform distribution of filled, neutral donors and empty, neutral traps and that local illumination causes photoionization of the donors. Chen also postulated the existence of a strong internal electric field. Under the influence of this electric field the carriers thus released migrate into the dark region where they are subsequently trapped. The result is a nonuniform charge distribution leading to a change in index of refraction via the electrooptic effect.

Chen made a number of observations which tend to support his internal field hypothesis. In his $LiNbO_3$ experiments, irradiation with a single laser beam of 2 mm diameter led to an index of refraction variation which could be explained only in terms of an unidirectional

drift of carriers along the symmetry axis of the crystal. Further investigations showed that a holographic grating could not be formed parallel to this axis implying that migration perpendicular to the axis could not occur. Also, the sensitivity to optical damage could be increased or decreased if an external field was applied in such a way as to increase or oppose the postulated internal field.[14] In addition, Chen found that in cubic KTN, recording was possible only in the presence of an external electric field.

The initial existence of a large internal field postualted by Chen is open to question.* Johnston[15] has pointed out that in the case of pyroelectric materials (of which ferroelectrics are a subclass) large internal fields are not required initially because the crystal symmetry permits variation in macroscopic polarization (electric dipole moment density) to result from the ionization or filling of certain trap sites, as well as from lattice polarization by a space-charge field. In this model the photoinduced polarization variation results in an electric field which then causes the photoexcited free carriers to drift out of the illuminated region. The resultant polarization distribution yields the required change in the refractive index via the electrooptic effect.

Johnston recognized the importance of defects or impurities to act as donors and traps in the writing process. He postulated an amphoteric defect associated with Nb-rich stacking faults in $LiNbO_3$.

*The internal field in a perfect poled ferroelectric is, according to Maxwell's equations, $E = -P/\varepsilon_0$. However, in a real crystal having finite conductivity, this field is expected to be compensated by the accumulation of free surface charge.

However, he did not demonstrate that these were truly the defects which are relevant. The situation was additionally complicated by Peterson, et al.,[16] who maintain that the damage susceptibility of $LiNbO_3$ is a function only of its iron content.

A different approach was taken by Amodei[17] who, in addition to recognizing the existence of electric field processes, stated that thermal diffusion of optically excited carriers should lead to observable index changes. Although this argument has intuitive appeal, it is not borne out by experimental evidence. Amodei has also shown that the sensitivity of $LiNbO_3$ can be increased by a factor of 20 by x- and gamma-irradiation. These results, which may be due solely to increased optical absorption in the irradiated materials (as discussed below), cast serious doubt upon the universality of the conclusions of Peterson.

It is evident from the preceding discussion that there is a great deal yet to be learned about the optical writing process in ferroelectric materials. We believe that the true key to improving the recording properties of these materials is increased understanding of the writing process. The fact that improvements in materials must be forthcoming in order to satisfy the system requirement on writing sensitivity may be seen by considering the sensitivity of $LiNbO_3$. This is the material for which the best index-of-refraction-change data now exists. Below, we use this data to relate the currently known characteristics of this material to the memory requirement.

According to data published by Chen,[13] the maximum observed index change in $LiNbO_3$ exceeds 10^{-3}, so that there is good reason to believe that at least ten holograms can be recorded in the same volume. The shortest exposure for which Chen displays data is 20 msec. In the linear region, his data indicate that for a 20 msec exposure on a 1 mm area,

$$\Delta n = 10^{-3} E \quad ,$$

where E is the energy (in joules) per pulse incident upon the area. Assuming no reciprocity failure, the desired Δn of 10^{-4} per pulse would require 0.1 joule. Therefore, in order to meet the current systems requirements, an increase in efficiency by a factor of 2000 is required.

In order to arrive at a better understanding of the origin of this low efficiency, the utilization of the writing light can be considered on the microscopic scale. We will assume a defect based writing mechanism, although it is not necessary to explicitly assume Johnston's. It is not reasonable to have more than one or two percent of the unit cells with these defects so the defect density will not significantly exceed $10^{17}/mm^3$. Chen's data indicate that 2.5 joules/mm^2 are required to saturate the index change in $LiNbO_3$ ($\Delta n_{max} = 1.3 \times 10^{-5}$). We now make the following assumptions:

1. The saturation condition reported by Chen involved the ionization of all of the defects in the illuminated region.
2. The electron mean free path is sufficiently long so that in reaching the equilibrium condition only one absorbed photon per depleted trap is required.
3. Each photon absorbed results in the ionization of a donor in the beam and the filling of a trap outside the beam.

Using these assumptions, the number of (absorbed) photons required for saturation would be $10^{17}/mm^3$. According to Chen, the number of incident photons actually required to saturate a sample about 0.5 mm thick is 6×10^{18} photons/mm^2. We thus conclude that one photon in 120 is absorbed in a 0.5 mm path, or that the absorption coefficient

of the material is approximately 0.17 cm^{-1}. For a 1 mm thick slab of $LiNbO_3$, about one photon in 60 will be absorbed. We believe that the volume illumination of this material would remain sufficiently uniform if as many as one-third of the incident photons were absorbed. Thus, if the absorption coefficient could be increased, there is a potential increase of a factor of 20 in writing efficiency.

It is known that for many materials, most notably the rare-earth ions in solid hosts, the transfer of excitation from one ion to another can be a very efficient process, possibly much more efficient than the absorption of an incident photon. This suggests the possibility of suitably doping $LiNbO_3$ to absorb a large fraction of the incident light, whch excitation would then be transferred to the damage site. The statement by Johnston that "impurity addition has little effect on the index damage, up to levels at which coloration is readily apparent, when damage susceptibility generally increases," tends to support this speculation.

The recently reported effects of doping[18] and of radiation damage upon the sensitivity of $LiNbO_3$ and $BaNbO_3$ also tend to support the above arguments. Sensitivity enhancements of as much as 25 results from the γ-irradiation of $LiNbO_3$, a diffraction efficiency of 10%. Significantly better results were obtained with iron doped $LiNbO_3$, a 40% diffraction efficiency being achieved in a 2.5 mm thick sample with 10^{-2} j/mm^2. This brings the current sensitivity of the ferroelectrics within a factor of 150 of the desired value. The possibility of achieving further improvements are discussed below.

There are, in addition to $LiNbO_3$, a number of materials which exhibit reversible "optical damage". In general, these materials are composed of solid solutions of alkali or alkaline-earth oxides with Group IV or Group V oxides. The three component nature of these compounds usually allows some local variation in the stoichiometry and

then the possibility of amphoteric defects. Examples of materials which exhibit this behavior are[15] the pyroelectric materials ($LiNbO_3$, $LiTaO_3$, $CaNb_2O_7$, $Ba_2Nb_5O_{15}$ and $BaTiO_3$); the cubic materials ($SrTiO_3$, KTN, and bismuth germanium); and modified lead zirconate titanate ceramics.

The ceramics suffer from pronounced light scattering, so that they would not be suitable thick storage materials. The cubic materials require the presence of an electric field for both the read and write operations. This is not an intrinsic disadvantage and in fact may be a useful control mechanism in some circumstances. However, the sensitivity of the cubic materials to optically induced refractive index change is much lower than that of the pyroelectric materials. We therefore conclude that additional study of the pyroelectrics is the most probable way to obtain improved ferroelectric recording materials.

In the ferroelectrics, the changes in the ordinary and extraordinary indices of refraction are related to the polarization change by[15]

$$\delta n_o = - \frac{n_o^3 \, r_{13} \, \delta P_3}{2(\epsilon_{33}-1)} \quad , \qquad (5.10)$$

and

$$\delta n_e = - \frac{n_e^3 \, r_{33} \, \delta P_3}{2(\epsilon_{33}-1)} \quad , \qquad (5.11)$$

Here ϵ_{33} is the dielectric constant and r_{13} and r_{33} are the electro-optic coefficients.

The quantity measured by Chen is the change in the difference of the two indices, i.e., the change in the birefringence. He found $\delta n_e >> n_o$, so that in measuring $\Delta(n_e - n_o)$ he was in essence measuring δn_e. From Eqs. 5.10 and 5.11 we see that

$$\Delta n = \delta n_e - \delta n_o = \frac{\delta P_3}{2(\epsilon_{33}-1)} \left[n_o^3 r_{13} - n_e^3 r_{33}\right] . \qquad (5.12)$$

Johnston describes the amphoteric defect as having three possible charge states (D^+, D^0, D^-) differing by one electronic charge and notes that polarization variations will be proportional to the local differences between D^+ and D^- densities. Assuming fully ionic bonding he finds $\delta P_3 \propto \alpha (\rho_+ + \rho_-) P_S$, where P_S is the spontaneous polarization for all of the material in the neutral state D^0, ρ_+ and ρ_- are the D^+ and D^- densities and α is the fractional change in P_S corresponding to a unit change in electronic charge at one defect site. Equation 5.12 may now be written as

$$\Delta n = \alpha \frac{(\rho_+ + \rho_-) P_S (n_o^3 r_{13} - n_e^3 r_{33})}{2(\epsilon_{33} - 1)} , \qquad (5.13)$$

It is important to note that the right hand side of Eq. (5.13) may be divided into a damage sensitive part and a damage insensitive part. In comparing $LiNbO_3$ with other materials it is convenient to consider first the damage insensitive part which includes the spontaneous polarization, the ordinary and extraordinary indices of refraction, the dielectric constant, and the electrooptic coefficients. These parameters vary widely from one material to another, and indeed there are several materials for which certain of these parameters have more

favorable values than the corresponding ones in $LiNbO_3$. However, it must be emphasized that predictions cannot be based on a comparison of a single parameter. For example, at room temperature $Sr_{.75}Ba_{.25}Nb_2O_6$ has a value of r_{33} which is a factor of 50 larger than that in $LiNbO_3$,[19] however, this gain is negated by the fact the dielectric constant of $Sr_{.75}Ba_{.25}Nb_2O_6$,[20] is a factor of 300 larger than that in $LiNbO_3$.

It is obvious that one must consider the entire damage insensitive part, which we designate by

$$z = \frac{P_S}{2} \frac{n_o^3 r_{13} - n_e^3 r_{33}}{\varepsilon_{33}-1} , \qquad (5.14)$$

and must take into account the relationships which exist between these parameters. According to the theory of diDoMenico and Wemple[21] the spontaneous polarization, the dielectric constant and the electro-optic coefficients of all oxygen-octahedron ferroelectrics are related in the following way:

a) For polarization along a 3-fold axis

$$\frac{r_{13}}{\varepsilon_{33}-1} = \frac{2}{3} \left[g_{11} + 2g_{12} - g_{44} \right] \frac{P_S}{\varepsilon^3} , \qquad (5.15)$$

$$\frac{r_{33}}{\varepsilon_{33}-1} = \frac{2}{3} \left[g_{11} + 2g_{12} + 2g_{44} \right] \frac{P_S}{\varepsilon^3} , \qquad (5.16)$$

b) For polarization along a 4-fold axis

$$\frac{r_{13}}{\varepsilon_{33}-1} = 2g_{12} \frac{P_S}{\varepsilon^3} , \qquad (5.17)$$

$$\frac{r_{33}}{\epsilon_{33}-1} = 2g_{11}\frac{P_S}{\zeta^3} \quad , \qquad (5.18)$$

where ζ is a sort of packing fraction which varies between 1 and 1.2 and the g's are the same for all oxygen-octahedron ferroelectrics. For spontaneous polarization vectors lying along-3-fold and 4-fold crystalline axes we need to consider the following quantities respectively.

$$z_{6v} = \frac{P_S^2}{\zeta^3}\left[(n_o^3 - n_e^3)\left(\frac{g_{11}+2g_{12}}{2}\right) - \frac{g_{44}(n_o^3+2n_e^3)}{3}\right] \quad , \qquad (5.19)$$

$$z_{4v} = \frac{P_S^2}{\zeta^3}\left[g_{12}\,n_o^3 - g_{11}\,n_e^3\right] \quad . \qquad (5.20)$$

Since $g_{11} - g_{12} - g_{44} \approx 0$, these equations may be approximated by:

$$-z_{6v} \approx \frac{P_S^2}{\zeta^3}\,\frac{g_{44}(n_o^3+2n_e^3)}{3} \quad , \qquad (5.21)$$

and

$$-z_{4v} \approx \frac{P_S^3}{\zeta^3}\,g_{44}\,n_o^3 \quad . \qquad (5.22)$$

Using the fact that $g_{44} \approx 0.12\ m^2/c^2$ for all these materials and the fact that the packing fraction ζ is proportional to the quantity

$(n^2 - 1)$, we have evaluated the damage-insensitive factor in the expression for the index change Δn for several materials which have been suggested for holographic storage media. The results are shown in Table 5.2. It is seen that without consideration of the damage-sensitive part of Eq. 5.4, none of the materials listed in Table 5.2 can be expected to show as great a sensitivity to optical damage as found in the case of $LiNbO_3$. In fact, the z values of many of these materials are so inferior to the z value of $LiNbO_3$ that there is little justification for examining the damage sensitive contribution in these cases.

For further consideration of those materials having z values comparable to that in $LiNbO_3$ and for the purpose of considering improved performance of $LiNbO_3$ itself, we now discuss $\alpha(\rho_+ + \rho_-)$, the damage-sensitive part of the index change given in Eq. 5.13. In general, there are two ways to increase the density of charged defects. The first is to increase the number of amphoteric defects in the specimen. However, Johnston has pointed out that in the case of $LiNbO_3$ there is an upper limit of about 1 to 2% for stacking fault defects and substantial increases above this level are not expected in related materials. Even if one considers the possibility that other defects and/or impurities such as Fe are responsible for optical damage, it is doubtful that substantial increases in the starting impurity level can be employed because the absorption coefficient would increase to such a point that uniform illumination of the thick hologram would be precluded. The second method for increasing the number of charged defects is to increase the cross section for photoexcitation of a single defect site. This possibility, which has already been discussed, is also limited by the amount of absorption which can be tolerated in the thick hologram. Even with a factor of 20 improvement by these techniques the writing sensitivity of $LiNbO_3$ would remain a factor of 150 smaller than the system requirement.

Material	Type	P_s	ζ	N_o	N_c	Z	Ref. No.
$LiNbO_3$	6V	.71	1.2	2.29	2.20	.39	21,22
$LiTaO_3$	6V	.50	1.2	2.177	2.182	.18	21,22
$Ba_2NaNb_5O_{15}$	4V	.40	1.3	2.3		.26	21,22
KTN	4V	.17	1	2.275		.04	21,22,23
$Sr_{.5}Ba_{.5}Nb_2O_6$	4V	.25	1.06	2.312		.078	21,24,25
$Sr_{.25}Ba_{.75}Nb_2O_6$	4V	.18	1.06	2.314		.04	21,24,25
$KSr_2Nb_5O_{15}$	4V	.17	1.05	2.250		.034	21,25,26
$K_3Li_2Nb_5O_{15}$	4V	.25	1	2.277		.089	21,27
$K_{.8}Na_{.2}Ba_2Nb_5O_{15}$	4V	.38	1.03	2.315		.20	28,21

The properties tabulated are: symmetry of polarization axis, magnitude of spontaneous polarization P_s, the "packing fraction" ζ, the ordinary and extraordinary indices of refraction n_o and n_c at .63μ, and z, the damage insensitive term.

TABLE 5.2. Properties of Several Ferroelectric Materials

The only parameter which has not yet been considered is α, the fractional change in P_S corresponding to a unit change in electronic charge at one defect site. Unfortunately, this parameter, which provides the only hope for greatly improved performance of ferroelectrics, is the most difficult to discuss because it involves the detailed nature of the writing process. In particular, the relevant defect must be identified and, as previously pointed out, this detail is the subject of great controversy. Therefore, we believe that further experiments to elucidate the role of defects in the writing process are essential to the improved performance of ferroelectric materials. Below we outline key points which should be considered.

1. It is evident that an internal (or external) electric field is required for efficient writing. The following questions regarding this field should be answered.

   a) What is its function?
   b) What is its origin in the noncubic material?

In addition it is of interest to know, perhaps as a corollary to a), why the thermal diffusion process is not sufficient to produce observable index changes.

2. It is also known that impurities are important in the writing process. They may play any or all of the following roles.

   a) Centers for the absorption of optical energy,
   b) Sources of electric fields after photoionization, or
   c) Sources of polarization after photoionization.

The exact function of the impurities must be determined.

3. There has been very little said about the dynamics of the writing process. The system concept calls for a writing time of less than 10^{-3} sec. The dynamics of the writing process should be investigated both to see if they are consistent with this requirement and because a knowledge of the dynamics will lead to a better understanding of the writing process.

The following are some of the investigations which should be undertaken in an attempt to illucidate the preceding points.

1. A calculation should be performed to see if a skewed charge distribution gives rise to a larger Δn than a symmetric distribution to see if a possible function of the electric field is to produce such a skewed distribution of charges.

2. Mobilities and lifetimes of free carriers in typical ferroelectrics should be measured to see if the required local electric fields can be arrived at by either a thermal or imposed drift of carriers which is consistent with these measured properties.

3. Determine if the optically induced polarization is a function of the impurities by measuring polarization as a function of concentration for samples under various types of illumination.

4. For a variety of impurity levels, look at the time dependence of Δn including times long after the writing is accomplished to see if writing speed, or Δn_{max}, or both depend upon impurity concentrations. This should help determine the role of the impurities, i.e., absorption vs. polarization centers.

5. Investigate the dynamics of the writing process, in particular seeing if the process is power or energy dependent, and if migration rates are involved which might limit writing speed.

6. Investigate the iron hypothesis by using other impurities in an iron free crystal.

7. ESR studies of the defect sites such as those planned by Dr. T. Estle of Rice University should be pursued to help determine the nature of the optically active defects.

5.3.2 Photochemical Effects in Organic Materials

Organic Photochromics - We use the word photochromic in a general manner to describe a material which undergoes a change in optical density at a particular wavelength when irradiated by light. In the case of organic photochromics this change is usually the result of a molecular change, a change in composition of the photosensitive material. These materials have received wide consideration as candidates for the photo-active materials of holographic memories and have been demonstrated to be effective storage media for holograms. They are used, as are silver halide films, as amplitude holograms. Photochromics offer the advantage of not requiring development and suffer the disadvantage of being less sensitive than silver halide films. They share a disadvantage common to amplitude holograms: low diffraction efficiency. To try to take advantage of the increased efficiency of phase gratings, we therefore explored in organic photochromics the effect discussed above for inorganics, namely, the possibility of writing a phase grating based upon the anomalous dispersion accompanying the photochromism. At issue was the possibility that Δn could be made large without having an optical density so large as to reduce diffraction efficiency.

To investigate the possibility of writing a phase grating in an organic material, we chose to look at solutions of dyes rather than photochemically created molecules. Anamalous dispersion depends upon the absorption curve of a material and not its composition. Hence we

felt that, should large enough values of Δn be found, photochromic systems could be fabricated to satisfy the other requirements. Measurements of the refractive index of solutions of two dyes were made near the principle visible absorption bands of the dyes as a function of wavelength. Our measurements on methylene blue indicate that an index change of 8.5×10^{-5} would be accompanied by an optical density change of 1.4 per cm. This is equivalent to $\Delta n = 6 \times 10^{-5}$/OD/cm which is just slightly better than Hammer's $SrTiO_3$ data. The comments concerning the inorganic photochromics therefore apply here also.

Photopolymers - In this category we include molecules which undergo changes in molecular weight upon exposure to light. The attendant change in index of refraction results from a change in density or a change in the position of the absorption band of the altered molecules. These materials have received considerable attention[29,30] because of their high sensitivity. Jenney reports sensitivities as high as 6×10^{-6} joules/mm^2 for dye sensitized polymerizations.

High sensitivities can be realized because a single photon can result in a large number of monomer units being incorporated into a single molecule. As a result of this built-in chemical amplification, it is not unusual for thousands of monomeric units to be combined. Unfortunately the process is generally not reversible. In certain cases it is possible to effect a depolymerization but on severely limited scale. Each bond broken requires a photon so that erasure, even when possible, would require several orders of magnitude more energy than writing.

Several reversible polymerizations are known[31,32] but none of them polymerize by a chain mechanism. They consequently lack the high sensitivity quoted above. Each uses a reversible photodimerization as a means of changing the index of refraction. Dimerization is a special case of polymerization in which the polymer consists of two monomeric units,

and is, in several instances, reversible. In addition, many of these reactions will take place in the solid state, in crystalline monomers, or in crystalline dimers. Several of these reactions have also been shown to occur in highly viscous fluids, namely polymeric matrices. Large changes in index have been demonstrated in such systems. However, the sensitivity is probably too low for the present application even though hologram formation has been demonstrated in these materials. For example, the molar concentration of anthracene in crystalline anthracene is about 7 moles/ℓ. Assuming a quantum yield of formation of the dimer of about 0.5, then 0.5 j/mm^2 are required[31] to get $\Delta n = 10^{-3}$. Assuming (very inaccurately in this concentration range) that $\Delta n = 10^{-4}$ requires 1/10 that amount of energy, then 5×10^{-2} j/mm^2 are needed.

No data are available which would permit calculation of the sensitivity of the polyhexamethylene-α-truxillamide system described in the paper by Takahashi.[34]

Thermoplastics - Thermoplastic materials have in recent years been studied extensively as media for holographic information storage. In a typical application a supporting electrode is coated with a photoconductor which in turn is coated with a thermoplastic material. The supporting electrode is grounded while a corona discharge is used in a selected atmosphere to spray a charge on the surface of the thermoplastic. Upon irradiation the charge migrates from the supporting electrode, through the photoconductor, to the back surface of the thermoplastic. As a result the field across the thermoplastic in the irradiated area is larger than the field across the thermoplastic in the unirradiated area. A current is passed through the supporting electrode and the resultant resistive heating causes the thermoplastic to soften and allows it to flow. Due to the electrostatic forces it becomes thinner in irradiated areas than in unirradiated areas. Erasure is accomplished

by heating the thermoplastic to a higher temperature in the absence of a field thereby permitting the thermoplastic to flow and become uniform. The organic compounds studied for such application range in structure from small molecules such as wood rosin derivatives to plasticized high polymers.

Although considerable research is still being carried out with thermoplastics, it is clearly evident from past work that holographic recording devices based on such materials are well suited for some applications. Materials are presently available, for example, with the ability to withstand several hundred write/erase cycles with little deterioration in properties. For best stability, i.e., lack of fatigue, a thermoplastic material for a reversible holographic device should be chemically inert. Since the materials are subjected to corona charging and thermal cycling the requisite inertness becomes extraordinarily difficult to achieve. While no material actually meets this criterion some organic compounds are sufficiently inert to meet the requirements for certain applications.

Thermoplastics will fatigue, if recycled sufficiently. Such fatigue is most frequently the result of the compound's sensitivity to either light, heat,or the electronics or ions which result from the corona discharge to which the materials are subjected. The thermoplastic is usually found to dimerize or otherwise polymerize so as to produce a new chemical species with different physical properties. Less commonly, the thermoplastic material will react with other available organic chemicals or degrade into simpler, smaller compounds. Regardless of the particular chemical modification undergone by the thermoplastic, such modification effect the slow but continuous alteration of the thermoplastic's physical properties. Generally with increasing fatigue, higher temperature becomes required to effect development and erasure. This higher temperature then causes the accelerated degradation of the original thermoplastic material.

In addition to these considerations of fatigue, there are other less critical, but nevertheless annoying, shortcomings associated with currently available thermoplastic materials. For example, ion implantation, the magration of isolated change from the surface of the thermoplastic into the bulk of the material is frequently cited as an important cause of background noise.

At present thermoplastics are the material of choice for thin holograms. Their sensitivity of 0.75×10^{-6} j/mm^2 for a diffraction efficiency of 16% compares favorably to most other recording media. There has been considerable effort expended in the design of increasingly superior resins.[35]

Cis-Trans Isomerization - It was suggested by a Battelle staff member, Dr. Henry Grotta, that of the geometric isomers known as cis-trans isomers, the cis and trans members might differ in refractive index. Since reversible conversion from one member to the other is often possible this suggestion opened a new class of materials for consideration. A brief survey of the literature indicated index differences as large as 10^{-2} between cis-trans pairs. Larger values can be expected.

Cis and trans isomers are molecules which have the same chemical constituents but different molecular geometry due to hindered rotation about a carbon-carbon double bond. For the sake of clarity we shall limit our discussion of cis-trans isomers to derivatives of ethane CH_3-CH_3. This molecule may be visualized as two tetrahedra sharing a common apex, with the carbon atoms at the centers of the tetrahedra and the hydrogen atoms or other atoms bonded to the carbon at the free apices. The rotation around the C-C bond is free.* Thus, if a molecule such as CH_2Cl-CH_2Cl is drawn as

*Actually it is hindered slightly with an energy barrier to rotation of about 5-10 kcal/mole.

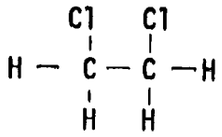

this, at room temperature, is equivalent to

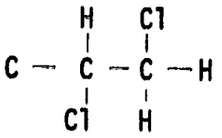

or any other arrangement of H and Cl atoms in which the atoms are bonded to carbon. The situation is different when there is a double bond between the carbon atom, as in derivatives of ethene

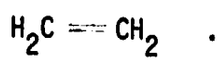

This compound may be visualized as having the carbon atoms in the center of two tetrahedra which share a common edge. The two tetrahedra cannot rotate with respect to one another.** That is, in this case rotation about the carbon-carbon bond is restricted. Consequently the compounds

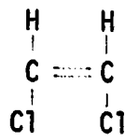

and

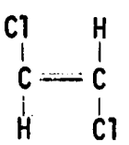

are not identical and differ in density, dipole moment, melting point, chemical properties, and refractive index. The geometry of the molecule is such that the centers of the four atoms bonded

**The barrier to rotation in this case is an order of magnitude higher than the barrier for the single bond.

to the carbon atoms are coplanar. If the molecule has bulky constituents on it, such as

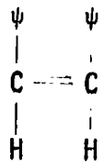

(I)

where the symbol ψ represents a benzene ring, then the configuration (I), called the cis configuration, will not be a coplanar molecule, because of the size of the benzene rings. The configuration (II)

(II)

is not so constrained and will be a planar molecule. This latter isomer is called the trans configuration, or the trans isomer. If we were to substitute bulky constituents for the hydrogen atoms on the molecule II then it too could be made nonplanar. The point we wish to make is that it is possible to choose substituents so that only one isomer is planar. Planarity is important because it determines the distribution of charge in the molecule. In the planar molecule II the π electrons of the two rings and the carbon carbon bond are delocalized. The result is a highly polarizable molecule. Further, if appropriate substituents are placed on the rings of molecule II some net separation of charge may be affected, resulting

in a permanent dipole moment. In the absence of planarity as in molecule I, charge delocalization occurs on each but cannot occur through the carbon carbon bond. Consequently the polarizability of I is expected to be lower than that of II and the dipole moment of molecule I lower than that of molecule II.

The refractive index increases with increasing polarizability and with increasing permanent dipole moment.* It can be seen that because of charge delocalization the polarizability of the trans form is greater than that of the cis form. If in addition the appropriate substituents are added to proper positions in the molecule a net separation of charge will be effected resulting in an increase in permanent dipole moment of the trans form as compared with the cis form.

These pairs are of potential utility because, as we have stated earlier reversible transformation between members of the pair can be achieved optically.

The photochemistry of these transformations is complex but has been extensively studied. The transformations can be sensitized by the addition of appropriate molecules. Irradiation in the absorption band of the sensitizer causes the isomerization reaction. Furthermore, the final cis-trans ratio (photostationary state) depends upon the sensitizer used. Mechanistic arguments have been advanced,

---

*This follows from the Lorentz-Lorenz equation

$$R = \left(\frac{4\pi N}{3}\right)\alpha + \left(\frac{4\pi N}{3}\right)\frac{\mu^2}{3kT} = \frac{n^2+1}{n^2+2}\frac{M}{\rho}$$

where R is the molar refractivity, μ is the permanent dipole moment, α the polarizability, M the molecular weight, and ρ the density.

notably by Hammond and his coworkers[36] which relate the cis-trans ratio of the photostationary state of the sensitized photoreaction to the triplet energy of the sensitizer. In order to rationalize the results it is necessary to involke nonspectroscopic states, the existance of which currently lacks confirmation. The case of α-methylstibene[36] is of particular interest since the molecule lends itself well to the kind of chemical manipulation which is expected to effect the refractive index difference between the cis and trans members of the pair. Further, by judicious choice of sensitizer mixtures it should be possible to choose sensitizer pairs which result in widely differing cis-trans ratios and which have significantly different absorption spectra. Thus it becomes possible to manipulate the cis-trans ratio by choosing a wavelength which will excite only that sensitizer which results in the desired cis-trans ratio. The cis-trans ratio, and consequently the refractive index, can then be controlled through the choice of wavelength. This permits different wavelength to be used, if desired, for write/read/erase functions. Since the sensitizer is not consumed, the light absorption of the writing radiation remains the same irrespective of the number of holograms occupying the same volume, an advantage not enjoyed with for example directly excited photochromics.

An example will serve to illustrate the application of these compounds. The photostationary state achieved with α-methylstilbene sensitized by duroquionone has a cis-trans ratio of 0.2, while the photostationary state attained with the eosin sensitized reaction is cis-trans = 9.0.

The absorption maximum of eosin is at 519 nm and of duroquinone at 335 nm. There is significant absorption of duroquinone at 350 nm which corresponds approximately to an absorption minimum of eosin. Thus the two sensitizers may be excited independently. The initial composition of our system will be 90 percent cis isomer and 10 percent trans isomer. The hologram is written with light absorbed by eosin,

519 nm. When this material is light struck the composition changes. The maximum change corresponds to cis-trans ratios of 0.20 rather than the initial 9.0. Thus the refractive index of the light struck material has changed. The hologram may be read with radiation absorbed by neither sensitizer so the hologram will be unperturbed by the reading process. It may be erased by irradiating uniformly with light absorbed by duroquionone. This will restore the original composition.

The feasibility of this approach was assessed by preparing cis and trans α-methylstilbene.[37,38] A 1% solution of each in methanol was prepared and the refractive index of cis versus trans α-methylstilbene was measured in a Phoenix differential refractometer. The results are given in Figure 5.1.

The molar absorption coefficient of both cis and trans α-methylstilbene is nominally zero at these wavelengths. From Figure 5.1, the Δn measured for α-methylstilbene at about 550 nm at a concentration of 5×10^{-2} mol/ℓ is 4.5×10^{-4}. We shall assume that the system is sensitized and that we are writing with 500 nm, and that the concentration of the sensitizer is adjusted so that 50% of the light is absorbed. The quantum yield of the sensitized reaction is about 0.5.[36] In a 1 mm cube (10^{-6} ℓ) the mass of material which would have to be transformed is 10^{-6} ℓ $\times 5 \times 10^{-2}$ mol/ℓ $= 5 \times 10^{-8}$ which is 3×10^{16} molecules. Because of the quantum yield of 0.5 and an absorption of 50% this requires an incident energy density of 1.2×10^{17} photons/mm^2 - 4.8×10^{-2} j/mm^2. This is the energy required to obtain $\Delta n = 4.5 \times 10^{-4}$. If we assume that n varies linearly with concentration in this concentration range then 1.2×10^{-2} joules incident on 1 mm^2 would be required to obtain $\Delta n = 10^{-4}$ in a material 1 mm thick.

An increase in efficiency of about 200 is necessary to meet the goal of this program. However, since the system chosen was one of known photochemistry and was not chosen on the basis of maximizing Δn, this result is highly encouraging. Detailed calculations based on the Lorentz-Lorenz equation have shown that it is realistic to expect to come to within an order of magnitude of the recording material criteria using cis-trans materials.

There are several ways of increasing the difference in index between the cis and trans forms. As was noted earlier, it is desired to obtain a large increase in the charge delocalization in the trans form. This can be accomplished by substituting groups which supply or withdraw charge from the benzene rings of α-methylstilbene. These substituents should be placed on a para position giving para, para'-derivatives of stilbene. Examples of groups which supply charge are $-N(CH_3)_2$ and $-OCH_3$, and those which withdraw charge are $-NO_2$ and -CN. These should be particularly effective when used in combination.

It is to be expected that the addition of these substituents will increase the stability of the trans form relative to the cis form and may consequently affect the desired photochemical reaction adversely. A tradeoff might therefore be necessary between maximizing Δn (trans versus cis), and obtaining a useful photochemical reaction. As yet, the fatigue characteristics of these materials are now known. The reactions are thought to proceed via the triplet state of the stilbene derivative. Direct excitation is usually to a singlet excited state, more energetic than the triplet. Thus the sensitized reaction requires that the stilbene derivative undergo fewer dissipative processes than in the direct reaction. This is likely to improve stability. Ultimately, fatigue characteristics will be determined by measurement.

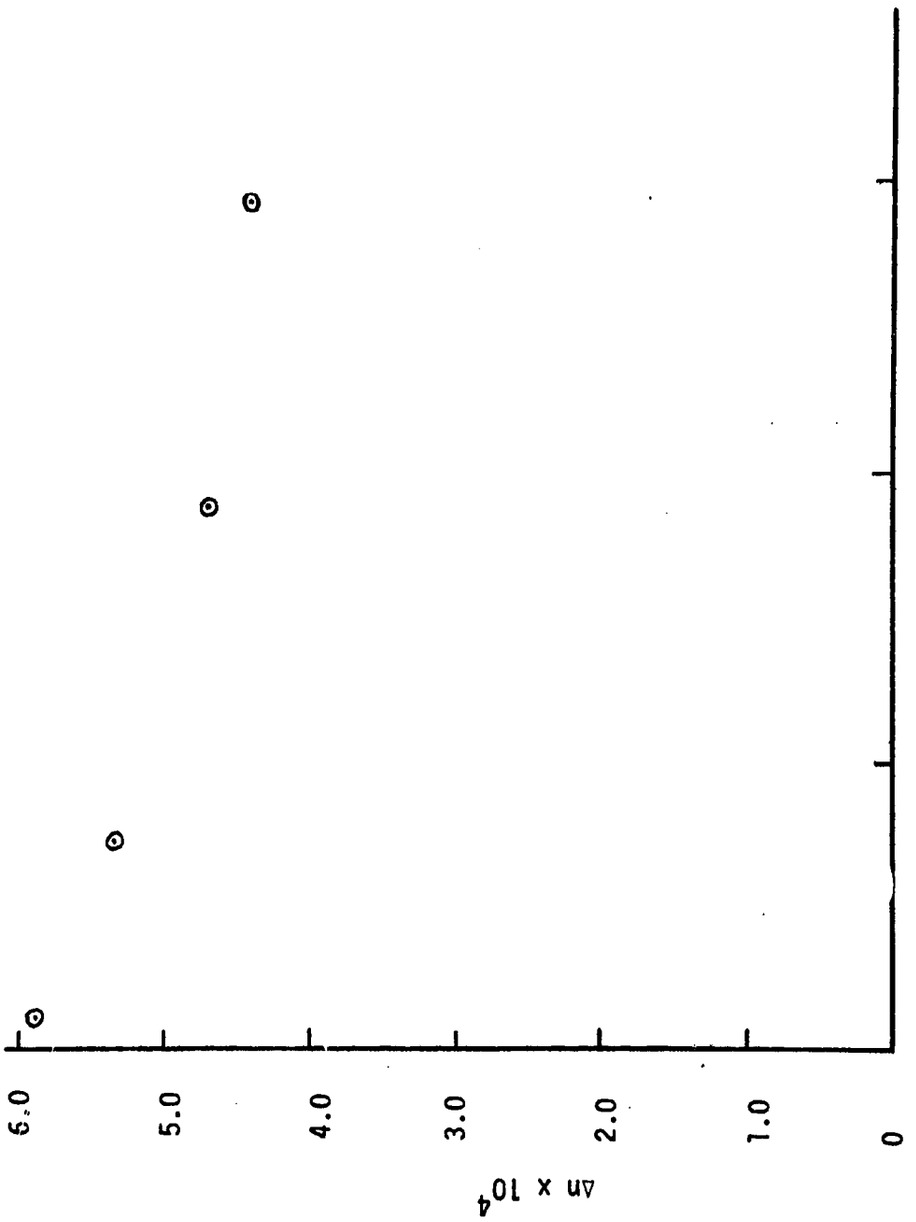

FIGURE 1
Δn for cis vs. trans α- methylstilbene
(1% by Wt. in Methyl Alcohol, T = 25 C)

It is extremely difficult to predict the magnitude of Δn which might result. It is, to begin with, difficult to find literature values for Δn for cis-trans pairs, and they are usually given for small molecules in whcih density effects on refractive index either predominate or tend to vitiate dipole moment or delocalization effects. Differences between the cis and trans members are usually about 10^{-2}, while we find 5×10^{-4} for a 1% solution of the stilbene. It is likely that about an order of magnitude increase may be expected unless a component due to the proximity of a new absorption band appears.

These reactions have been the subject of several investigations, principally because of the unusual dependence of the cis-trans ratio on the nature of the sensitizer. We have chosen to consider the substitued stilbenes because of this feature and because these molecules lend themselves to the chemical manipulation described above which should increase Δn. Some consideration should be given to other, more complex isomers in an effort to glean other useful systems from the photochemical literature.[39]

5.4 Memory Material Test Set Up

A holographic materials evaluation system was assembled for determining sensitivity and resolution characteristics of candidate memory materials. A 1 watt argon-ion and a 70-milliwatt helium/neon laser were used as sources. The evaluation system was constructed on a large vibrationally-isolated granite optical table. The laser beam at the desired recording wavelength could be directed through a spatial-filter, beam expander-collimater unit to obtain a 2-inch diameter collimated beam or could be used at its original output size of a few mm diameter. This beam was divided by a variable-ratio beam splitter and, through a succession of planar mirrors, each beam was directed toward a sample holder. The spatial frequency of the interference pattern produced at the sample holder was determined

by the angle between the two beams and the wavelength of the recording radiation. A second wavelength is selected from among those available and is directed to the sample holder at an angle appropriate to play out the hologram simultaneously with the recording process.

This system was checked out using samples of Hughes photopolymer. The recording was made with the red output of the He-Ne laser at an angle of about 35° between the beams. This produces a grating of 900 lines/mm spatial frequency. The argon-ion laser was operated at low power so that only the low threshold cyan output was obtained. This was expanded to about a 1 cm diameter and directed at an angle to the sample such that it would play out any grating formed in the sample. The diffracted readout beam was directed by a mirror to a detector which was in turn connected to a chart recorder. It was therefore possible to record the dynamic response of the sample as a holographic recording medium. It was found in the trial runs that gratings exhibiting a diffraction efficiency of roughtly 3 percent could be produced in about 20 seconds after a 2 second induction period with power density of about 1/3-mw/cm^2. This is equivalent to an energy density of about 7×10^{-5} j/mm^2 to reach the peak diffraction.

5.5 Conclusions and Recommendations

The criteria for a memory material are sufficiently in number and severity that, at the initiation of the Material Optimization Program, there was no a priori reason to believe that they could all be satisfied by any class of materials. As was discussed earlier in this section, all known categories of recording materials were first considered in light of the qualitative criteria for the memory material. Those which had properties which were consistant with these criteria were then considered in light of the quantitative requirements.

It is the principle conclusion of the present study that there are at least two classes of materials which satisfy all of the qualitative requirements and have the capability of satisfying all but one of the quantitative criteria. The material classes are the ferroelectric materials and the cis-trans isomers. Both of these material classes fail to meet the writing sensitivity to within a factor of ten of the desired value. If this predicted value cannot be exceeded, it will, of course, require some modification of the basic system concept. Either a laser with a higher average power or a laser amplifier will be required, or a slower writing rate must be accepted.

Due to the fact that considerably more effort has been expended on the study of writing by optical damage in ferroelectrics than on the study of writing processes in cis-trans isomers, the state of the art of hologram formation in the former class of materials is at a much more advanced level. Consequently, it is recommended that immediate emphasis be placed on a continuation of the study of the cis-trans materials in an effort to locate, as soon as possible, any serious problems which have not been anticipated by the present work. Several secondary efforts should also be pursued. These include a continued study of the ferroelectric materials with particular emphasis upon the elucidation of the writing mechanism, and a continuing search for additional materials and mechanisms which may be developed into successful read/write/erase holographic memory materials.

RECORDING MEDIA BIBLIOGRAPHY AND REFERENCES

In this section are included general representative references to each of the materials listed in Table 5.1. This list is followed by the citations which correspond to the numbered references in Section 5.

Silver Halide Films

Holography, H. M. Smith, Wiley Interscience, New York City, (1969).

Dichromated Gelatin

R. K. Curran, "Mechanism of Hologram Formation in Dichromated Gelatin," Appl. Opt., 9, 1651 (1970).

M. Chang, "Improved Dichromated Gelatin for Holographic Recording," Optical Society Meeting, Hollywood, Fla., p. 27 (Sept. 28 - Oct. 2, 1970).

Photopolymers

W. S. Colburn and K. A. Haines, "Volume Hologram Formation in Photopolymer Materials," Applied Optics 10, 1636 (1971).

R. H. Wopschall, "Dry Photopolymer Film for Recording Holograms," 1971 Spring Meeting of Opt. Soc. of Am. (Apr. 5-8, 1971).

D. H. Close, et al., "Hologram Recording on Photopolymer Materials," Appl. Phys. Letters, 14, 159 (1969).

W. J. Tomlinson, I. P. Kaminow, E. A. Chandross, R. L. Fork and W. T. Silfvast, "Photoinduced Refractive Index Increase in Poly(Methylmethacrylate) and its Applications," Applied Phys. Letters, 16, 486 (1970).

Photoresists

M. J. Beesley and J. G. Castledine, "The Use of Photoresist as a Holographic Recording Medium," Appl. Opt., 9, 2720 (1970).

Thermoplastics

H. R. Anderson, Jr., E. A. Bartkus, and J. A. Reynolds, "Molecular Engineering in the Development of Materials for Thermoplastic Recording," I.B.M. J. Res. Develop., 140, March (1971).

Liquid Crystal

J. D. Margerum, T. D. Beard, W. P. Bleha, Jr., and S. Y. Wong, "Transparent Phase Images in Photoactivated Liquid Crystals:, Appl. Phys. Letters, 19, 216 (1971).

J. D. Margerum, J. Nimoy, and S. Y. Wong, "Reversible Ultraviolet Imaging with Liquid Crystals," Appl. Phys. Letters, 17, 51 (1970).

T. Sakusabe and S. Kobayashi, "Infrared Holography with Liquid Crystals," Jap. J. Appl. Phys., 10, 758 (1971).

Magnetic Materials

R. S. Mezrich, "Curie-Point Writing of Magnetic Holograms on MnBi," Appl. Phys. Letters 14, 132 (1969).

H. Wieder, et al., "A Study of Thermomagnetic Remanence Writing on EuO," J. Appl. Phys. 42, 3458 (1971).

G. Fan, K. Pennington, and J. H. Greinev, "Magnetic-Optic Hologram," J. Appl. Phys. 40, 974 (1969).

1. A. L. DaLisa, "Photoanodic Engraving of Holograms on Silicon," Appl. Phys. Letters 17, 208 (1970).

2. A. L. DaLisa, et al., "Holographic Recording on Silicon," Optical Society Meeting, Hollywood, Fla., p. 28 (Sept. 28 - Oct. 2, 1970).

3. R. G. Brandes, F. P. Laming, and A. D. Pearson, "Optically Formed Dielectric Gratings in Thick Films of Arsenic-Sulfur Glass," Appl. Opt. 9, 1712 (1970).

4. S. A. Keneman, "Hologram Storage in Arsenic Trisulfide Thin Films," Appl. Phys. Letters 19, 205 (1971).

5. B. W. Faughman, D. L. Staebler, and Z. J. Kiss "Inorganic Photochromic Materials," Applied Solid State Science, Vol. 2, p. 120, Academic Press (1971).

6. D. R. Bosomworth and H. J. Gerritsen, "Thick Holograms in Photochromic Materials:, Appl. Opt. 7, 95 (1968).

7. J. M. Hammer, "Photochromic Change in Refractive Index," Appl. Phys. Letters 13,318 (1968).

8. D. Kermisch, "Efficiency of Photochromic Gratings," J. Opt. Soc. Am., 61, No. 9, pp. 202 (1971).

9. Z. J. Kiss, "Photochromics," Physics Today, p. 42 (Jan., 1970).

10. Y. R. Shen and N. Bloembergen, Phys. Rev. 133, A 515 (1964).

11. Y. R. Shen, Phys. Rev. 134, A 661 (1964).

12. S. A. Keneman, G. W. Taylor, A. Miller and W. H. Fonger, "Storage of Holograms in a Ferroelectric-Photoconductor Device," Appl. Phys. Letters 17, 173 (1970).

13. F. S. Chen, "Optically Induced Change of Refractive Indices in $LiNbO_3$ and $LiTaO_3$," J. Appl. Phys. 40, 3380 (1969).

14. F. S. Chen, J. T. LaMacchia and D. B. Fraser, "Holographic Storage in Lithium Niobate," Appl. Phys. Letters 13, 223 (1968).

15. W. D. Johnston, Jr., "Optical Index Damage in $LiNbO_3$ and Other Pyroelectric Insulators," J. Appl. Phys. 41, 3279 (1970).

16. G. E. Peterson, A. M. Glass, and T. J. Negran, "Control of the Susceptibility of Lithium Niobate to Laser-Induced Refractive Index Changes," Appl. Phys. Letters 19, 130 (1971).

17. J. J. Amodei, "Electron Diffusion Effects During Hologram Recording in Crystals," Appl. Phys. Letters 18, 22 (1971).

18. J. J. Amodei, private communication.

19. A. M. Glass, Jr., Appl. Phys. 40, 4699 (1969).

20. I. S. Rez, Soviet Physics Uspekhi 10, 759 (1968).

21. M. DiDomenico, Jr., and S. H. Wemple "Oxygen-Octahedra Ferroelectrics. I. Theory of Electrooptical and Nonlinear Optical Effects," J. Appl. Phys. 40, 720 (1969).

22. J. T. Milek and S. J. Wells, "Linear Electrooptic Modulator Materials," Electronic Properties Information Center Report S-14 Jan., 1970.

23. S. H. Wemple and M. DiDomenico, "Oxygen-Octahedra Ferroelectrics II," J. Appl. Phys. 40, 735 (1969).

24. E. L. Venturini, et al., "Refractive Indices of Strontium Barium Nichate," J. Appl. Phys. 39, 343 (1968).

25. G. Burns and A. W. Smith, "Properties of New and Useful Tungsten-Bronze Niobates," IEEE J. Quanl. Elec. CE-4, 584 (1968).

26. E. A. Giess, et al., "Ferroelectric and Optical Properties of $KSr_2Nb_5O_{15}$," Appl. Phys. Letters 11, 233 (1967).

27. L. F. Vau Uitert, et al., "A New and Stable Nonlinear Optical Material," Appl. Phys. Letters 11, 161 (1967).

28. A. W. Smith, et al., "Optical and Ferroelectric Properties of $K_xNa_{1-x}Ba_zNb_5O_{15}$," J. Appl. Phys. 42, 250 (1971).

29. M. J. Tomlinson, I. P. Kaminow, E. A. Chandross, R. L. Fork, and W. J. Silfrost, "Photoinduced Refractive Index Increase in Poly(Methyl-methacrylate)," Appl. Phys. Letters 16, 486 (1970).

30. J. A. Jenney, "Holographic Recording with Photopolymers:, J. Opt. Soc. Am., 60, 1155 (1970).

31. E. A. Chandross, W. J. Tomlinson, R. L. Fork, A. A. Lamola, and C. A. Pryde, paper presented at Symposium on Unconventional Photographic Systems, Society of Photographic Scientists and Engineers, Oct., 1971.

32. K. S. Wei and R. Livingston, "Reversible PHotodimerization of Anthracene and Tetracene," Photochem. and Photobiol. 6, 229 (1965).

33. R. Livingston and K. S. Wei, "Reversible Photochemical Dimerization of Acenaphtylene I. The Reaction in Liquid Solutions," J. Phys. Chem. 71, 541 (1967).

34. H. Takahashi, M. Sakuragi, and M. Hasegawa, "A Photodegradable Polymer: Polyhexamethylene-α-Truxillamide," Polymer Letters, 9, 685 (1971).

35. G. S. Hammond, J. Saltiel, A. A. Lamola, N. J. Turro, J. S. Bradshaw, D. O. Cowan, R. C. Counsell, V. Vogt, and C. D. Dalton, "Mechanisms of Photochemical Reactions in Solution. XXII. Photochemical Cis-trans Isomerization," J. Am. Chem. Soc., 86, 3197 (1964).

36. A. Zwierjak and H. Pines, "Equilibration of Cis- and Trans-Methylstilbene in Presence of Potassium t-Butoxide as Catalyst," J. Org. Chem. 27, 4084 (1962).

37. D. J. Cram and F. A. A. Ellrafey, "Studies in Stereochemistry. X. The Rule of 'Steric Control of Asymmetric Induction' in the Synthesis of Acryclic Systems," J. Am. Chem. Soc., 74, 5828 (1952).

38. See for example, A. Schonberg, G. O. Schenck, and O. A. Newmiller, "Preparative Organic Photochemistry," Springer-Verlag, New York (1968).

6

REFERENCES

1. "Optical Read/Write Memory System Design," Quarterly Progress Report 8104-Q-1, Electro-Optics Center, Radiation Incorporated; prepared for NASA-MSFC under contract NAS 8-26360, November 1970.

2. "Optical Read/Write Memory System Design," Final Technical Report, 8104-F-1, Electro-Optics Center, Radiation Incorporated; prepared for NASA-MSFC under Contract NAS 8-26360, February 1971.

3. "Optical Read/Write Memory System Components," Third Quarterly Progress Report 8105-Q-3, Electro-Optics Center, Radiation Incorporated; prepared for NASA-MSFC under Contract NAS 8-26672, November 1971.

4. "Optical Read/Write Memory System Components," First Quarterly Progress Report 8105-Q-1, Electro-Optics Center, Radiation Incorporated; November 1971.

5. L. Silberstein, Phil. Mag. 44, 257 (1922).
L. Silberstein, J. Opt. Soc. Am 31, 343 (1941).

6. See references in "A Signal and Noise Analysis of Graining Emulsions," Ph.D. Thesis by S. A. Benton (1968), University Microfilm 70-14, 453.

7. "Investigation of Optical Memory Techniques, Final Report," Prepared under Contract No. NAS 12-2200 by Radiation Incorporated (October 1970).

8. H. Kogelnik, "Coupled Wave Theory for Thick Hologram Gratings," B.S.T.J. 48, 2909, 1969.

9. M. Chang, "Dichromated Gelatin of Improved Optical Quality," Appl. Opt. 10, 2550, (1970).

10. W-H. Lee and M. O. Greer, "Noise Characteristics of Photographic Emulsions Used for Holography," J. Opt. Soc. Am. 61, 402, 1971.

11. C. B. Burckhardt, "Storage Capacity of an Optically Formed Spatial Filter for Character Recognition," Appl. Opt. 6, 1359 (1967).

12. E. L. O'Neil, Introduction to Statistical Optics, Ch. 7 (Addison Wesley 1963).

13. C. R. Berry, R. P. Loveland, The Silver Halide Grain in The Theory of Photographic Process, edited by C. E. Kenneth Mees and T. H. James, Third Edition (MacMillan 1966).

14. "Optical Read/Write Memory System Components," Second Quarterly Progress Report 8105-Q-2, Electro-Optics Center, Radiation Incorporated; prepared for NASA-MSFC under Contract NAS 8-26672, August 1971.

15. Haertling, G. H., "Electro-Optic Ceramic Materials," Proceedings of the 1971 WESCON Technical Papers, SEssion 31, Paper 31/1, San Francisco, California, August 24-27, 1971.

16. Haertling, G. H. and C. E. Land, "Hot Pressed (Pb, La) (Zr, Ti) O_3 Ferroelectric Ceramics for Electro-Optic Applications," Jour. Amer. Ceramic Soc., Vol. 54, No. 1, pp 1-11, January 1971.

17. Maldonado, J. R., and A. H. Meitzler, "Strain-Biased Ferroelectric-Photoconductor Image Storage and Display Devices," Proc. IEEE, Vol. 59, No. 3, pp. 368-382, March 1971.

18. Maldonado, J. R., and A. H. Meitzler, "Ferroelectric Ceramic Light Gates Operated in a Voltage-Controlled Mode," IEEE Trans. on Electron Devices, Vol. ED-17, No. 2, pp. 148-156, February 1970.

19. Roberts, H. N., "Strain-Biased PLZT Input Devices (Page Composers) For Holographic Memories and Optical Data Processing," to be published in Applied Optics, February 1972.

20. Land, C. E., and P. D. Thacher, "Ferroelectric Ceramic Electro-optic Materials and Devices," Proc. IEEE, Vol. 57, No. 5, pp. 751-768, May 1969.

21. Friesem, A. A., and H. N. Roberts, "Investigation of Optical Memory Techniques," Proceedings of Conference on Holographic Instrumentation Applications (NASA SP-248), Ames Research Center, Moffett Field, California, pp. 73-88, January 13-14, 1970.

22. Roberts, H. N. and A. Kozma, "PLZT Input Transducers for Coherent Optical Memories and Processors," Paper 18.6. IEEE/OSA Conference on Laser Engineering and Applications, Washington, D.C., June 2-4, 1971.

23. Klein, M. V., Optics, John Wiley and Sons, Inc., New York, pp. 495-502, 1970.

24. Lipson, S. G., and H. Lipson, Optical Physics, Cambridge University Press, London, pp. 131-136, 1969.

25. Stone, J. M., Radiation and Optics, McGraw-Hill, New York, Chapter 17, 1963.

26. Conversations with A. H. Meitzler and J. R. Maldonado at Bell Telephone Laboratories.

27. Smith, W. D., and C. E. Land, "Scattering Mode Ferroelectric-Photoconductor Image Storage and Display Devices," to be published in Applied Physics Letters, February 15, 1972.

28. W. E. Glenn, "Thermoplastic Recording," J. Appl. Phys., 30, 1870, (1959).

29. R. W. Gundlach and C. J. Claus, "A Cyclic Xerographic Method Based on Frost Deformation," Phot. Sci. Eng., 7, 14, (1963).

30. J. Gaynor and S. Aftergut, "Photoplastic Recording" Phot. Sci. Eng., 209, (1963).

31. J. C. Urbach, "The Role of Screening in Thermoplastic Xerography" Phot. Sci. Eng., 10, 287 (1966).

32. J. C. Urbach and R. W. Meier, "Thermoplastic Xerographic Holography" Appl. Opt. 5, 666 (1966).

33. J. Gaynor and G. J. Sewell, "Photocharge Process" Phot. Sci. Eng. 11, 204, (1967).

34. L. H. Lin and M. L. Beauchamp, "Write-Read-Erase in Situ Optical Memory Using Thermoplastic Holograms," Appl. Opt., 9, 2088 (1970).

35. H. R. Anderson, E. A. Bartkus, J. A. Reynolds, "Molecular Engineering in the Development of Materials for Thermoplastic Recording," IBM J. Res. Develop., March, 1971.

36. A. A. Friesem and J. L. Walker, "Thick Absorptive Recording Media in Holography," Appl. Opt. 9, 201 (1970).

37. David E. Callahan and J. R. Torley, "Performance Characteristics of Pulsed Phototransist Structures Under Various Conditions," IEEE April 1968.

7

NEW TECHNOLOGY

A new technology report as required by the contract will be submitted on or before 30 April 1972.

APPENDIX A

POLARIZATION MODULATION CONCEPTS AND CONFIGURATIONS WITH STRAIN-BIASED PLZT

In this Appendix we describe the electro-optic concepts which can be applied to a block data composer (BDC) using strain-biased PLZT which has inherent memory. A brief description of the BDC operation is that (1) linearly polarized light is required, (2) electrically controlled birefringence switching in PLZT changes light polarization states, and (3) these changes are converted to light intensity variations by a polarization analyzer. The properties of PLZT which permit such operation are described. The conversion of light polarization state modulation to light intensity modulation is analytically demonstrated. The nature of optical property changes in PLZT resulting from electrical control signals and strain-biasing is discussed and illustrated with experimental data.

STRAIN-BIASED ELECTRO-OPTIC OPERATION OF PLZT

Our purpose is to discuss the operation and to show how PLZT will work in a BDC by comparing its operation with a classical device. Therefore, in this section we first briefly describe the operation of a mechanically controlled Babinet-Soliel compensator which uses birefringent crystalline quartz. We then relate this description to the characteristics of electrically controlled PLZT ceramics. The importance of strain-bias, which permits switching signals to be applied to transparent electrodes on optical entrance and exit faces of PLZT, is also considered.

Certain transparent crystals, such as calcite and quartz, are inherently birefringent (doubly refracting). These crystals can be cut and oriented so that one component of linearly polarized light propagating

through it experiences the ordinary index of refraction n_o, and the orthogonally polarized component experiences the extraordinary index of refraction n_e. The birefringence $\bar{n}$ is defined for such materials by $\bar{n} = n_e - n_o$. The phase retardation of one polarization component relative to the other at the exit face of the crystal is $\phi = 2\pi b\bar{n}/\lambda$ where b is the crystal thickness and λ is the free space wavelength of the light. Familiar and useful optical devices — such as Nicol and Glan-Thompson polarizers, quarter-wave and half-wave plates, and the Babinet-Soliel compensator — are constructed with these birefringent materials[23-25]. We wish to consider the properties of the Babinet-Soliel compensator (B-SC) in more detail and relate these to the switching properties of PLZT as an aid to the understanding of how PLZT performs as an electrically controlled phase retarding medium.

A B-SC constructed with crystalline quartz is, in essence, a variable phase retarder (see Figure A-1). For a given setting, two orthogonal components of linearly polarized light propagating through the aperture of the device are phase retarded relative to each other at each point in the aperture by an amount

$$\phi_q(x) = \frac{2\pi\bar{n}_q b(x)}{\lambda} \qquad \text{(A-1)}$$

where $\bar{n}_q$ is the biregringence of quartz and b(x) is the difference in thickness of one quartz block relative to the other for a compensator setting of x. The two quartz blocks (one of which is cut along a diagonal) are oriented such that an ordinary wave (which sees n_o) in the first becomes an extraordinary wave (which sees n_e) in the second, and vice versa.[25]

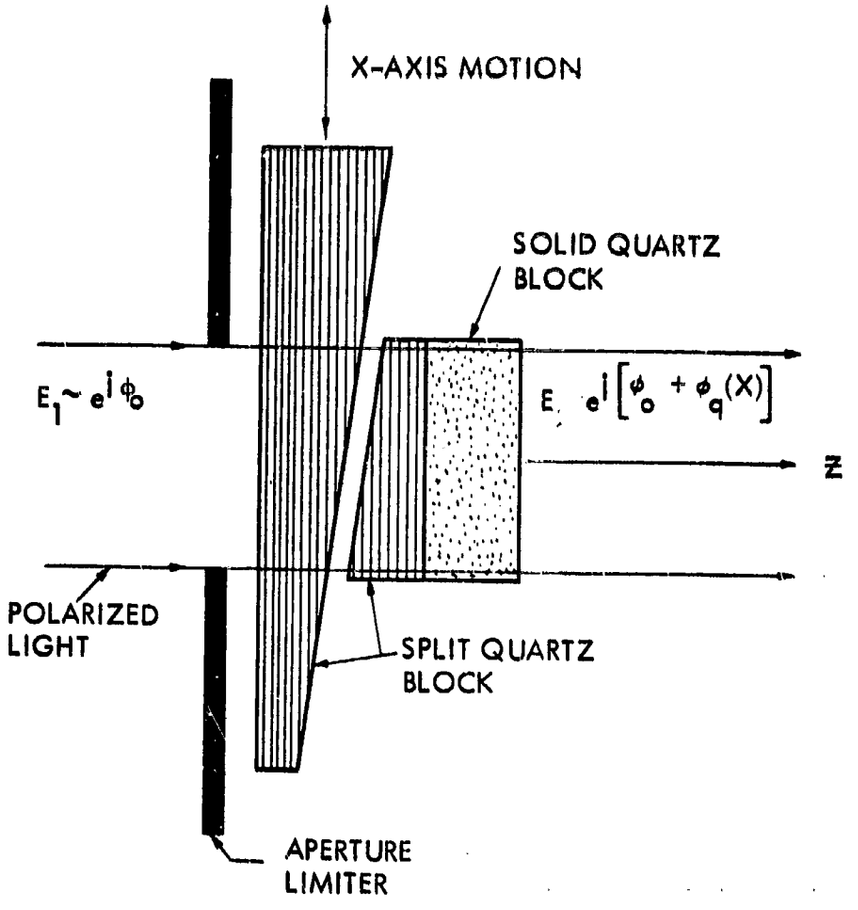

FIGURE A-1. BABINET-SOLIEL COMPENSATOR

A-3

The phase retardation $\phi_q(x)$ in Equation A-1 is varied by changing b(x) with a fixed $\bar{n}_q$. Thus, thickness difference is a mechanically controlled parameter while birefringence is fixed. It is important to note that a certain relative orientation of the optical axes of the two quartz blocks is necessary to produce the desired effect.

In PLZT, thickness is fixed at some b and phase retardation is controlled electrically by changing the state of birefringence. Thus, we can write that

$$\phi_p(V) = \frac{2\pi b \bar{n}_p(V)}{\lambda} \qquad \text{(A-2)}$$

where $\bar{n}_p(V)$ is the birefringence induced by an electrical control signal V. The roles of thickness and birefringence have been interchanged in PLZT relative to the B-SC operation, and electrical rather than mechanical controls are incorporated. As with the B-SC, the directions along which refraction change effects occur in PLZT must be oriented so that these changes couple to orthogonally polarized light components. The important impact of this fact is that longitudinal electrical control signals applied to transparent electrodes in the path of the light must induce birefringence effects in the two orthogonal transverse directions (in the plane of the PLZT).

In initial experiments[18,20] with unstrained PLZT, it was shown that the switching electric fields in PLZT had to be perpendicular to the light path to produce relative phase retardation between the two orthogonally polarized light components. Electrode configurations for two-dimensional matrix addressing were complex, allowing less than 10 percent of a PLZT plate to be active. Later it was discovered that logitudinal electric fields applied with transparent electrodes induce useful relative phase retardation changes if the PLZT is placed under a transverse linear strain (in the plane of the PLZT plate).[17,19] The switchable birefringence in the

transverse strain-biased mode, with longitudinal electric fields, is less than in the unstrained mode with transverse electric fields by a factor depending on the strain level (typically a factor of 2 to 3). However, the switchable levels are high enough to produce half-wave relative phase retardations (the optimum level) with reasonable plate thicknesses (0.075 to 0.150 mm) and drive voltages (under 300 volts).

With these facts, we are lead to modify the expression in Equation A-2 to read,

$$\phi_p(V_z,S_x) = \frac{2\pi b \bar{n}_p(V_z,S_x)}{\lambda} \qquad \text{(A-3)}$$

where ϕ_p now depends on a longitudinal electrical signal V_z and a transverse strain-bias S_x.

A simplified test configuration for a single switchable PLZT element is shown in Figure A-2. The polarizer P_1 linearly polarizes the incident light at 45 degrees to the strain axis (the x-axis in this case). Two equal amplitude light components polarized along x and along y, respectively, are incident on the PLZT with this setting. As this beam propagates through the PLZT, the two orthogonally polarized components experience a relative phase retardation given by Equation A-3. We can therefore write the optical phase retardation states which result from different electrical excitation states as,

$$\phi_{p1} = \frac{2\pi b}{\lambda}(n_x - n_y)_1 = \frac{2\pi b}{\lambda}\bar{n}_{p1}(V_{z1},S_x)$$

$$\phi_{p2} = \frac{2\pi b}{\lambda}(n_x - n_y)_2 = \frac{2\pi b}{\lambda}\bar{n}_{p2}(V_{z2},S_x)$$

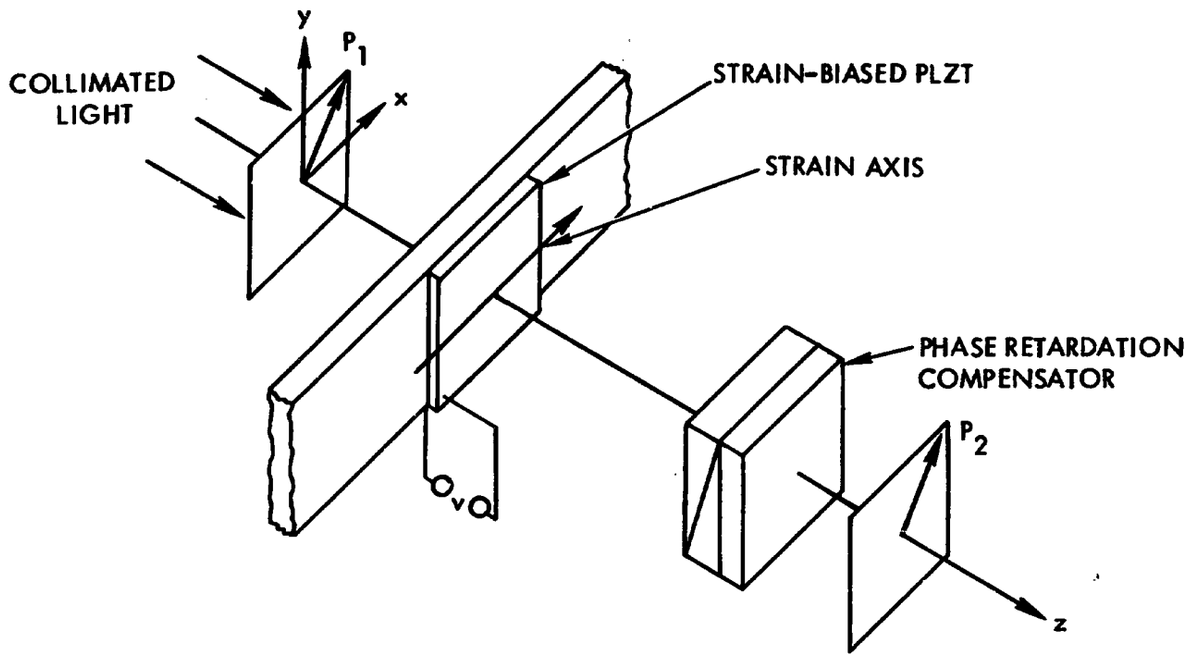

FIGURE A-2. STRAIN-BIASED PLZT WITH TRANSPARENT ELECTRODES IN ONE PRACTICAL OPTICAL MODULATION ARRANGEMENT

which can be combined to obtain the total relative phase retardation as a function of V_{z1}, V_{z2}, and some fixed S_x as,

$$\Delta\phi_p = \frac{2\pi b}{\lambda}(\bar{n}_{p2}-\bar{n}_{p1}) = \frac{2\pi b}{\lambda}\Delta\bar{n}_p(V_{z1}, V_{z2};S_x) \quad . \qquad (A\text{-}4)$$

The quantity $\Delta\bar{n}_p(V_{z1}, V_{z2};S_x)$ is the switchable birefringence. It is the difference between the birefringence which exists following a V_{z1} control voltage pulse and the birefringence which exists following a V_{z2} control voltage pulse at a constant strain-bias level of S_x. Note that $\Delta\phi_p$ is inversely proportional to light wavelength λ. Equation A-4 therefore describes a design condition for some specified wavelength of incident light. For different wavelengths, the strain S_x can be modified to reoptimize switching conditions. The experimentally determined dependence of $\Delta\bar{n}_p$ on tensile strain is depicted in Figure A-3.

In summary, we have demonstrated that $\bar{n}_p$ is an electrically controllable parameter which can be used to alter the optical transmissivity of a device that consists of PLZT between properly oriented polarizers (see Figure A-2). The arrangement of polarizers P_1 and P_2, the strain-biased PLZT with transparent electrodes, and the phase retardation compensator shown in Figure A-2 illustrates a scheme for converting these birefringence changes to intensity changes in the light transmitted through P_2. This conversion process is described in detail in the next section. The phase retardation compensator shown here allows us to adjust the bias level of birefringence. This is used to better study the switching between the different birefringence levels, and will not be used in the holographic memory system.

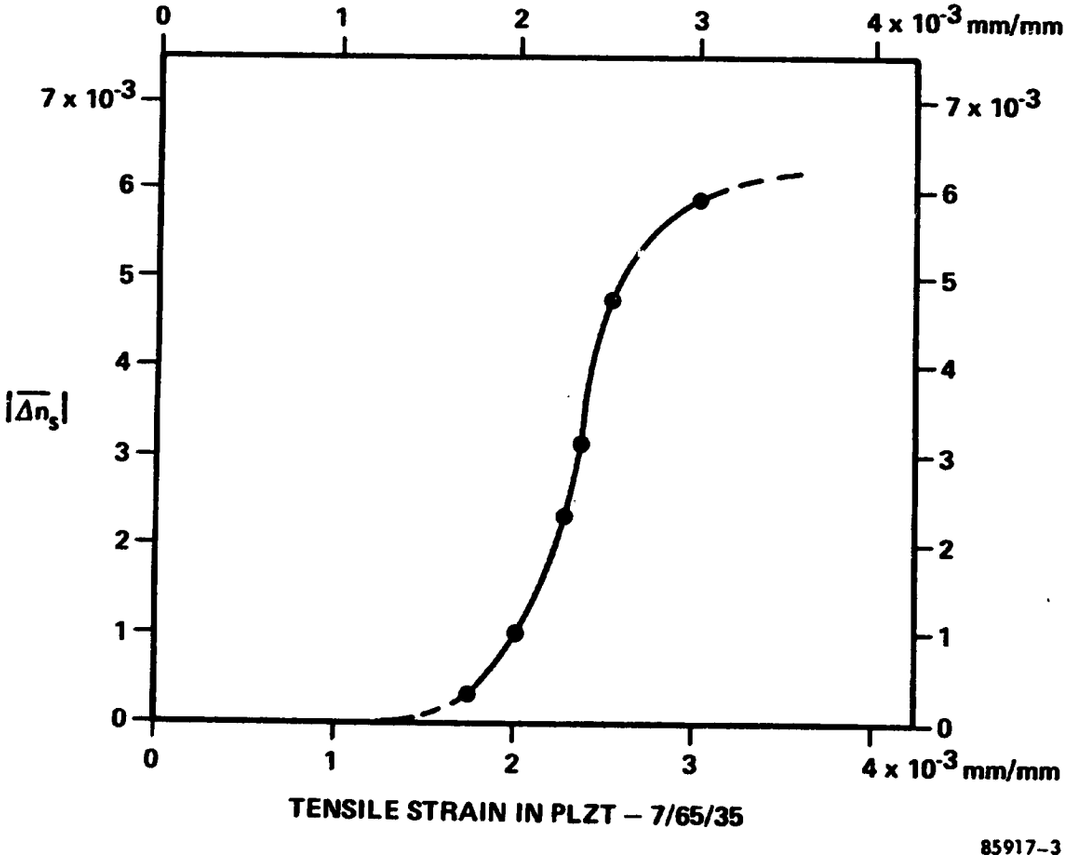

FIGURE A-3. SWITCHABLE BIREFRINGENCE VERSUS TENSILE STRAIN IN PLZT

POLARIZATION MODULATION CONCEPTS

In this section we derive the important relationships between transmitted light intensity and PLZT birefringence.

An electro-optic material responds to an applied voltage with changes in the index of refraction along particular axes. The particular axes are related to the direction of the applied electric field by an electro-optic tensor. For strain-biased PLZT, the reference coordinate system can be chosen so that an electric field E_z induces detectable changes along the x and y axes (i.e., changes in n_x and n_y). The relation for a general electro-optic material is given by,

$$\Delta n_p = -\frac{n_p^3}{2} R_{pq} f(E_q) \qquad \text{(A-5)}$$

where n_p is the average index of refraction, R_{pq} is an electro-optic coefficient, and $f(E_q)$ is some function of E_q. For a material having a linear electro-optic effect, $f(E_q) = AE_q$ where A is some constant. For a material such as PLZT which has hysteresis, $f(E_q)$ is a more complicated function which must account for the previous history of applied voltages, for the nonlinearity associated with polarizable ferroelectrics, and for the strain-bias level, as indicated in Equation A-3.

To describe how these effects can be applied to the BDC, we consider the configuration shown in Figure A-2. Strain-biased PLZT is sandwiched between transparent electrodes deposited on the entrance and exit faces so that an electric field E_z can be generated along z. The material thickness along z is b. The shape of the transparent electrodes determines the shape of the switched region (small squares for the BDC). A monochromatic light beam having wavelength λ passes through polarizer P_1,

which is oriented at 45 degrees to the x and y axes. The light field incident on the electro-optic material can therefore be described approximately by

$$\vec{E}_i = \frac{E_o}{(2)^{1/2}} (\vec{a}_x + \vec{a}_y)\, e^{jknz},$$

where we have suppressed the time dependence $e^{j\omega t}$ since it is common to all such terms. E_o is the maximum wave amplitude, $\vec{a}_x$ and $\vec{a}_y$ are unit vectors along x and y, $k = 2\pi/\lambda$, and n is the index of refraction of the medium between P_1 and the strain-biased PLZT. We let $z = 0$ at the entrance face of the PLZT and let the x and y components of $\vec{E}_i$ experience index of refractions n_x and n_y where n_x and n_y are not necessarily equal. Then, after passing through the PLZT, the electric field of the light wave at the PLZT exit face is given by

$$\vec{E}_e = \frac{BE_o}{(2)^{1/2}} (\vec{a}_x e^{jkn_x b} + \vec{a}_y e^{jkn_y b})$$

where B is a constant less than one which accounts for reflection and absorption losses. We may rewrite this expression as

$$\vec{E}_e = \frac{BE_o}{(2)^{1/2}} e^{jkn_x b} (\vec{a}_x + \vec{a}_y e^{jk(n_y - n_x)b})$$

In Figure A-2 a polarizer P_2 is shown oriented parallel to P_1 to transmit the light component polarized in the $(\vec{a}_x + \vec{a}_y)$ direction. The component of the light wave electric field $\vec{E}_f$ transmitted by P_2 is given by

$$\vec{E}_f = \left\{ \vec{E}_e \cdot [C2^{-1/2}(\vec{a}_x + \vec{a}_y)] \right\} 2^{-1/2}(\vec{a}_x + \vec{a}_y) ,$$

where C is a constant smaller than one which accounts for losses in P_2 and the scalar or "dot" product is indicated in brackets $\{\cdot\}$. We can put $\vec{E}_f$ in the form

$$\vec{E}_f = \frac{BCE_o}{(2)^{1/2}} e^{jkn_x b} \frac{1 + e^{jk(n_y - n_x)b}}{2} (\vec{a}_x + \vec{a}_y) .$$

The factor in brackets [ ] is affected by an electrical control signal. The relative phase retardation between the x and y components of the transmitted light electric field, $\vec{E}_f$, is then:

$$\phi = k(n_y - n_x)\, b = \frac{2\pi(n_y - n_x)b}{\lambda} .$$

We now define the transmissivity of the system, T_f to be

$$T_f = \frac{|\vec{E}_f|}{|\vec{E}_i|} = \left| A \frac{1 + e^{j\phi}}{2} \right| = A \cos \frac{\phi}{2}$$

where A = BC. If P_2 were rotated 90 degrees, we could get $T_f' = A \sin \frac{\phi}{2}$.

The intensity $I_2(\phi)$ of the light transmitted by P_2 is proportional to $|\vec{E}_f|^2$. Thus,

$$\frac{I_2(\phi)}{I_o} = T_f^2 = A^2 \cos^2(\tfrac{\phi}{2}) \qquad \text{(A-6)}$$

or, with P_2 rotated 90 degrees,

$$\frac{I_2'(\phi)}{I_o} = T_f'^2 = A^2 \sin^2\left(\frac{\phi}{2}\right), \qquad \text{(A-7)}$$

where $I_o = |E_o|^2$. Here I_o is the maximum (ON) transmitted intensity which occurs in Equation (A-6) for ϕ equal to even multiples of π. The minimum (OFF) transmitted intensity occurs for ϕ equal to odd multiples of π. Thus, we have

OFF conditions: $(n_y - n_x)_{OFF} = \frac{\lambda}{2b}(2m-1)$ $m = 1, 2, 3, \ldots$

ON conditions: $(n_y - n_x)_{ON} = \frac{\lambda}{b} m'$ $m' = 0, 1, 2, \ldots$

Typically, operation is between m = 1 and m' = 1 states. The output light intensity from polarizer P_2 can be controlled if the quantity $(n_y - n_x)$ can be controlled. As noted earlier, the electro-optic effect provides precisely this control with strain-biased PLZT.

If we assume that switching from ON to OFF states is accomplished with a net phase difference of $|\phi_{ON} - \phi_{OFF}| = \pi$, then we show that

$$b = \frac{\lambda}{2|(n_y - n_x)_{ON} - (n_y - n_x)_{OFF}|} = \frac{\lambda}{2\overline{\Delta n}_p} \qquad \text{(A-8)}$$

Therefore, the material thickness b can be selected based on measured or known refractive index differences which will exist in the ON and OFF states in the strain-biased PLZT. The design relation described in Equation A-8 is met at λ = 632.8 nm with the PLZT strained to S_x 2.4 x 10^{-3} mm/mm (tension) with b 0.1 mm.

ELECTRICAL CONTROL OF OPTICAL STATES — HYSTERESIS EFFECTS AND MEMORY

In this section we experimentally show the nature of the optical changes induced in PLZT by changes in the applied voltage. One way to illustrate these optical changes is to obtain the hysteresis relationship and the associated birefringence relationship so that the intensity of the light can be calculated as a function of applied voltage. A much simpler (and more accurate) method is to display the intensity of the light directly as a function of voltage so that intermediate measurements and calculations are not needed.

The procedure is to apply a 60 Hz drive signal to a strain-biased sample of PLZT and to display the intensity of the transmitted light as the vertical signal on an oscilloscope. A sample of 60 Hz sinusoidal drive signal is taken as the horizontal signal. We can vary the peak voltage as well as the amount of applied strain to generate a family of operational curves. The hysteresis relation between transmitted light intensity (I) and PLZT drive voltage (V_z) for different amounts of strain is illustrated in Figure A-4. These traces are 60 Hz hysteresis curves with a 60 Hz drive voltage reaching peaks of 190 volts, as indicated. The relationships between the I-V_z, the $\overline{\Delta n}_p$ - V_z, the P_r-V_z, and the $\overline{\Delta n}_p$ - P_r hysteresis curves are illustrated in Figure A-5. The top curve in Figure A-5 is a trace of I-V_z data obtained at $S_x = 2.25 \times 10^{-3}$ mm/mm; note the arrows indicating the direction of change with V_z. The quantity P_r is the polarization field in the PLZT and P_R is the maximum remanent ($V_z = 0$) polarization which can be established (a zero voltage "saturation" state).

The $\overline{\Delta n}_p$ - V_z curve was obtained by relating it, point-by-point, to the I-V_z data with $I/I_o = \cos^2(\Delta\phi_p/2)$. Here $\Delta\phi_p = (2\pi/\lambda)b\overline{\Delta n}_p$. The P_r-V_z curve was supplied by the material manufacturer (Honeywell).

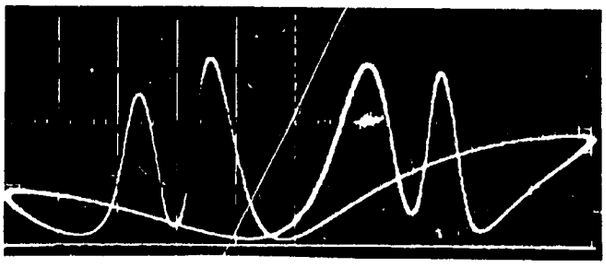

(a) $S_x = 3.0 \times 10^{-3}$ mm/mm

I = 0

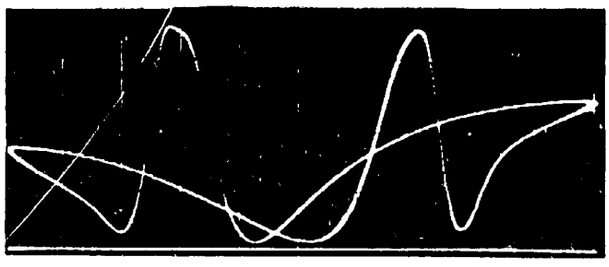

(b) $S_x = 2.37 \times 10^{-3}$ mm/mm

I = 0

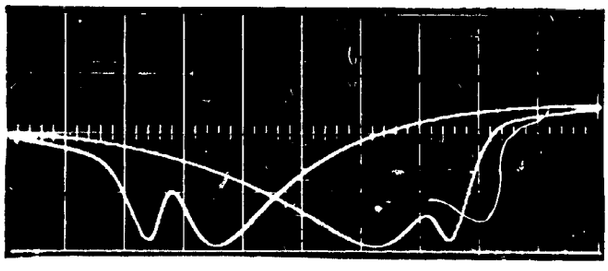

(c) $S_x = 2.0 \times 10^{-3}$ mm/mm

I = 0

-190 80 V_z=0 +80 +190

(Volts)

FIGURE A-4. LIGHT INTENSITY VERSUS 60 Hz VOLTAGE HYSTERESIS WITH DIFFERENT TENSILE STRAINS

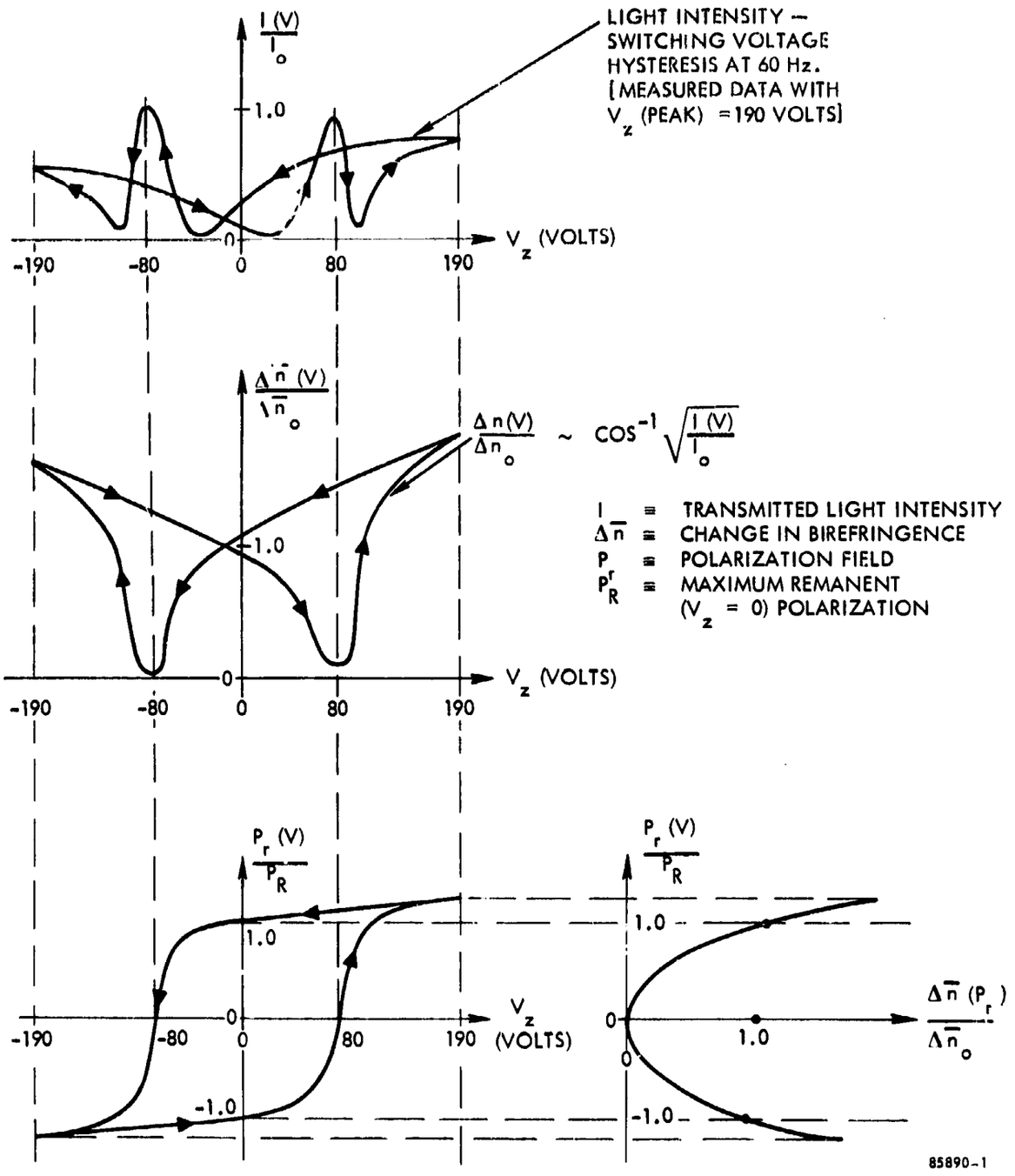

FIGURE A-5. HYSTERESIS RELATIONSHIPS FOR PLZT

The $\overline{\Delta n}_p$ - P_r curve was obtained by mapping the $\overline{\Delta n}_p$ - V_z curve onto the P_r-V_z curve, as indicated in Figure A-5.

Note that near V_z = ±80 volts (the coercive voltage), the quantities I, $\overline{\Delta n}_p$, and P_r all change rapidly. Near P_r = 0, $\overline{\Delta n}_p$ goes through a minimum while near $P_r = P_R$, $\overline{\Delta n}_p$ is near a maximum.

The data in Figure A-5 clearly indicate that optical transmission states in PLZT are a function of the history of electrical control signals in a nonlinear manner. The specific sequence of electrical control signals which is used to matrix address a two-dimensional array of display elements is not explicitly shown in These data. This sequence is described in Section 4.3.5.